Metallostar assemblies based on dithiocarbamates for use as MRI contrast agents

Hannah L. Perry,[a,b,+] Il-Chul Yoon,[a+] Nicolas G. Chabloz,[a] Susannah Molisso,[a] Graeme J. Stasiuk,[b] René M. Botnar[b] and James D. E. T. Wilton-Ely*[,a]

[a] *Department of Chemistry, Imperial College London, Molecular Sciences Research Hub, White City Campus, London, W12 0BZ, UK.*
[b] *School of Biomedical Engineering and Imaging Sciences, King's College London, St Thomas' Hospital, London, SE1 7EH, UK.*
+ These authors contributed equally

E-mail: j.wilton-ely@imperial.ac.uk

Abstract

Two different octadentate gadolinium chelates based on DO3A and DOTAGA chelates (hydration number q = 1) have been used to prepare a series of bi-, tri- and tetrametallic *d-f* mixed-metal complexes. The piperazine-based dithiocarbamate linker ensures that rotation of the gadolinium chelates is restricted, leading to enhanced relaxivity (r_1) values, which increase with overall mass and the number of gadolinium units. The r_1 value (at 10 MHz, 25 °C) per Gd unit rises from 5.0 mM^{-1} s^{-1} for the Gd-DO3A-NH_2 monogadolinium chelate to 9.2 mM^{-1} s^{-1} in a trigadolinium complex with a ruthenium(III) core. Using a 1.5 T clinical scanner operating at 63.87 MHz (25 °C), an 86% increase in relaxivity per gadolinium unit is observed for this multimetallic compound compared to clinically-approved Dotarem. The gadolinium complexes based on the DOTAGA chelate also performed well at 63.87 MHz, with a relaxivity value of 9.5 mM^{-1} s^{-1} per gadolinium unit being observed for the trigadolinium *d-f* mixed-metal complex with a ruthenium(III) core. The versatility of dithiocarbamate coordination chemistry thus provides access to a wide range of *d-f* hybrids with potential for use as high-performance MRI contrast agents.

Keywords: Gadolinium, dithiocarbamate, imaging, MRI, metallostar

Introduction

Magnetic resonance imaging (MRI) is a non-invasive medical imaging technique which provides detailed anatomical images with the highest spatial resolution of all the non-ionizing and non-invasive imaging modalities.[1] Different tissues are characterized by MR-specific relaxation parameters (longitudinal relaxation time, T_1; transverse relaxation time, T_2) and differing proton densities. The intrinsic soft tissue contrast observed enables detailed anatomical images to be acquired using MRI. However, due to the poor contrast often observed between different tissue types (such as healthy and diseased), contrast agents[2] are often employed in order to alter and accelerate the relaxation of water protons in healthy and diseased tissue, thereby improving the image detail and contrast. This is achieved by the presence of an exogenous paramagnetic species (e.g., trivalent gadolinium), which affects both T_1 recovery and T_2 decay due to its strong local magnetic moment. Higher relaxivity values (in $mM^{-1}s^{-1}$) correlate with better contrast enhancement.[2] The contrast agents currently used in a clinical setting are almost all based on paramagnetic ($4f^7$) trivalent gadolinium ions. Examples of these monogadolinium compounds are Dotarem® and Primovist® (Figure 1), which are both extracellular probes with a non-specific biodistribution. Their design features an octadentate chelate, which prevents loss of the toxic gadolinium ion, while still allowing a single coordination site for a water molecule (q = 1). The release of gadolinium cations into the body leads to the formation of salts with endogenous anions, such as phosphate or carbonate. On entering tissues, these species stimulate an inflammatory response, which results in scarring of the tissue. This nephrogenic systemic fibrosis (NSF) can lead to severe renal impairment in patients and has led to restrictions in the use of contrast agents with acyclic chelates.[2]

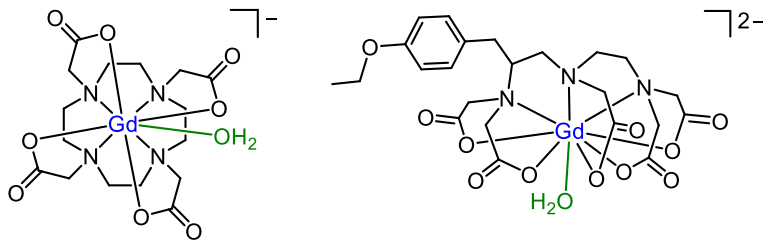

Dotarem® Primovist®

Figure 1. Two commonly used, clinically-approved gadolinium contrast agents, which both have a hydration number (q) of one.

Interactions between the paramagnet and coordinated and surrounding water molecules leads to an improvement in the relaxation rates of the surrounding water protons, enhancing image contrast and signal-to-noise performance.[2] Due to the inherent low sensitivity of MRI, very high concentrations (typically 0.1 mmol per kg patient weight) of contrast agent are required and so efforts have been made to increase the relaxivity performance of each Gd^{3+} ion. This could also reduce the amount of contrast agent that needs to be administered.

The attachment of Gd^{3+} complexes to larger assemblies such as polymers and nanoparticles has been successfully used to dramatically increase the relaxivity per Gd^{3+} ion. This can be explained in terms of the rotational correlation time, which increases when the assembly rotates slowly, leading to enhanced relaxation rates. In addition, the degree to which the relaxation of water protons changes is due to the multimeric effect which stems from the increased, localized contrast agent concentration.[2]

Pioneering work by Tóth,[3] Helm,[4] Parac-Vogt[5] and Desreux[6] has focused on the synthesis of molecular multimetallic gadolinium compounds, either with an organic or metal-based core. These assemblies have demonstrated impressive relaxivity in many cases. However, one pitfall common to all polygadolinium approaches is the difficulty in eliminating internal rotation of the individual gadolinium chelates, which undermines the potential for extremely high relaxivity enhancement.

For over a decade we have focused on the development of a wide range of routes to multimetallic compounds,[7] with the use of dithiocarbamates ($R_2NCS_2^-$) being a recurring feature.[8] This has been driven partly by the ease of formation of dithiocarbamates from (usually secondary) amines in the presence of base and carbon disulfide.[9] The fact that dithiocarbamate compounds are known for their ability to coordinate to all the transition metals in all common oxidation states (both high and low) indicates the vast potential that dithiocarbamates with additional functionality could promise.[9,10]

In 2014, we reported for the first time how dithiocarbamates could be used to incorporate gadolinium units into multimetallic assemblies, or onto the surface of gold nanoparticles.[11] These materials showed promising relaxivity behavior, however, the

hexacoordinate coordination of the Gd^{3+} ion (q = 3) raised concerns over the potential loss of this toxic ion under physiological conditions. This led to new designs based on an octadentate coordination environment, such as that found in Dotarem® (Fig. 1).[12] The present work describes how these improved and highly stable gadolinium chelates can be employed in the generation of multimetallic compounds based on both *d*- and *f*-block metals, along with an assessment of their performance in MRI contrast enhancement.

Results and discussion

Two polydentate chelates designed for the immobilization of gadolinium on the surface of gold nanoparticles,[13,14] **Gd-DO3A-DTC** and **Gd-DOTAGA-DTC,** were used to provide gadolinium chelates with either a neutral or anionic environment for the Gd ion. It was expected that the charge on this part of the molecules would have a significant impact on the interaction of water with the paramagnetic ion and hence modify the relaxivity observed.

The **Gd-DO3A-NH2** and **Gd-DOTAGA-NH2** precursors were prepared by a straightforward multi-step route starting from commercially-available cyclen, as reported previously (Scheme 1).[13,14] The corresponding dithiocarbamates, **Gd-DO3A-DTC** and **Gd-DOTAGA-DTC** were prepared and isolated shortly before use as the ammonium precursors are more suitable for long-term storage than these reactive species.

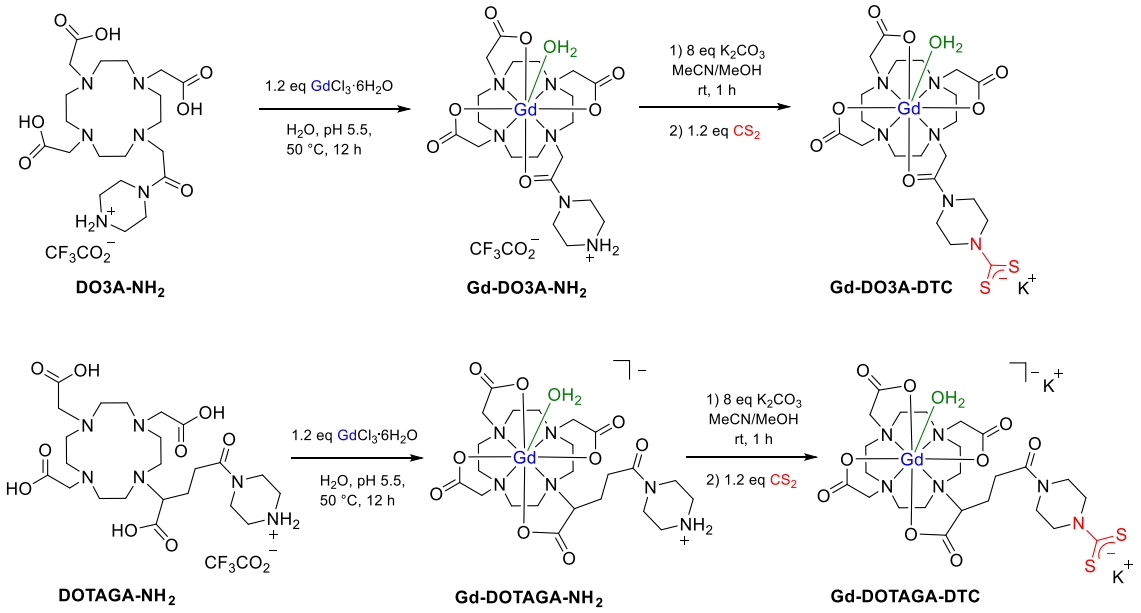

Scheme 1. Synthesis of **Gd-DO3A-DTC** and **Gd-DOTAGA-DTC.**

Synthesis of multimetallic d-f hybrids

The benefit of using reliable linkers, such as pyridyl donors, to form multimetallic *d-f* hybrids for use in imaging applications has been demonstrated by Faulkner and co-workers.[15] While less frequently employed than nitrogen-based donors, the dependable reactivity and versatility of dithiocarbamate ligands[9] make them ideally suited to the construction of multimetallic assemblies.[8] Accordingly, the dithiocarbamate, **Gd-DO3A-DTC**, was used to prepare a series of multimeric molecular gadolinium compounds through addition of suitable transition metal precursors (Scheme 2). In order to enable characterization by nuclear magnetic resonance spectroscopy, the lanthanum analogues of the compounds were additionally prepared. The synthesis of **La-DO3A-NH$_2$** and **La-DO3A-DTC** is described in the Supporting Information.

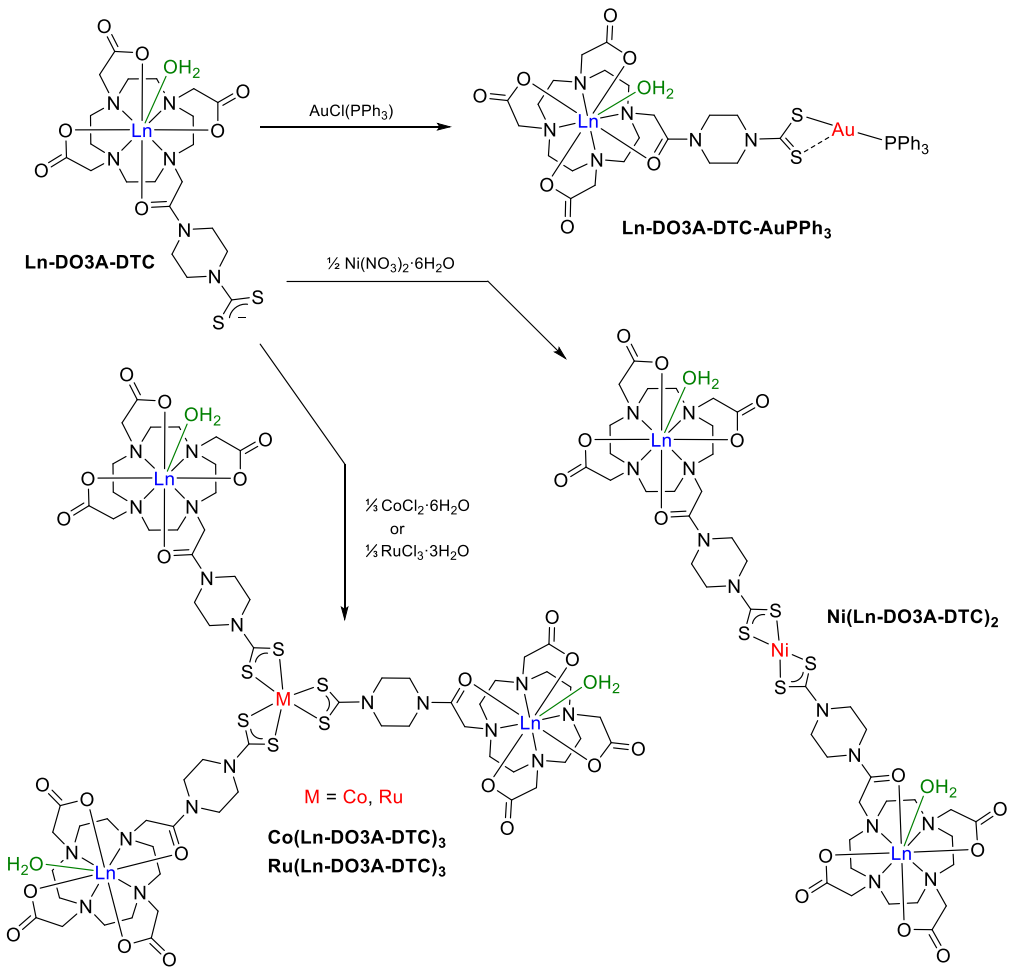

Scheme 2. Synthesis of mono-, bi- and trigadolinium compounds based on **Ln-DO3A-DTC** (Ln = La, Gd).

Dithiocarbamate complexes of gold are well known,[9] particularly of gold(I), in which this 1,1'-dithio ligand typically bonds in an anisobidentate manner. The versatile starting material, [AuCl(PPh_3)], was chosen for reaction with the lanthanum complex, **La-DO3A-DTC** (Scheme 2). After stirring at room temperature in the dark for one hour, the precipitated KCl salt was removed by filtration and the product was isolated and analyzed by $^{31}P\{^1H\}$ nuclear magnetic resonance (NMR) spectroscopy. This revealed a shift of the PPh_3 resonance from 33.2 ppm in the starting material to 37.3 ppm in the product. The $^{13}C\{^1H\}$ NMR spectrum displayed a resonance at 213.3 ppm for the CS_2 carbon nucleus,[9] while the ^1H NMR spectrum showed broadened peaks attributed to the DO3A-piperazine chelate in addition to aromatic resonances for the phosphine ligand. The IR spectrum revealed an absorption at 1599 cm^{-1} (C=O stretch) as well as a feature at 1430 cm^{-1} attributed to the C-N stretch, and a peak at 999 cm^{-1} assigned as the ν_{C-S} absorption of the dithiocarbamate ligand.[9] Along with a molecular ion for $[M - H_2O]^+$ at *m/z* 1142 in the mass spectrum (MALDI, +ve mode), these data confirmed the formulation of the product as **La-DO3A-DTC-AuPPh$_3$**. The gadolinium analogue, was then synthesized from **Gd-DO3A-DTC** using the same protocol to yield an off-white powder, **Gd-DO3A-DTC-AuPPh$_3$**. Infrared analysis supported the preparation of this analogous product with typical bands for the PPh_3 ligand along with peaks at 1679 ($\nu_{C=N}$), 1603 ($\nu_{C=O}$), 1396 (ν_{C-N}) and 994 cm^{-1} (ν_{C-S}). These features are consistent with the anisobidentate binding mode for the dithiocarbamate ligand, which is typical for gold(I) complexes.[9]

Compound **La-DO3A-DTC** was added to nickel nitrate hydrate causing a rapid color change with the pale blue solution becoming bright yellow. This was then stirred for an hour at room temperature (Scheme 2) to give **Ni(La-DO3A-DTC)$_2$** as a pale green powder. The solid state infrared spectrum of **Ni(La-DO3A-DTC)$_2$** indicated the presence of the dithiocarbamate-DO3A ligand with characteristic peaks at 1671 ($\nu_{C=N}$), 1599 ($\nu_{C=O}$), 1403 (ν_{C-N}) and at 1003 cm^{-1} (ν_{C-S}). The corresponding reaction between **Gd-DO3A-DTC** and $Ni(NO_3)_2 \cdot 6H_2O$ followed the same pathway to afford a pale green powder, **Ni(Gd-DO3A-DTC)$_2$**. The infrared spectrum of this compound confirmed the presence of the dithiocarbamate ligand with absorptions at similar values to those found for **Ni(La-DO3A-DTC)$_2$**. Mass spectrometry was used to further characterize **Ni(La-DO3A-DTC)$_2$** and **Ni(Gd-DO3A-DTC)$_2$**.

Following the successful preparation of bimetallic monogadolinium and trimetallic digadolinium complexes, attention then turned to the synthesis of tetrametallic trilanthanide complexes (Scheme 2). Compound **La-DO3A-DTC** was added to $CoCl_2 \cdot 6H_2O$ leading to a rapid change in solution color from pale pink to dark green. After stirring for an hour at room temperature and filtration through Celite, all solvent was removed to afford a dark green solid, formulated as **Co(La-DO3A-DTC)$_3$**. The infrared spectrum of this compound confirmed the presence of the DO3A-dithiocarbamate ligand with similar absorptions to those found for the other complexes. The gadolinium analogue, **Co(Gd-DO3A-DTC)$_3$**, was prepared in the same manner. In common with many literature examples,[9] reaction of a divalent cobalt precursor leads to the isolation of a trivalent diamagnetic tri(dithiocarbamate) product. **Ru(La-DO3A-DTC)$_3$** and **Ru(Gd-DO3A-DTC)$_3$** were synthesized following a similar procedure to that used for their cobalt analogues using $RuCl_3 \cdot 3H_2O$. Formation of these $RuLn_3$ complexes was accompanied by a color change from black to dark green. Infrared spectroscopy and mass spectrometry confirmed the successful synthesis of the desired tetrametallic trigadolinium complexes. An investigation of the magnetic properties through both the Evans NMR method and measurement using a magnetic susceptibility balance led to μ_{eff} values between 1.92 – 2.10 BM, strongly suggesting only one unpaired electron and a low-spin $(t_{2g})^5(e_g)^0$ configuration for the trivalent ruthenium center.

In a similar manner, the dianionic **Gd-DOTAGA-DTC** compound was added to various transition metal salts to form anionic multimeric molecular gadolinium compounds (Scheme 3). As expected, spectroscopic data for these compounds were found to be similar to those described above. Characterization details for these compounds can be found in the Electronic Supplementary Information.

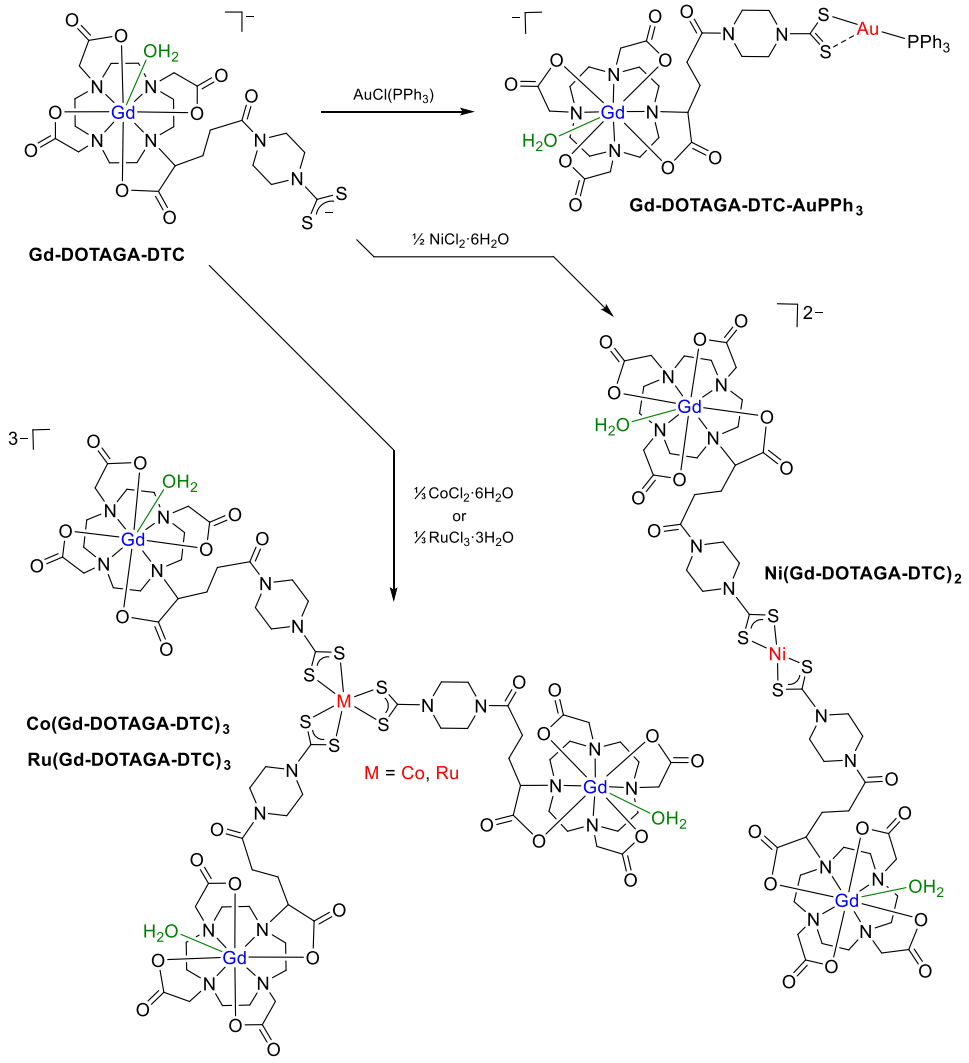

Scheme 3. Synthesis of mono-, di- and trigadolinium compounds based on **Gd-DOTAGA-DTC**. All countercations are potassium ions.

Macrocyclic chelates with carboxylate arms, such as **Gd-DOTAGA-DTC** often have faster water exchange rates (contributing to higher relaxivity) than macrocyclic chelates with amide arms (like **Gd-DO3A-DTC**).[12] The coordination environment of **Gd-DOTAGA-DTC** mimics that found in the leading, clinically-used contrast agent, Dotarem®, which is known for its high kinetic stability (logK_{GdL} of 25.3).[1] This fact provides reassurance (particularly in the context of Nephrogenic Systemic Fibrosis, NSF) that the toxic gadolinium(III) ion will not be released under biological conditions.

The synthesis described above resulted in a series of analogous multimetallic complexes bearing the **Gd-DO3A-DTC** and **Gd-DOTAGA-DTC** units. This allowed their relaxivity to be evaluated and their potential as MR contrast agents to be determined.

Relaxivity measurements

Using a 0.01-10 MHz fast field-cycling NMR relaxometer (0.25 Tesla SMARtracer®, Stelar), the relaxivity performance of the polygadolinium compounds was established and compared to **Gd-DO3A-NH2** and **Gd-DOTAGA-NH2** (chosen in preference to the corresponding dithiocarbamates due to their greater stability) as well as the clinically-approved standard, Dotarem®. The data point at 63.87 MHz was acquired using a 1.5 T clinical MRI scanner, which operates only at room temperature (25 °C). Fluorescence lifetime measurements reported in previous studies[13,14] for the europium analogues, **Eu-DO3A-NH2** and **Eu-DOTAGA-NH2** confirmed the expected hydration value of q = 1 for the octadentate chelates. Both **Gd-DO3A-NH2** and **Gd-DOTAGA-NH2** were found to possess a higher relaxivity than Dotarem®, likely due to the slightly higher molecular mass, which is known to enhance relaxivity.[2] The Nuclear Magnetic Relaxation Dispersion (NMRD) profiles of these chelates are shown in Figure 2. The presence of an amide arm, such as that found in **Gd-DO3A-NH2**, has been reported to potentially impact negatively on the relaxivity,[16] however, this does not seem to be a significant factor in the performance of the chelate design reported here.

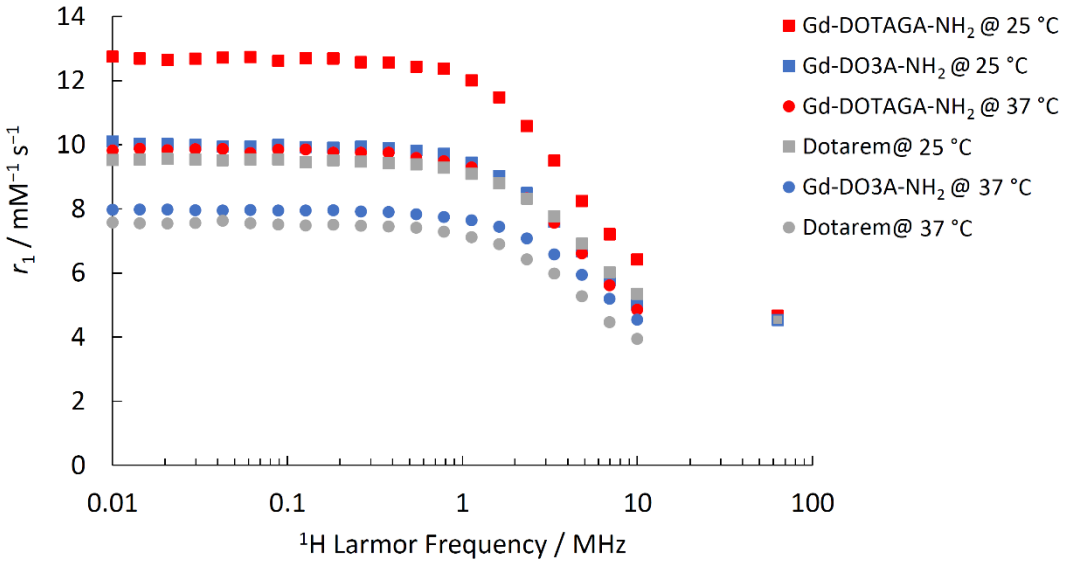

Figure 2. NMRD profiles of Dotarem®, **Gd-DO3A-NH2**, **Gd-DOTAGA-NH2** at 25 and 37 °C.

The relaxivity of the various multimetallic assemblies was also measured at 25 and 37 °C in water and NMRD profiles determined. It is known that an increase in mass of the gadolinium-containing unit results in an enhancement of the relaxivity[17,18] due to slow tumbling and a reduction in the rotational freedom experienced by each individual Gd unit. However, it was anticipated that a particularly pronounced enhancement would be observed for the materials prepared in this study. In addition to the increased mass, the rigidity of the piperazine rings and the multiple bond character of the dithiocarbamate and amide bonds also limit rotational freedom and thus enhance relaxivity. Previous designs based on an organic or metal core often allow rotation about the axis of the tether and this can have a detrimental effect on the relaxivity.[3-6]

Using the Evans method to determine the gadolinium concentration,[19] the relaxivity of **Gd-DO3A-DTC-AuPPh$_3$** at 0.01 MHz was found to be 11.3 and 10.3 mM^{-1} s^{-1} at 25 and 37 °C, respectively (Figure 3). As the temperature increases, the rate of internal freedom of rotation increases and this results in a reduction in the relaxivity of the complex. Although the relaxivity maintained a constant value at Larmor frequencies between 0.01 and 1 MHz, at Larmor frequencies beyond 1 MHz, the relaxivity of the complex decreased with increasing frequency – a typical effect seen in small molecular contrast agents.[20] The relaxivity of **Gd-DO3A-DTC-AuPPh$_3$** at 10 MHz was found to be 6.4 and 5.6 mM^{-1} s^{-1} at 25 and 37 °C, respectively.

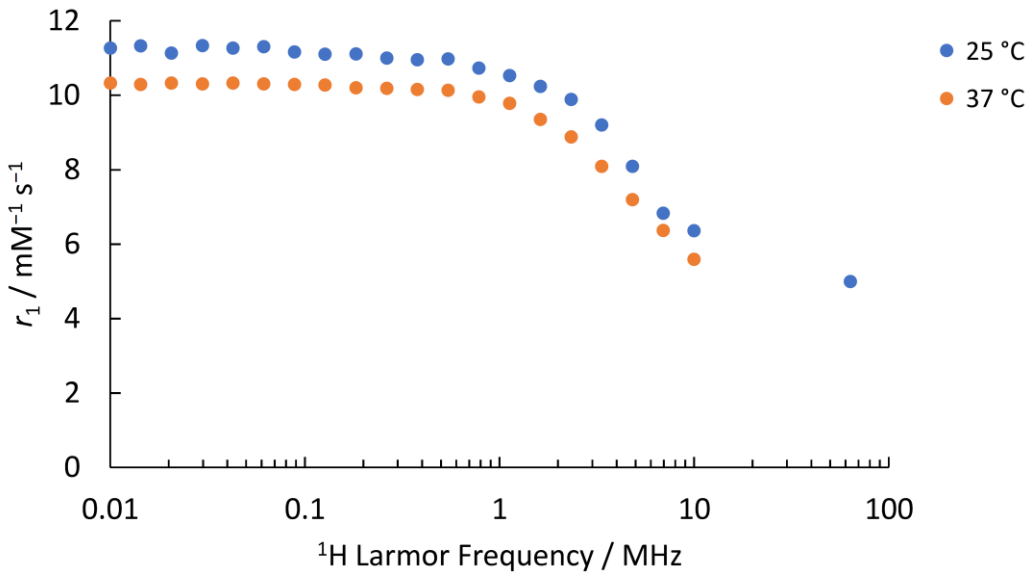

Figure 3. The NMRD profiles of **Gd-DO3A-DTC-AuPPh$_3$** at 25 and 37 °C.

This represents a modest improvement on the r_1 value of **Gd-DO3A-NH$_2$** at 10 MHz (5.2 mM^{-1} s^{-1} at 25 °C and 4.5 mM^{-1} s^{-1} at 37 °C) and this enhancement can be attributed to the additional mass provided by the AuPPh$_3$ unit slowing the rotational correlation time. The trimetallic (digadolinium) complex, **Ni(Gd-DO3A-DTC)$_2$**, was found to display r_1 values (at 10 MHz) per Gd^{3+} ion of 6.1 and 5.5 mM^{-1} s^{-1} at 25 and 37 °C, respectively (Figure 4). Again, this represents an increase over the relaxivity of **Gd-DO3A-NH$_2$** and is a similar value to that measured for **Gd-DO3A-DTC-AuPPh$_3$**. This is not surprising given their similar mass. The overall relaxivity (at 10 MHz) of **Ni(Gd-DO3A-DTC)$_2$** was found to be 12.2 mM^{-1} s^{-1} and 10.9 mM^{-1} s^{-1} at 25 and 37 °C, demonstrating the benefits of an increased gadolinium payload.

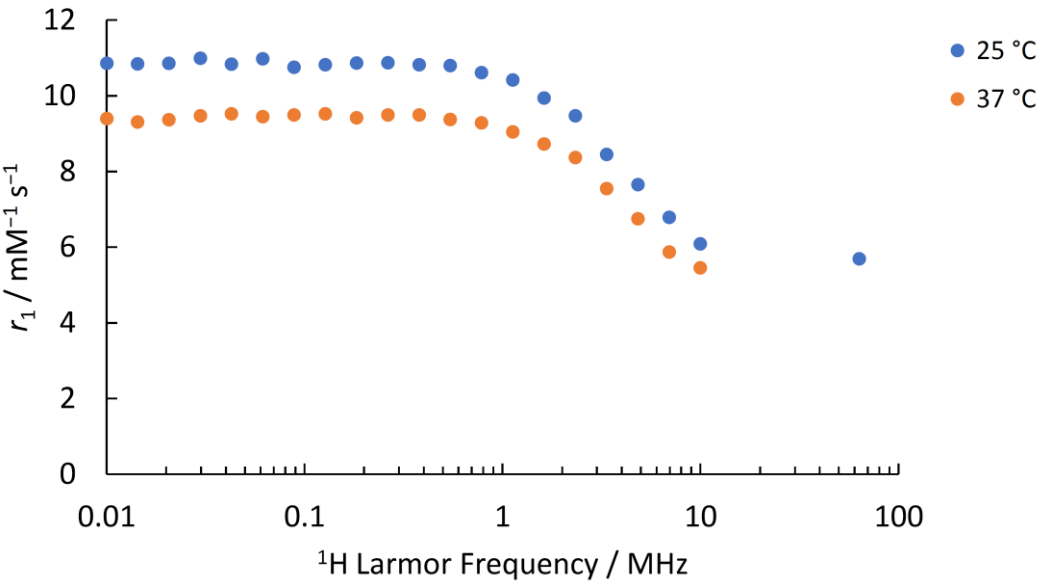

Figure 4. The relaxivity values per Gd^{3+} ion for **Ni(Gd-DO3A-DTC)$_2$** at 25 and 37 °C.

NMRD studies performed on **Co(Gd-DO3A-DTC)$_3$** revealed this trigadolinium compound to display relaxivity values per gadolinium ion (at 10 MHz) of 10.5 (25 °C) and 9.7 (37 °C) mM^{-1} s^{-1} (Figure 5). This is almost double the value obtained for monometallic **Gd-DO3A-NH$_2$** and also a significant improvement on the di-gadolinium complex, **Ni(Gd-DO3A-DTC)$_2$**.

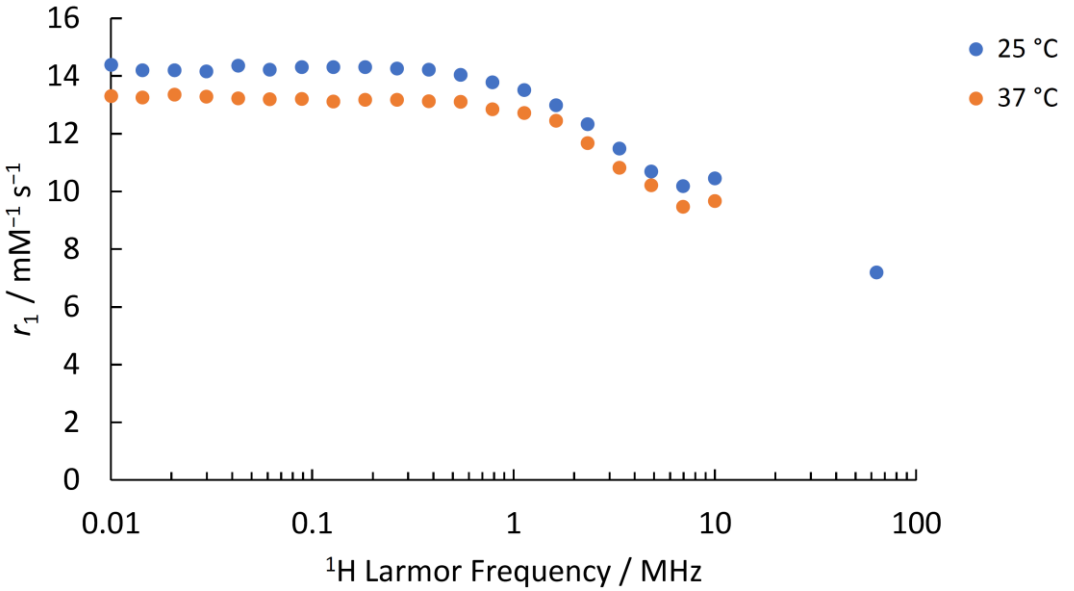

Figure 5. The relaxivity values per Gd^{3+} ion for **Co(Gd-DO3A-DTC)$_3$** at 25 and 37 °C.

The rigidity of the dithiocarbamate-piperazine linker (with multiple bond character in both amide and dithiocarbamate units) decreases the internal rotation in the complexes thus increases relaxivity. However, in the mono- and di-gadolinium complexes, this boost in relaxivity is limited by the rapid overall rotation of the complexes. It appears that the mass of **Co(Gd-DO3A-DTC)$_3$** causes the overall rotation to decrease sufficiently to allow the gains in relaxivity from the reduced internal motion to be observed. This results in a reduced temperature dependence; the difference between the r_1 values recorded at 25 and 37 °C is significantly smaller than that found in the complexes of lower mass. As the molecular mass increases, this reduction will continue until the increase in temperature leads to the situation where rotational correlation time is no longer a limiting factor. Figure 5 also shows an increase in relaxivity as the frequency approaches 10 MHz, which is a trend typical of macromolecular structures.[20] With three Gd^{3+} ions in the same molecular assembly, the high payload of gadolinium ions per complex gives an overall relaxivity for **Co(Gd-DO3A-DTC)$_3$** of 31.4 (25 °C) and 29.0 (37 °C) mM^{-1} s^{-1}. This is almost 6 times the r_1 value of **Gd-DO3A-NH$_2$** and is comparable to the trigadolinium species synthesized by Desreux and coworkers.[6]

A second tri-gadolinium complex based on Gd-DO3A-DTC was prepared using a ruthenium core (**Ru(Gd-DO3A-DTC)$_3$**). It performed similarly to **Co(Gd-DO3A-DTC)$_3$**, with relaxivity values at 10 MHz of 9.2 mM^{-1} s^{-1} and 8.5 mM^{-1} s^{-1} at 25 °C and 37 °C, respectively (Figure 6). These values increase to 27.6 mM^{-1} s^{-1} and 25.6 mM^{-1} s^{-1} when

considering the overall relaxivity of the tri-gadolinium complex. The same trend in relaxivity, with an upswing between 7 and 10 MHz, was observed with **Ru(Gd-DO3A-DTC)$_3$** just as it had been with **Co(Gd-DO3A-DTC)$_3$**.

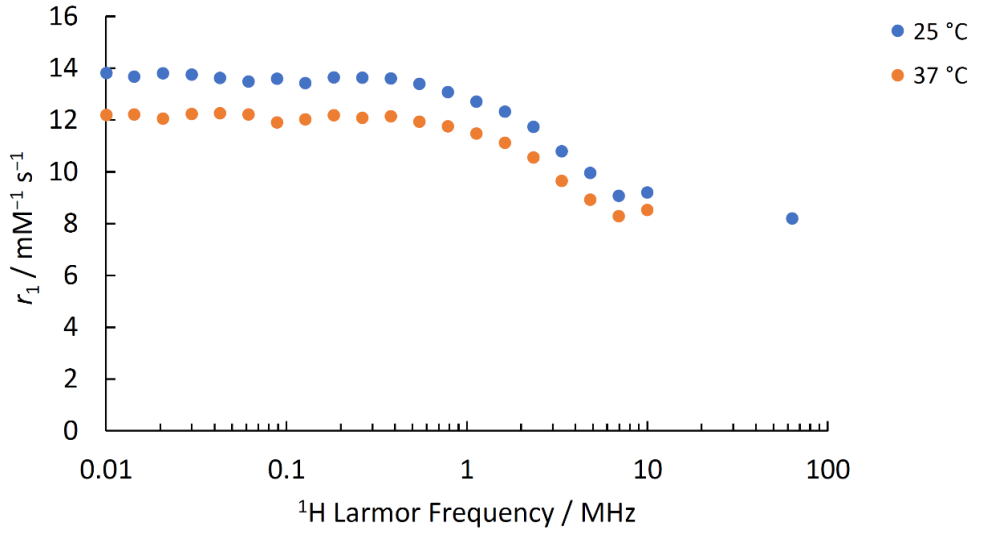

Figure 6. The relaxivity values per Gd^{3+} ion for **Ru(Gd-DO3A-DTC)$_3$** at 25 and 37 °C.

A comparison of the complexes in this study based on Gd-DO3A-DTC at 25 °C is provided in Figure 7.

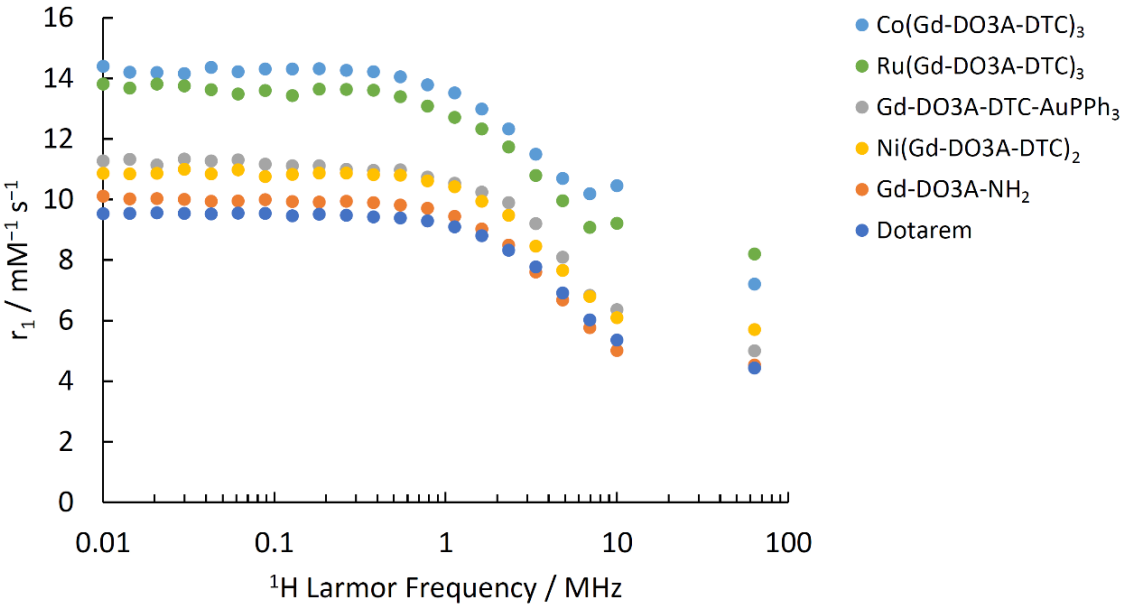

Figure 7. Summary of the relaxivity per Gd^{3+} ion of Dotarem®, **Gd-DO3A-NH$_2$**, **Gd-DO3A-DTC-AuPPh$_3$**, **Ni(Gd-DO3A-DTC)$_3$**, **Co(Gd-DO3A-DTC)$_3$** and **Ru(Gd-DO3A-DTC)$_3$** at 25 °C.

The DOTAGA-based complexes displayed similar trends in relaxivity to their DO3A-based analogues, with the gold and nickel complexes achieving relaxivity values of 6.9 and 7.2 mM^{-1} s^{-1}, respectively, and the cobalt and ruthenium complexes performing better with relaxivity values of 10.8 and 9.9 mM^{-1} s^{-1}, respectively, (10 MHz, 25 °C). The overall relaxivities of the DOTAGA-based complexes are displayed in Figure 8, to emphasize the benefit of incorporating multiple gadolinium chelates into a single assembly. The individual NMRD profiles of the DOTAGA-based complexes at 25 and 37 °C can be found in the Supporting Information, where the same characteristic 'upswing' in relaxivity that was seen with **Co(Gd-DO3A-DTC)$_3$** and **Ru(Gd-DO3A-DTC)$_3$** is replicated for **Co(Gd-DOTAGA-DTC)$_3$** and **Ru(Gd-DOTAGA-DTC)$_3$**.

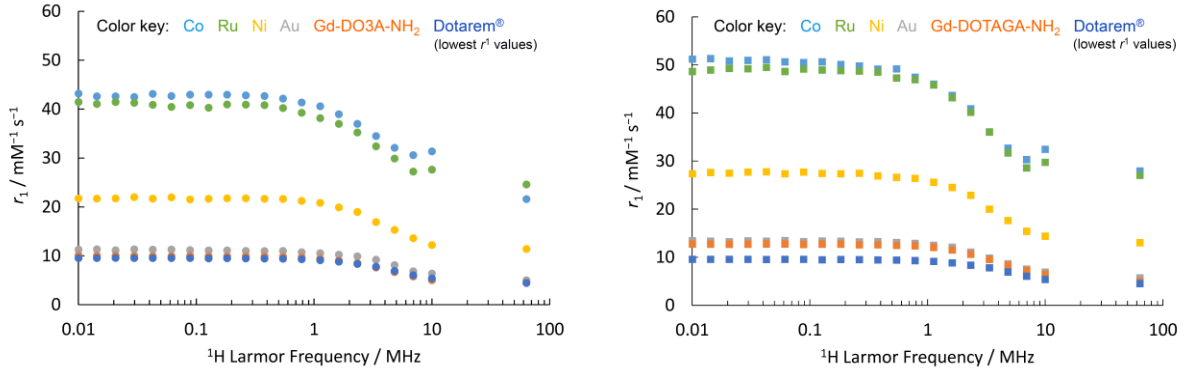

Figure 8. The overall relaxivity values of the DO3A-based metallostars (left) and the DOTAGA-based metallostars (right) at 25 °C. The central metal ion is distinguished by color: cobalt (light blue), ruthenium (green), nickel (yellow), gold (grey). Also displayed are **Gd-DO3A-NH$_2$** (orange circles) and **Gd-DOTAGA-NH$_2$** (orange squares) and Dotarem® (dark blue).

In order to provide a convenient numerical comparison, the r_1 values (10 MHz) at 25 °C and 37 °C for each complex are shown in Table 1, both per Gd^{3+} ion and overall. On increasing the temperature of the Dotarem® solution, relaxivity decreased from 5.4 to 4.0 mM^{-1} s^{-1}, which represented a 26% decrease. The relaxivity of **Ru(Gd-DOTAGA-DTC)$_3$**, on the other hand, decreased by only 3%, from 9.9 to 9.6 mM^{-1} s^{-1}. In fact, all the multimetallic complexes were far less affected by the temperature change than Dotarem®. This can be traced to their larger size, compared to Dotarem®, and the internal rigidity present in their structures. As the temperature was increased, the rotational motion of the smaller

Dotarem® chelates increased more significantly than that in the multimetallic complexes. This led to the relaxivity values for the multimetallic complexes being less affected by the temperature change than the relaxivity of Dotarem®.

Table 1. Summary of the relaxivity values (mM^{-1} s^{-1}) for the multimetallic complexes measured at 25 and 37 °C (10 MHz).

	25 °C		**37 °C**	
	***r*$_1$ per Gd**	***r*$_1$ overall**	***r*$_1$ per Gd**	***r*$_1$ overall**
Dotarem®	5.4	5.4	4.0	4.0
Gd-DO3A-NH$_2$	5.2	5.2	4.5	4.5
Gd-DO3A-DTC-AuPPh$_3$	6.4	6.4	5.6	5.6
Ni(Gd-DO3A-DTC)$_2$	6.1	12.2	5.5	10.9
Co(Gd-DO3A-DTC)$_3$	10.5	31.4	9.7	29.0
Ru(Gd-DO3A-DTC)$_3$	9.2	27.6	8.5	25.6
Gd-DOTAGA-NH$_2$	6.4	6.4	5.0	5.0
Gd-DOTAGA-DTC-AuPPh$_3$	6.9	6.9	5.9	5.9
Ni(Gd-DOTAGA-DTC)$_2$	7.2	14.4	5.9	11.9
Co(Gd-DOTAGA-DTC)$_3$	10.8	32.4	9.8	29.5
Ru(Gd-DOTAGA-DTC)$_3$	9.9	29.7	9.6	28.7

The T_1-weighted MR images of the compounds (Figure 9) were measured on a clinical scanner at 63.87 MHz (1.5 T) and compared to Dotarem®. This reveals that for the same concentration of Gd^{3+} ions (0.2 mM), significantly greater contrast can be achieved per Gd^{3+} unit in **Gd-DO3A-DTC-AuPPh$_3$** (r_1 = 5.0 ± 0.1 mM^{-1} s^{-1}), **Ni(Gd-DO3A-DTC)$_2$** (r_1 = 5.7 ± 0.1 mM^{-1} s^{-1}), **Co(Gd-DO3A-DTC)$_3$** (r_1 = 7.2 ± 0.1 mM^{-1} s^{-1}) and **Ru(Gd-DO3A-DTC)$_3$** (r_1 = 8.2 ± 0.1 mM^{-1} s^{-1}) compared to Dotarem® (r_1 = 4.4 ± 0.2 mM^{-1} s^{-1}).

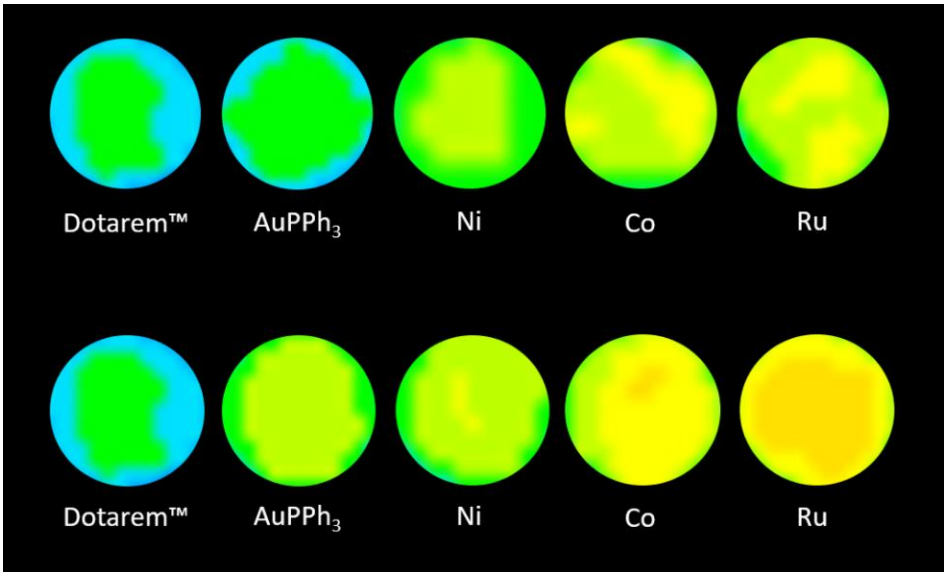

Figure 9. T_1-weighted MR images (shown in '16 colors', ImageJ) of the multimetallic complexes (DO3A-based, above, and DOTAGA-based, below) and Dotarem® at 25 °C, 63.87 MHz. $[Gd^{3+}]$ = 0.2 mM in all cases.

The multimetallic complexes based on the DOTAGA chelate consistently showed greater relaxivity values than their equivalent DO3A complexes, demonstrating the importance of the gadolinium chelate design. This is in spite of the short alkyl chain that features in the DOTAGA linker, which could facilitate undesirable internal flexibility. It appears that, in this case at least, the additional flexibility generated by this unsaturated linkage is not sufficiently significant to affect the relaxivity noticeably. It is also likely that other factors associated with the DOTAGA chelate, such as an increased water exchange rate at the metal center, provide a greater contribution to the observed relaxivity. The relaxivity values measured for the DOTAGA compounds at a clinical magnetic field strength were particularly impressive, with greater contrast being achieved by **Gd-DOTAGA-DTC-AuPPh$_3$** (r_1 = 5.9 ± 0.1 mM^{-1} s^{-1}), **Ni(Gd-DOTAGA-DTC)$_2$** (r_1 = 6.2 ± 0.1 mM^{-1} s^{-1}), **Co(Gd-DOTAGA-DTC)$_3$** (r_1 = 9.0 ± 0.2 mM^{-1} s^{-1}) and **Ru(Gd-DOTAGA-DTC)$_3$** (r_1 = 9.5 ± 0.1 mM^{-1} s^{-1}) compared to Dotarem® (r_1 = 4.4 ± 0.2 mM^{-1} s^{-1}). Most noteworthy were the tri-gadolinium complexes, **Co(Gd-DOTAGA-DTC)$_3$ and Ru(Gd-DOTAGA-DTC)$_3$**, whose relaxivity values at 1.5 T were at least twice that of Dotarem®.

Stability and toxicity studies

The design of the chelates used to complex the gadolinium ion is intentionally closely based on that of Dotarem®, one of the leading clinically-approved contrast agents. The stability of the chelate towards loss of gadolinium ions (and hence its toxicity) has been probed in previous studies.[13,14] This revealed that the addition of excess Zn^{2+} ions to **Gd-DO3A-NH$_2$** and **Gd-DOTAGA-NH$_2$** led to no change in the relaxivity values obtained, indicating that no displacement of Gd^{3+} ions occurred.[22]

Stability studies were repeated for the multimetallic complexes, again in the presence and absence of excess Zn^{2+} ions. When the multimetallic complexes were dissolved only in PBS (phosphate buffered saline, pH 7.4), there was no change in relaxivity for at least 72 hours, indicating that the multimetallic complexes had remained intact and not degraded in this time. When the multimetallic complexes were in the presence of 10 equivalents of Zn^{2+} ions, relaxivity once again remained constant, showing that no transmetallation had occurred between the Zn^{2+} and Gd^{3+} ions. These results were crucial for their potential use as clinical contrast agents as unchelated Gd^{3+} is known to be highly toxic, whereas chelated Gd^{3+} is generally well tolerated by the body.

In earlier studies, cytotoxicity assessment of the **Gd-DO3A-NH$_2$** and **Gd-DOTAGA-NH$_2$** gadolinium units revealed no toxicity to MCF-7 (breast cancer) or HeLa (cervical cancer) cells, even at concentrations of 250 μM.[13,14] In order to ascertain whether the multimetallic compounds described in this contribution had any adverse effects on cell viability, the same MTT (3-(4,5-dimethylthiazol-2-yl)-2,5-diphenyltetrazolium bromide) assay as previously reported[13,14] was carried out in HEK (human embryonic kidney) and HeLa cell lines. The multimetallic complexes all demonstrated low or no toxicity at concentrations up to 250 μM. In the HEK cell line, cell viability at 250 μM ranged from 82 ± 4% for **Co(Gd-DOTAGA-DTC)$_3$** (showing low toxicity) up to 106 ± 4% for **Ni(Gd-DO3A-DTC)$_2$** (showing no toxicity). In the HeLa cell line, cell viability at 250 μM ranged from 88 ± 2% for **Ru(Gd-DO3A-DTC)$_3$** to 103 ± 2% for **Co(Gd-DO3A-DTC)$_3$**.

The MTT cell viability assay was also performed on an additional complex, **Gd-DO3A-DTC-AuPPh$_2$PhCOOH** (Supporting Information). This multimetallic compound was prepared based on work by Goze, Bodio et al.[23] who demonstrated the antiproliferative

properties of a number of gold(I) phosphine dithiocarbamate complexes featuring a central cyclam motif. The empty cyclam was replaced with the Gd-DO3A chelate with the aim of creating a theranostic complex for combined MRI and cancer therapy. Unfortunately, no evidence of a therapeutic effect was observed following 24 hrs incubation of **Gd-DO3A-DTC-AuPPh$_2$PhCOOH** with HeLa (cervical cancer) cells as cell viability remained at 89%, even at a concentration of 250 μM. The addition of a carboxylic acid group to one of the phenyl rings was found to have little effect on the relaxivity of the complex as it performed very similarly to **Gd-DO3A-DTC-AuPPh$_3$** at magnetic field strengths up to 0.25 T (Larmor frequency of 10 MHz).

Cell uptake studies

The uptake study was designed to gather further information on the behavior of these multi-gadolinium systems in a biological environment. Due to the superior relaxivity performance of the DOTAGA-based contrast agents, compared to the equivalent DO3A-based complexes, only the DOTAGA-based agents were taken forward to the uptake studies. Additionally, the negative charge on the DOTAGA chelates and lack of amide arm make them more chemically similar to Dotarem®, which makes for easier comparison. By focusing on the DOTAGA-based agents, the charge density and lipophilicity was maintained (DOTAGA and Dotarem® both have a negative charge, whereas DO3A is neutral), which ensured that the uptake of gadolinium depended principally on changes in the structure of the agent (i.e. number of Gd^{3+} units per complex).

Uptake of the DOTAGA-based multimetallic complexes by HeLa cells (Figure 10) was determined after incubation with the complexes for 24 hours. Gadolinium concentration, not complex concentration, was kept constant for each of the contrast agents and the results showed that the uptake of gadolinium per cell increased as the number of gadolinium chelates per complex increased. The mass of gadolinium delivered to each cell increased from 1.2 ± 0.1 pg (**Gd-DOTAGA-DTC-AuPPh$_3$**) to 2.6 ± 0.2 pg (**Co(Gd-DOTAGA-DTC)$_3$**), which represents a uptake similar in mass to those achieved by other poly-gadolinium systems.[13,14] This supported our hypothesis that incorporating multiple gadolinium chelates into the same assembly results in a more efficient delivery of gadolinium into cells. Extrapolation of this

procedure from a cellular scale to a larger 'tissue scale' would lead to an uptake of micrograms or even milligrams, which is adequate for MR imaging, as has already been observed with small-molecule gadolinium complexes both *in vitro*[24] and *in vivo*.[25]

By keeping the concentration of gadolinium constant, it is possible to deduce that the increase in delivery of gadolinium is due to the design of the tetrametallic complexes, and not simply because the cells were incubated with more gadolinium. Furthermore, assessment of the ratio of gadolinium ions to central metal ions before and after uptake (Supporting Information) revealed no significant change, indicating that the complexes were entering the cells as a whole unit and therefore stable towards degradation, even under biological conditions.

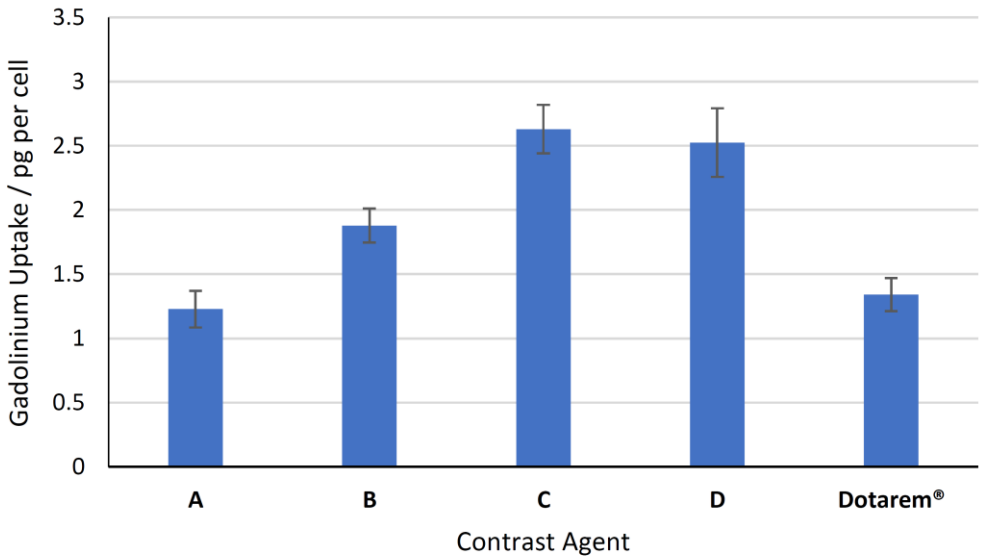

Figure 10. Uptake of **Gd-DOTAGA-DTC-AuPPh$_3$** (**A**), **Ni(Gd-DOTAGA-DTC)$_2$** (**B**), **Co(Gd-DOTAGA-DTC)$_3$** (**C**), **Ru(Gd-DOTAGA-DTC)$_3$** (**D**) and Dotarem® by HeLa cells following 24 h incubation.

Conclusions

A series of bi-, tri- and tetrametallic *d-f* mixed-metal complexes have been synthesized using either DO3A or DOTAGA-based gadolinium chelates to generate potential MRI contrast agents with consistently greater relaxivity values than Dotarem®, a clinically approved MRI

contrast agent. Most remarkable were **K_3[Co(Gd-DOTAGA-DTC)$_3$]** and **K_3[Ru(Gd-DOTAGA-DTC)$_3$]**, which achieved relaxivity values (per Gd^{3+} ion) more than twice the value of Dotarem® at clinical magnetic field strength. This can be partly attributed to the larger mass of the multimetallic complexes compared to Dotarem®, which leads to slower rotational motion and consequently greater relaxivity. However, a significant factor is also the rigidity of the piperazine-based dithiocarbamate linkers, which reduce the internal flexibility of the chelates and further enhance relaxivity.

A number of tests were performed to probe the stability, toxicity and cellular uptake of the multimetallic complexes. The stability tests revealed that the complexes were stable towards degradation and transmetallation and assessment of the gadolinium to central metal ion ratio before and after uptake by cells revealed that this stability towards degradation was maintained, even under biological conditions. MTT cell viability assays showed no evidence of toxicity, even at concentrations up to 250 μM, and cell uptake studies demonstrated the improved delivery of gadolinium into cells that is achieved when using a multi-gadolinium system.

The metallostar assemblies described here have shown great potential as multigadolinium MRI contrast agents. Given the versatility of dithiocarbamate coordination chemistry, there is a wealth of opportunity to further develop these multimetallic complexes into targeted, multimodal or theranostic agents by exchanging a gadolinium chelate for an appropriate dithiocarbamate-linked ligand. Such a modification would improve the clinical appeal of these assemblies whilst not enforcing a significant adjustment to an already straightforward synthetic route.

Supporting Information

Additional details are provided on characterization of the compounds described here along with details of relaxivity, cytotoxicity and cell uptake studies.

Acknowledgements

The authors wish to express their gratitude to the EPSRC Centre for Doctoral Training in Smart Medical Imaging (King's College London and Imperial College London) for provision of relaxometer facilities and a studentship (to H. L. P.). I.-C. Y. thanks Imperial College for the award of a President's PhD Scholarship and N. G. C. thanks the EPSRC for a DTP studentship. We are grateful to Mr Andrew Coulson for assistance with tissue culture facilities, Ms Patricia Carry for assistance with ICP-MS and Dr Giovanna Nordio for assistance with the MRI. G. J. S. would like to thank the MRC for funding (MR/T002573/1).

References

1. a) Bottrill, M.; Kwok, L.; Long, N. J. Lanthanides in magnetic resonance imaging. *Chem. Soc. Rev.* **2006**, *35*, 557-571; b) Hermann, P.; Kotek, J.; Kubíček, V.; Lukeš, I. Gadolinium(III) complexes as MRI contrast agents: ligand design and properties of the complexes. *Dalton Trans.* **2008**, *23*, 3027-3147.

2. a) Caravan, P. Strategies for increasing the sensitivity of gadolinium based MRI contrast agents. *Chem. Soc. Rev.* **2006**, *35*, 512-523; b) Lacerda, S.; Tóth, É. Lanthanide complexes in molecular magnetic resonance imaging and theranostics. *ChemMedChem* **2017**, *12*, 883-894. c) Li, H.; Meade, T. J. Molecular magnetic resonance imaging with Gd(III)-based contrast agents: challenges and key advances. *J. Am. Chem. Soc.* **2019**, *141*, 17025-17041; d) Banerjee, S. R.; Ngen, E. J.; Rotz, M. W.; Kakkad, S.; Lisok, A.; Pracitto, R.; Pullambhatla, M.; Chen, Z.; Shah, T.; Artemov, D.; Meade, T. J.; Bhujwalla, Z. M.; Pomper, M. G. Synthesis and evaluation of Gd^{III}-based magnetic resonance contrast agents for molecular imaging of prostate-specific membrane antigen. *Angew. Chem. Int. Ed.* **2015**, *54*, 10778-10782; e) Harrison, V. S. R.; Carney, C. E.; MacRenaris, K. W.; Waters, E. A.; Meade, T. J. Multimeric near IR-MR contrast agent for multimodal *in vivo* imaging. *J. Am. Chem. Soc.* **2015**, *137*, 9108-9116; f) Amoroso, A. J.; Pope, S. J. A. Using lanthanide ions in molecular bioimaging. *Chem. Soc. Rev.* **2015**, *44*, 4723-4742; g) Zech, S. G.; Eldredge, H. B.; Lowe, M. P.; Caravan, P. Protein binding to lanthanide(III) complexes can reduce the water exchange rate at the lanthanide. *Inorg. Chem.* **2007**,

46, 3576-3584; h) Giardiello, M.; Botta, M.; Lowe, M. P. Synthesis of lanthanide(III) complexes appended with a diphenylphosphinamide and their interaction with human serum albumin. *J. Incl. Phenom. Macrocycl. Chem.* **2011**, *71*, 435-444; i) Perry, H. L.; Botnar, R. M.; Wilton-Ely, J. D. E. T. Gold nanomaterials functionalised with gadolinium chelates and their application in multimodal imaging and therapy. *Chem. Commun.* **2020**, *56*, 4037–4046.

3. a) Livramento, J. B.; Tóth, É.; Sour, A.; Borel, A.; Merbach, A. E.; Ruloff, R. High relaxivity confined to a small molecular space: a metallostar-based, potential MRI contrast agent. *Angew. Chem. Int. Ed.* **2005**, *44*, 1480-1484; b) Livramento, J. B.; Sour, A.; Borel, A.; Merbach, A. E.; Tóth, É. A starburst-shaped heterometallic compound incorporating six densely packed Gd^{3+} ions. *Chem. Eur. J.* **2006**, *12*, 989-1003; c) Livramento, J. B.; Weidensteiner, C.; Prata, M. I. M.; Allegrini, P. R.; Geraldes, C. F. G. C.; Helm, L.; Kneuer, R.; Merbach, A. E.; Santos, A. C.; Schmidt, P.; Tóth, É. First *in vivo* MRI assessment of a self-assembled metallostar compound endowed with a remarkable high field relaxivity. *Contrast Media Mol. Imaging* **2006**, *1*, 30-39; d) Costa, J.; Balogh, E.; Turcry, V.; Tripier, R.; Le Baccon, M.; Chuburu, F.; Handel, H.; Helm, L.; Tóth, É.; Merbach, A. E. Unexpected aggregation of neutral, xylene-cored dinuclear Gd^{III} chelates in aqueous solution. *Chem. Eur. J.* **2006**, *12*, 6841-6851; e) Livramento, J. B.; Helm, L.; Sour, A.; O'Neil, C.; Merbach, A. E.; Tóth, É. A benzene-core trinuclear GdIII complex: towards the optimization of relaxivity for MRI contrast agent applications at high magnetic field. *Dalton Trans.* **2008**, *9*, 1195-1202; f) Tóth, É.; Vauthey, S.; Pubanz, D.; Merbach, A. E. Water exchange and rotational dynamics of the dimeric gadolinium(III) complex $[BO\{Gd(DO3A)(H_2O)\}_2]$: a variable-temperature and -pressure ^{17}O NMR study. *Inorg. Chem.* **1996**, *35*, 3375-3379; g) Sour, A.; Jenni, S.; Ortí-Suárez, A.; Schmitt, J.; Heitz, V.; Bolze, F.; Loureiro de Sousa, P.; Po, C.; Bonnet, C. S.; Pallier, A.; Tóth, E.; Ventura, B. Four gadolinium(III) complexes appended to a porphyrin: a water-soluble molecular theranostic agent with remarkable relaxivity suited for MRI tracking of the photosensitizer. *Inorg. Chem.* **2016**, *55*, 4545-4554; h) Schmitt, J.; Jenni, S.; Sour, A.; Heitz, V.; Bolze, F.; Pallier, A.; Bonnet, C. S.; Tóth, É.; Ventura, B. A porphyrin dimer–GdDOTA conjugate as a theranostic agent for one- and two-photon photodynamic therapy and MRI. *Bioconjugate Chem.* **2018**, *29*, 3726-3738; i) Schuhle, D. T.; Polasek, M.; Lukes, I.; Chauvin, T.; Tóth, É.; Schatz, J.; Hanefeld, U.;

Stuart, M. C. A.; Peters, J. A. Densely packed Gd(III)-chelates with fast water exchange on a calix[4]arene scaffold: a potential MRI contrast agent. *Dalton Trans.* **2010**, *39*, 185-191; j) Henig, J.; Tóth, É.; Engelmann, J.; Gottschalk, S.; Mayer, H. A. Macrocyclic Gd^{3+} chelates attached to a silsesquioxane core as potential magnetic resonance imaging contrast agents: synthesis, physicochemical characterization, and stability studies. *Inorg. Chem.* **2010**, *49*, 6124-6138.

4. a) Powell, D. H.; Dhubhghaill, O. M. N.; Pubanz, D.; Helm, L.; Lebedev, Y. S.; Schlaepfer, W.; Merbach, A. E. Structural and dynamic parameters obtained from ^{17}O NMR, EPR, and NMRD studies of monomeric and dimeric Gd^{3+} complexes of interest in magnetic resonance imaging: an integrated and theoretically self-consistent approach. *J. Am. Chem. Soc.* **1996**, *118*, 9333-9346; b) Costa, J.; Ruloff, R.; Burai, L.; Helm, L.; Merbach, A. E. Rigid $M^{II}L_2Gd_2^{III}$ (M = Fe, Ru) complexes of a terpyridine-based heteroditopic chelate: a class of candidates for MRI contrast agents *J. Am. Chem. Soc.* **2005**, *127*, 5147-5157; c) Moriggi, L.; Aebischer, A.; Cannizzo, C.; Sour, A.; Borel, A.; Bunzli, J.-C. G.; Helm, L. A ruthenium-based metallostar: synthesis, sensitized luminescence and ^{1}H relaxivity. *Dalton Trans.* **2009**, *12*, 2088-2095; d) Mieville, P.; Jaccard, H.; Reviriego, F.; Tripier, R.; Helm, L. Synthesis, complexation and NMR relaxation properties of Gd^{3+} complexes of $Mes(DO3A)_3$. *Dalton Trans.* **2011**, *40*, 4260-4267; e) Mousavi, B.; Chauvin, A.-S.; Moriggi, L.; Helm, L. Carbazole as linker for dinuclear gadolinium-based MRI contrast agents. *Eur. J. Inorg. Chem.* **2017**, *45*, 5403-5412; f) Fontes, A.; Karimi, S.; Helm, L.; Yulikov, M.; Ferreira, P. M.; André, J. P. Dinuclear DOTA-based Gd^{III} chelates- revisiting a straightforward strategy for relaxivity improvement. *Eur. J. Inorg. Chem.* **2015**, *9*, 1579-1591.

5. a) Dehaen, G.; Verwilst, P.; Eliseeva, S. V.; Laurent, S.; Vander Elst, L.; Muller, R. N.; De Borggraeve, W. M.; Binnemans, K.; Parac-Vogt, T. N. A heterobimetallic ruthenium-gadolinium complex as a potential agent for bimodal imaging. *Inorg. Chem.* **2011**, *50*, 10005-10014; b) Dehaen, G.; Eliseeva, S. V.; Kimpe, K.; Laurent, S.; Vander Elst, L.; Muller, R. N.; Dehaen, W.; Binnemans, K.; Parac-Vogt, T. N. A self-assembled complex with a titanium(IV) catecholate core as a potential bimodal contrast agent. *Chem. Eur. J.* **2012**, *18*, 293-302; c) Debroye, E.; Dehaen, G.; Eliseeva, S. V.; Laurent, S.; Vander Elst, L.; Muller, R. N.; Binnemansa, K.; Parac-Vogt, T. N. A new metallostar complex based on an aluminum(III) 8-

hydroxyquinoline core as a potential bimodal contrast agent. *Dalton Trans.* **2012**, *41*, 10549-10556; d) Verwilst, P.; Eliseeva, S. V.; Vander Elst, L.; Burtea, C.; Laurent, S.; Petoud, S.; Muller, R. N.; Parac-Vogt, T. N.; De Borggraeve, W. M. A tripodal ruthenium-gadolinium metallostar as a potential $\alpha_v\beta_3$ integrin specific bimodal imaging contrast agent. *Inorg. Chem.* **2012**, *51*, 6405-6411; e) Dehaen, G.; Eliseeva, S. V.; Verwilst, P.; Laurent, S.; Vander Elst, L.; Muller, R. N.; De Borggraeve, W.; Binnemans, K.; Parac-Vogt, T. N. Tetranuclear d-f metallostars: synthesis, relaxometric, and luminescent properties. *Inorg. Chem.* **2012**, *51*, 8775-8783; f) Ceulemans, M.; Debroye, E.; Vander Elst, L.; De Borggraeve, W.; Parac-Vogt, T. N. Luminescence and relaxometric properties of heteropolymetallic metallostar complexes with selectively incorporated lanthanide(III) ions. *Eur. J. Inorg. Chem.* **2015**, *25*, 4207-4216; g) Debroye, E.; Parac-Vogt, T. N. Towards polymetallic lanthanide complexes as dual contrast agents for magnetic resonance and optical imaging. *Chem. Soc. Rev.* **2014**, *43*, 8178-8192.

6. a) Comblin, V.; Gilsoul, D.; Hermann, M.; Humblet, V.; Jacques, V.; Mesbahi, M.; Sauvage, C.; Desreux, J. F. Designing new MRI contrast agents: a coordination chemistry challenge. *Coord. Chem. Rev.* **1999**, *185-186*, 451-470; b) Paris, J.; Gameiro, C.; Humblet, V.; Mohapatra, P. K.; Jacques, V.; Desreux, J. F. Auto-assembling of ditopic macrocyclic lanthanide chelates with transition-metal ions. Rigid multimetallic high relaxivity contrast agents for magnetic resonance imaging. *Inorg. Chem.* **2006**, *45*, 5092-5102.

7. a) Lin, Y. H.; Leung, N. H.; Holt, K. B.; Thompson, A. L.; Wilton-Ely, J. D. E. T. Bimetallic complexes based on carboxylate and xanthate ligands: synthesis and electrochemical investigations. *Dalton Trans.* **2009**, *38*, 7891-7901; b) Oliver, K.; White, A. J. P.; Hogarth, G.; Wilton-Ely, J. D. E. T. Multimetallic complexes of group 10 and 11 metals based on polydentate dithiocarbamate ligands. *Dalton Trans.* **2011**, *40*, 5852-5864; c) Naeem, S.; Ribes, A.; White, A. J. P.; Haque, M. N.; Holt, K. B.; Wilton-Ely, J. D. E. T. Multimetallic complexes and functionalized nanoparticles based on oxygen- and nitrogen-donor combinations. *Inorg. Chem.* **2013**, *52*, 4700-4713; d) Robson, J. A.; Gonzàlez de Rivera, F.; Jantan, K. A.; Wenzel, M. N.; White, A. J. P.; Rossell, O.; Wilton-Ely, J. D. E. T. Bifunctional chalcogen linkers for the stepwise generation of multimetallic assemblies and functionalized nanoparticles. *Inorg. Chem.* **2016**, *55*, 12982-12996; e) Toscani, A.; Jantan, K. A.; Hena, J. B.;

Robson, J. A.; Parmenter, E. J.; Fiorini, V.; White, A. J. P.; Stagni, S.; Wilton-Ely, J. D. E. T. The stepwise generation of multimetallic complexes based on a vinylbipyridine linkage and their photophysical properties. *Dalton Trans*. **2017**, *46*, 5558-5570.

8. a) Wilton-Ely, J. D. E. T.; Solanki, D.; Hogarth, G. Multifunctional dithiocarbamates as ligands towards the rational synthesis of polymetallic arrays: an example based on a piperazine-derived dithiocarbamate ligand. *Eur. J. Inorg. Chem.* **2005**, *20*, 4027-4030; b) Wilton-Ely, J. D. E. T.; Solanki, D.; Knight, E. R.; Holt, K. B.; Thompson, A. L.; Hogarth, G. Multimetallic assemblies using piperazine-based dithiocarbamate building blocks. *Inorg. Chem.* **2008**, *47*, 9642-9653; c) Knight, E. R.; Leung, N. H.; Thompson, A. L.; Hogarth, G.; Wilton-Ely, J. D. E. T. Multimetallic arrays: bi-, tri-, tetra-, and hexametallic complexes based on gold(I) and gold(III) and the surface functionalization of gold nanoparticles with transition metals. *Inorg. Chem.* **2009**, *48*, 3866-3874; d) Macgregor, M. J.; Hogarth, G.; Thompson, A. L.; Wilton-Ely, J. D. E. T. Multimetallic arrays: symmetrical and unsymmetrical bi-, tri-, and tetrametallic organometallic complexes of ruthenium(II) and osmium(II). *Organometallics* **2009**, *28*, 197-208; e) Hogarth, G. Rainford-Brent, E.-J. C.-R. C. R.; Kabir, S. E.; Richards, I.; Wilton-Ely, J. D. E. T.; Zhang, Q. Functionalised dithiocarbamate complexes: synthesis and molecular structures of 2-diethylaminoethyl and 3-dimethylaminopropyl dithiocarbamate complexes $[M\{S_2CN(CH_2CH_2NEt_2)_2\}_n]$ and $[M\{S_2CN(CH_2CH_2CH_2NMe_2)_2\}_n]$ (n = 2, M = Ni, Cu, Zn, Pd; n = 3, M = Co). *Inorg. Chim. Acta* **2009**, *362*, 2020-2026; f) Knight, E. R.; Cowley, A. R.; Hogarth, G.; Wilton-Ely, J. D. E. T. Bifunctional dithiocarbamates: a bridge between coordination chemistry and nanoscale materials. *Dalton Trans.* **2009**, *4*, 607-608; g) Knight, E. R.; Leung, N. H.; Lin, Y. H.; Cowley, A. R.; Watkin, D. J.; Thompson, A. L.; Hogarth, G.; Wilton-Ely, J. D. E. T. Multimetallic arrays: symmetrical bi-, tri- and tetrametallic complexes based on the group 10 metals and the functionalisation of gold nanoparticles with nickel-phosphine surface units. *Dalton Trans.* **2009**, *19*, 3688-3697; h) Hurtubise, V. L.; McArdle, J. M.; Naeem, S.; Toscani, A.; White, A. J. P.; Long, N. J.; Wilton-Ely, J. D. E. T. Multimetallic complexes and functionalized nanoparticles based on unsymmetrical dithiocarbamate ligands with allyl and propargyl functionality. *Inorg. Chem.* **2014**, *53*, 11740-11748; i) Toscani, A.; Heliövaara, E. K.; Hena, J. B.; White, A. J. P.;

Wilton-Ely, J. D. E. T. Multimetallic alkenyl complexes bearing macrocyclic dithiocarbamate ligands. *Organometallics* **2015**, *34*, 494-505.

9. Hogarth, G. Transition Metal Dithiocarbamates: 1978–2003. *Prog. Inorg. Chem.* **2005**, *53*, 71-561.

10. a) Coucouvanis, D. The chemistry of the dithioacid and 1,1-dithiolate complexes. *Prog. Inorg. Chem.* **1970**, *11*, 233-371; b) Coucouvanis, D. The chemistry of the dithioacid and 1, 1-dithiolate complexes, 1968–1977. *Prog. Inorg. Chem.* **1979**, *26*, 301-469.

11. Sung, S.; Holmes, H.; Wainwright, L.; Toscani, A.; Stasiuk, G. J.; White, A. J. P.; Bell, J. D.; Wilton-Ely, J. D. E. T. Multimetallic complexes and functionalized gold nanoparticles based on a combination of d- and f-elements. *Inorg. Chem.* **2014**, *53*, 1989-2005.

12. Stasiuk, G. J.; Long, N. J. The ubiquitous DOTA and its derivatives: the impact of 1,4,7,10-tetraazacyclododecane-1,4,7,10-tetraacetic acid on biomedical imaging. *Chem. Commun.* **2013**, *49*, 2732-2746.

13. Chabloz, N. G.; Wenzel, M. N.; Perry, H. L.; Yoon, I.-C.; Molisso, S.; Stasiuk, G. J.; Elson, D. S.; Cass, A. E. G.; Wilton-Ely, J. D. E. T. Polyfunctionalized nanoparticles bearing robust gadolinium surface units for high relaxivity performance in MRI. *Chem. Eur. J.* **2019**, *25*, 10895-10906.

14. Chabloz, N. G.; Perry, H. L.; Yoon, I.-C.; Coulson, A. J.; White, A. J. P.; Stasiuk, G. J.; Botnar, R. M.; Wilton-Ely, J. D. E. T. Combined magnetic resonance imaging and photodynamic therapy using polyfunctionalized nanoparticles bearing robust gadolinium surface units, *Chem. Eur. J.* **2020**, *26*, 4552–4566.

15 a) Koullourou, T.; Natrajan, L.; Bhavsar, H.; Pope, S. J. A.; Feng, J.; Kauppinen, R.; Narvainen, J.; Shaw, R.; Scales, E.; Kenwright, A.; Faulkner, S. Synthesis and spectroscopic properties of a prototype single molecule dual imaging agent comprising a heterobimetallic rhenium−gadolinium complex. *J. Am. Chem. Soc.* **2008**, *130*, 2178-2179; b) Sørensen, T. J.; Faulkner, S. Multimetallic lanthanide complexes: Using kinetic control to define complex multimetallic arrays. *Acc. Chem. Res.* **2018**, *51*, 2493−2501.

16. Ou, M.; Chen, Y.; Chang, Y.; Lu, W.; Liu , G.; Wang, Y. Synthesis, complexation and water exchange properties of Gd(III)–TTDA-mono and bis(amide) derivatives and their binding affinity to human serum albumin. *Dalton Trans.* **2007**, *26*, 2749-2759.

17. a) Marradi, M.; Alcántara, D.; Martínez de la Fuente, J.; García-Martín, M. L.; Cerdán S.; Penadés, S. Paramagnetic Gd-based gold glyconanoparticles as probes for MRI: tuning relaxivities with sugars. *Chem. Commun.* **2009**, *26*, 3922–3924; b) Nithyakumar, A.; Alexander, V. Tri- and tetranuclear Ru^{II}-Gd^{III}_2 and Ru^{II}-Gd^{III}_3 d-f heterometallic complexes as potential bimodal imaging probes for MRI and optical imaging. *New J. Chem*. **2016**, *40*, 4606-4614; c) Eggenspiller, A.; Michelin, C.; Desbois, N.; Richard, P.; Barbe, J.-M.; Denat, F.; Licona, C.; Gaiddon, C.; Sayeh, A.; Choquet, P.; Gros, C. P. Design of porphyrin-dota-like scaffolds as all-in-one multimodal heterometallic complexes for medical imaging. *Eur. J. Org. Chem.* **2013**, *29*, 6629-6643.

18. Moriggi, L.; Cannizzo, C.; Dumas, E.; Mayer, C. R.; Ulianov, A.; Helm, L. Gold nanoparticles functionalized with gadolinium chelates as high-relaxivity MRI contrast agents. *J. Am. Chem. Soc.* **2009**, *131*, 10828-10829.

19. Evans, D. F. The determination of the paramagnetic susceptibility of substances in solution by nuclear magnetic resonance. *J. Chem. Soc.* **1959**, *0*, 2003-2005.

20. Zhou, Z.; Lu, Z. Gadolinium-based contrast agents for magnetic resonance cancer imaging. *Wiley Interdiscip. Rev. Nanomed. Nanobiotechnol.* **2013**, *5*, 1-18.

21. Tóth, É.; Helm, L.; Merbach, A. *The Chemistry of Contrast Agents in Medical Magnetic Resonance Imaging*, 2 ed., John Wiley & Sons, **2013**.

22. Laurent, S.; Vander Elst, L.; Copoix, F.; Muller, R. N. Stability of MRI paramagnetic contrast media: a proton relaxometric protocol for transmetallation assessment. *Invest. Radiol.* **2001**, *36*, 115-122.

23. Florès, O.; Velic, D.; Mabrouk, N.; Bettaïeb, A.; Tomasoni, C.; Robert, J.-M.; Paul, C.; Goze, C.; Roussakis, C.; Bodio, E. Rapid synthesis and antiproliferative properties of polyazamacrocycle-based bi- and tetra-gold(I) phosphine dithiocarbamate complexes. *ChemBioChem* **2019**, *20*, 2255-2261.

24. Stasiuk, G. J.; Minuzzi, F.; Sae-Heng, M.; Rivas, C.; Juretschke, H.-P.; Piemonti, L.; Allegrini, P. R.; Laurent, D.; Duckworth, A. R.; Beeby, A.; Rutter, G. A.; Long, N. J.

Dual-modal magnetic resonance/ fluorescent zinc probes for pancreatic β-cell mass imaging. *Chem. Eur. J.* **2015**, *21*, 5023-5033.

25. Rivas, C.; Stasiuk, G. J.; Gallo, J.; Minuzzi, F.; Rutter, G. A.; Long, N. J. Lanthanide(III) complexes of rhodamine-DO3A conjugates as agents for dual-modal imaging. *Inorg. Chem.* **2013**, *52*, 14284-14293.

For ToC use:

Metallostar assemblies based on dithiocarbamates for use as MRI contrast agents

Hannah L. Perry, Il-Chul Yoon, Nicolas G. Chabloz, Susannah Molisso, Graeme J. Stasiuk, René M. Botnar and James D. E. T. Wilton-Ely*

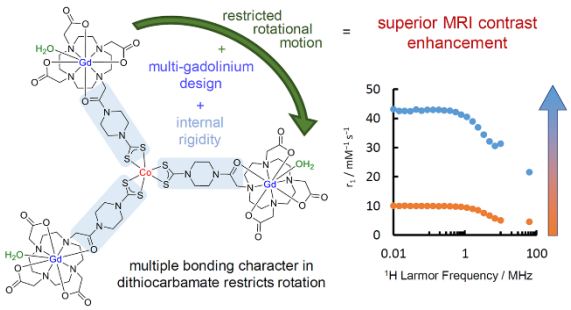

[75 words]

Two different octadentate gadolinium chelates (hydration number, q = 1) have been used to prepare a series of multimetallic d-f mixed-metal complexes for use as MRI contrast agents. The piperazenyl dithiocarbamate linker ensures that rotation of the gadolinium chelates is restricted, leading to enhanced relaxivity (r_1) values, which increase with overall mass and the number of gadolinium units. The versatility of dithiocarbamate coordination chemistry provides access to a wide array of other potential d-f hybrids.

Keywords: Gadolinium, dithiocarbamate, Imaging, MRI, metallostar

Supporting Information

Metallostar assemblies based on dithiocarbamates for use as MRI contrast agents

Hannah L. Perry,[a,b,+] Il-Chul Yoon,[a+] Nicolas G. Chabloz,[a] Susannah Molisso,[a] Graeme J. Stasiuk,[b] René M. Botnar[b] and James D. E. T. Wilton-Ely*,[a]

[a] *Department of Chemistry, Imperial College London, Molecular Sciences Research Hub, White City Campus, London, W12 0BZ, UK.*
[b] *School of Biomedical Engineering and Imaging Sciences, King's College London, St Thomas' Hospital, London, SE1 7EH, UK.*
+ These authors contributed equally

E-mail: j.wilton-ely@imperial.ac.uk

S1. General considerations

All chemicals and solvents were purchased from Alfa-Aesar, Sigma-Aldrich and VWR and were used without further purification, unless otherwise indicated. The compounds **[DO3A-NH$_2$]**O_2CCF_3,[1] K**[La-DO3A-DTC]**[1] and K_2**[Gd-DOTAGA-DTC]**[2] were prepared as described previously. All experiments and manipulations of compounds were conducted in

air, unless otherwise specified. Solvent mixtures are volume/volume mixtures. A Waters LCT Premier ES-ToF (ESI) spectrometer and a Waters Micromass MALDI-ToF spectrometer were used to collect all mass spectra. Standard FTIR spectra were measured using a Perkin Elmer Spectrum GX spectrometer and an Agilent Technologies Cary 630 spectrometer, both fitted with an attenuated total reflection (ATR) accessory. Fluorescence measurements in solution were carried out using a HORIBA Scientific Fluoromax-4P spectrofluorimeter (University of Hull). NMR spectroscopy was performed at 25 °C using a Bruker AV400 or 500MHz spectrometers at room temperature in D_2O unless otherwise stated. ^{1}H NMR and ^{13}C NMR chemical shifts (δ) were referenced to the residual non-deuterated solvent signal and the ^{13}C signal of the deuterated solvent respectively. The deuterated solvents were all purchased from Sigma Aldrich. NMRD profiles were recorded using a SMARTracer 0.25 T (0.01-10 MHz) bench-top fast field cycling NMR relaxometer (King's College London - Imperial College London CDT in Smart Medical Imaging). MRI was performed at St. Thomas' Hospital London (King's College London) at 25 °C on a clinical 1.5 T MRI Scanner (Philips Ingenia, Philips Medical Systems) using a modified Look-Locker imaging (MOLLI) T_1 sequence.

S2. Experimental Section

Preparation of [La-DO3A-NH$_2$]O_2CCF_3

[DO3A-NH$_2$]O_2CCF_3, prepared as described previously[1] (0.70 g, 1.19 mmol) and $LaCl_3 \cdot 7H_2O$ (0.55 g, 1.48 mmol) were dissolved in water (25 mL). The pH was adjusted to pH 5.6 with 1M NaOH. The solution was then stirred at room temperature for 1 h before increasing the temperature to 50 °C and stirring for a further 48 h. The solution was cooled to room temperature before adjusting to pH 10.9. The mixture was then stirred for 40 min to allow any $La(OH)_3$ to precipitate from solution. The mixture was placed in a centrifuge and the supernatant was collected. The pH was adjusted to pH 6.5 and xylenol orange was used to confirm the absence of free La^{3+}. The solvent was removed under reduced pressure to yield the product as a hygroscopic white powder. Yield: 800 mg (91%). IR: 3418 [ν(O-H)], 1673 [ν(C=N)], 1599 [ν(C=O)], 1435 [ν(C-N)], 1204, 1174, 1122 [ν(C-O)] cm^{-1}. ^{1}H NMR (400 MHz, D_2O) δ 2.31-4.03 (m(br), 34H, NCH_2) ppm. $^{13}C\{^{1}H\}$ NMR (101 MHz, D_2O) δ 179.6,

179.5, 179.4 (s x 3, $CH_2\underline{C}O$), 172.0 (s, NCO), 162.9 (q, $O\underline{C}CF_3$, J_{FC} = 35.4 Hz), 116.4 (q, CF_3, J_{FC} = 293.0 Hz), 60.5, 60.4, 60.3 (s x 3, $\underline{C}H_2CO_2$), 57.0 (s, $\underline{C}H_2CO_2$), 53.1, 49.3 (s(br) x 2, C_4H_8), 46.4, 44.2, 43.9, 43.5, 30.3, 30.2, 30.1, 29.9 (s x 8, NCH_2CH_2N) ppm. MS (ES +ve) *m/z* (abundance %): 609 (100) $[M - H_2O]^+$.

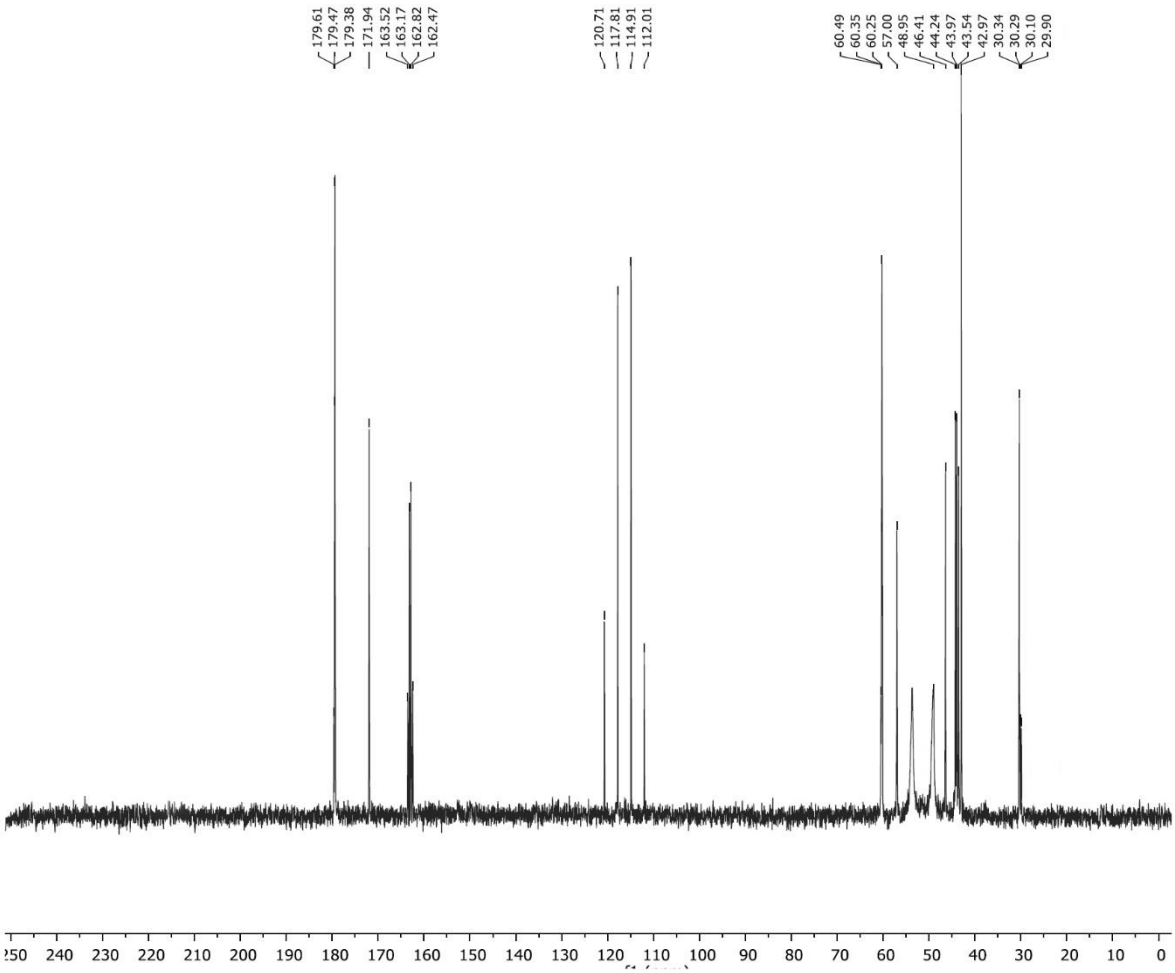

Figure S2-1. $^{13}C\{^1H\}$ NMR spectrum of **[La-DO3A-NH_2](O_2CCF_3)** in D_2O.

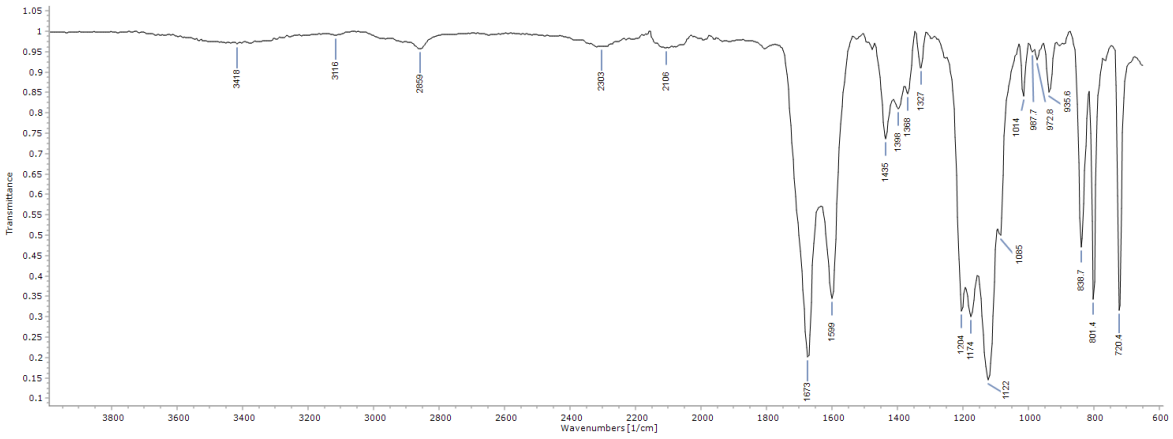

Figure S2-2. Solid-state infrared spectrum of **[La-DO3A-NH$_2$](O$_2$CCF$_3$)**.

Preparation of K**[La-DO3A-DTC**]

[La-DO3A-NH$_2$]O$_2$CCF$_3$ (0.80 g, 1.08 mmol) and K$_2$CO$_3$ (1.23 g, 8.90 mmol) were dissolved in a 1:3 mixture of methanol and water (20 mL) and stirred for 1 h. CS$_2$ (80 µL, 1.32 mmol) was added and the solution was stirred at room temperature for a further hour. The reaction mixture was then filtered through Celite and the pale-yellow solution was collected. The solvent was removed under reduced pressure to yield a pale yellowish solid. Yield: 730 mg (91%). IR (solid state): 3496 [ν(O-H)], 1670 [ν(C=N)], 1643 [ν(C=O)], 1424 [ν(C-N)], 1204, 1178, 1129 [ν(C-O)], 1003 [ν(C-S)] cm^{-1}. ^{1}H NMR (400 MHz, D$_2$O) δ 2.06-4.00 (m(br), 32H, CH$_2$) ppm; ^{13}C{^{1}H} NMR (126 MHz, D$_2$O) δ 233.6 (s, CS$_2$), 179.6 (s, NCO), 163.1 (s, CH$_2$CO), 60.7, 60.3 (s x 2, CH$_2$CO$_2$), 53.8 (s(br), NC$_4$H$_8$N), 51.7, 51.3, (s x 2, NCH$_2$CH$_2$N), 50.2 (s(br), NC$_4$H$_8$N), 48.9, 44.3, 43.6, 27.1 (s x 4, NCH$_2$CH$_2$N) ppm. MS (ES −ve) *m/z* (abundance %): 683 (100) [M − H$_2$O]$^-$.

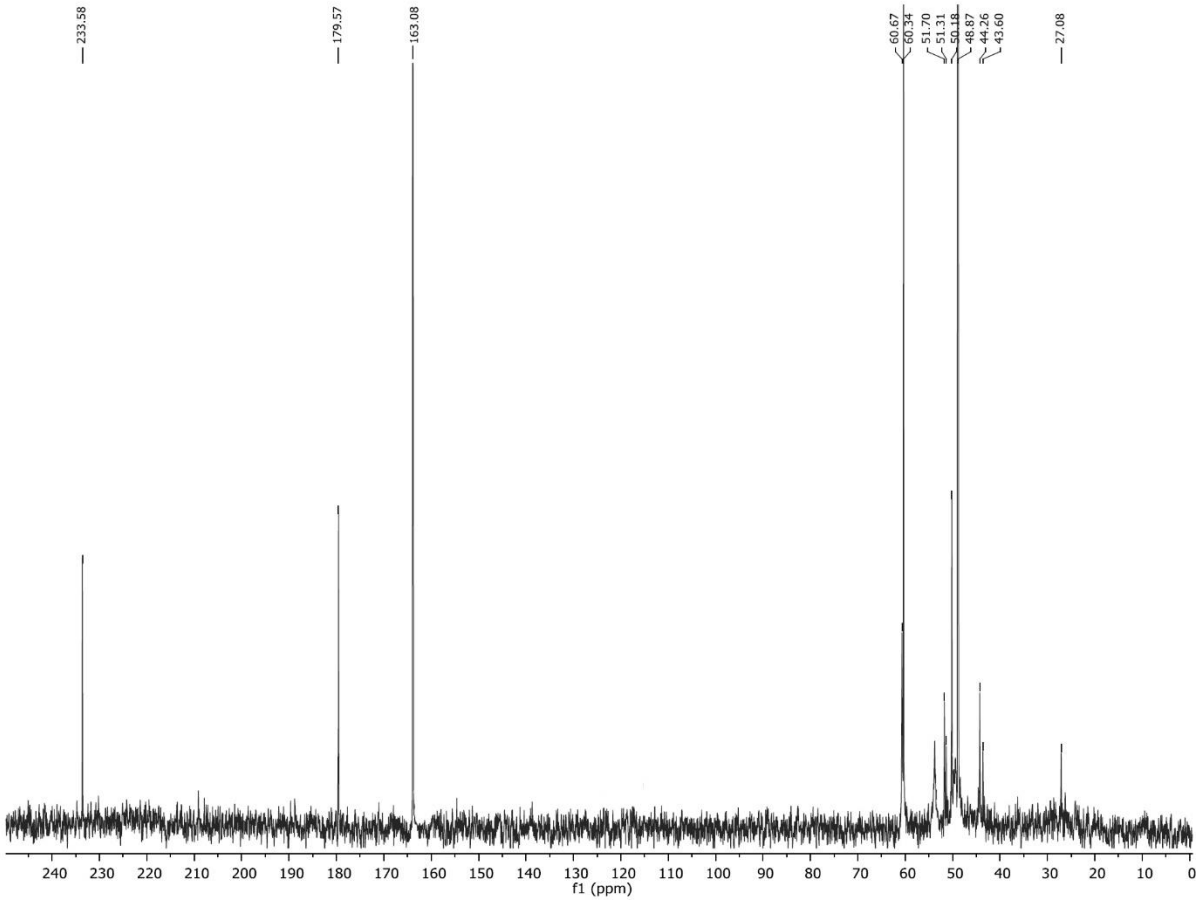

Figure S2-3. $^{13}C\{^{1}H\}$ NMR spectrum of K**[La-DO3A-DTC]** in D_2O.

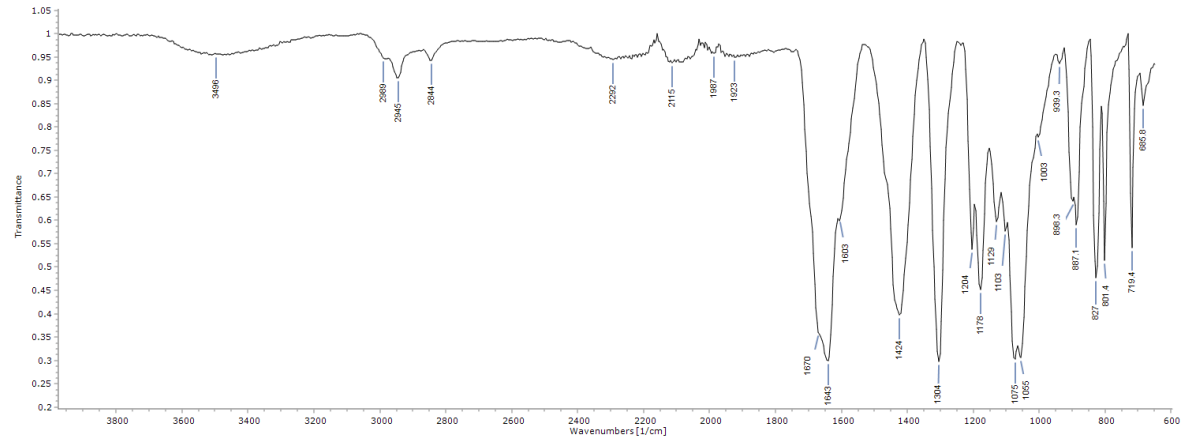

Figure S2-4. Solid-state infrared spectrum of K**[La-DO3A-DTC]**.

Preparation of [La-DO3A-DTC-AuPPh$_3$]

[AuCl(PPh$_3$)] (99 mg, 0.20 mmol) was dissolved in a 1:3 mixture of acetone and water (10 mL) and K[**La-DO3A-DTC**] (0.15 g, 0.20 mmol) was added, causing the precipitation of a colorless salt. The solution was stirred in the dark, at room temperature for 1 h and the precipitate was filtered through Celite. The solvent was removed under reduced pressure to afford the product as an off-white powder. Yield: 195 mg (84%). IR (solid state): 3420 [ν(O-H)], 2851 [aromatic ν(C-H)], 1673 [ν(C=N)], 1599 [ν(C=O)], 1430 [ν(C-N)], 1204, 1174, 1120 [ν(C-O)], 999 [ν(C-S)] cm^{-1}. ^{1}H NMR (400 MHz, DMSO-d_6) δ 7.47-7.64 (m, 15H), 1.90-4.05 (m(br), 32H) ppm. ^{13}C{^{1}H} NMR (126 MHz, DMSO-d_6) δ 213.3 (s, CS_2), 173.9, 173.6 (s x 2, C=O), 133.8 (d, *o/m*-C_6H_5, J_{PC} = 13.7 Hz), 132.2 (s, *p*-C_6H_5), 129.6 (*o/m*-C_6H_5, J_{PC} = 11.4 Hz), 128.7 (*ipso*-C_6H_5, J_{PC} = 58.0 Hz), 62.5, 61.5 (s(br) x 2, $\underline{C}H_2CO_2$), 53.5 (s(br), NC_4H_8N), 49.2 (s(br), NCH_2CH_2N) ppm. ^{31}P{^{1}H} NMR (162 MHz, D_2O) δ 37.3 (s, PPh_3) ppm. MS (MALDI +ve) *m/z* (abundance %): 1142 (42) $[M - H_2O]^+$.

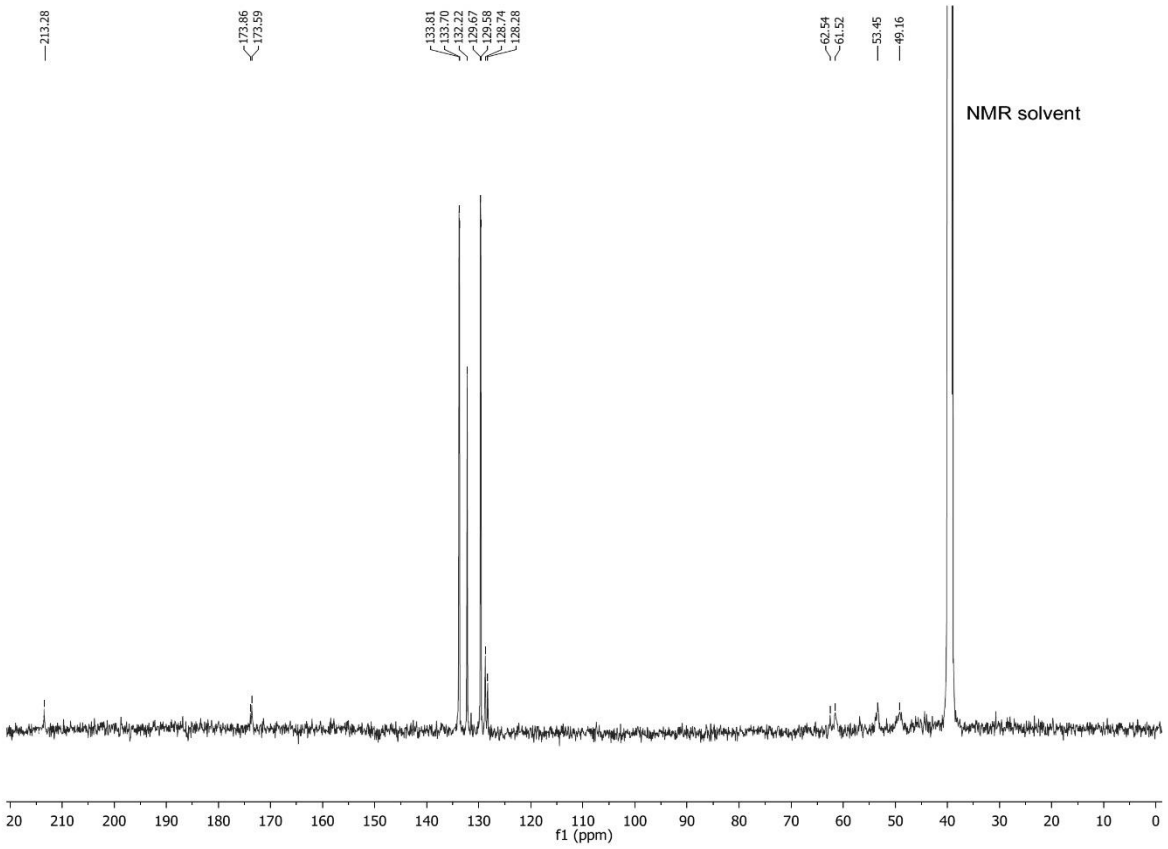

Figure S2-5. ^{13}C{^{1}H} NMR spectrum of **[La-DO3A-DTC-AuPPh$_3$]** in DMSO-d_6.

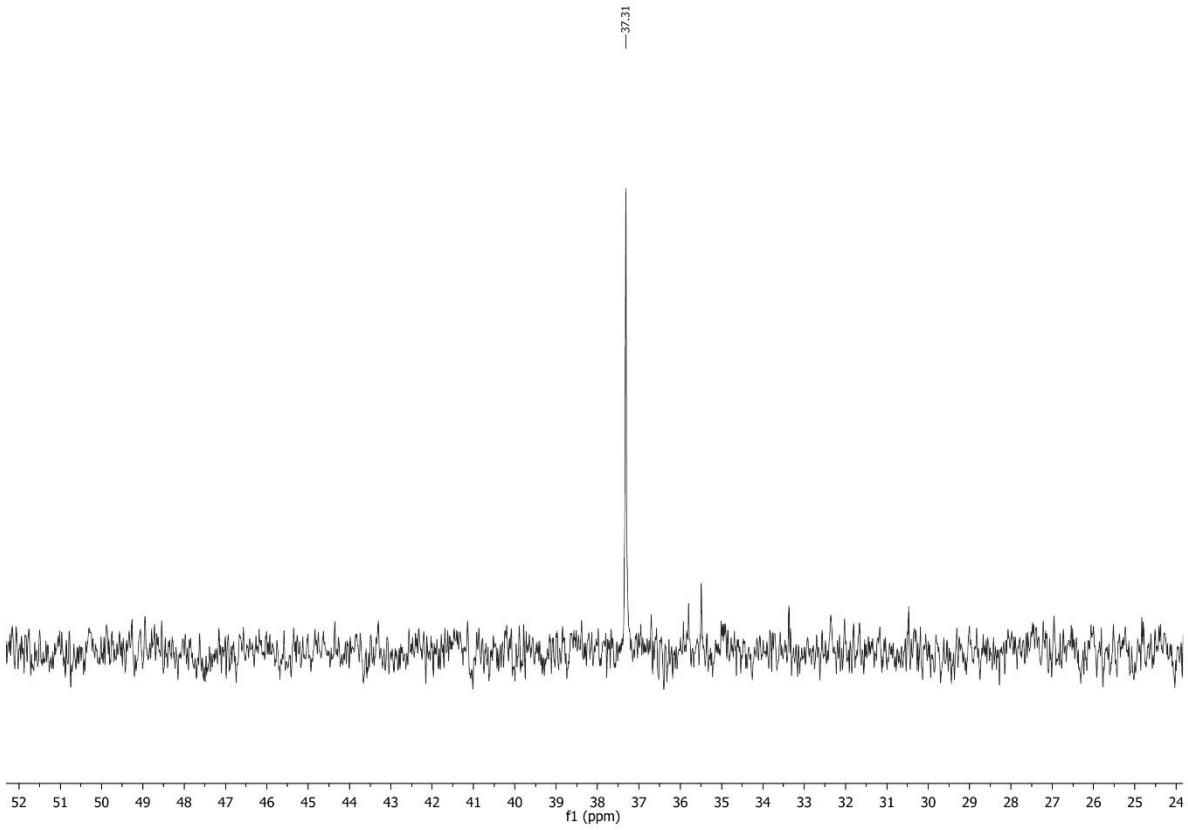

Figure S2-6. $^{31}P\{^{1}H\}$ NMR spectrum of **[La-DO3A-DTC-AuPPh$_3$]** in D_2O.

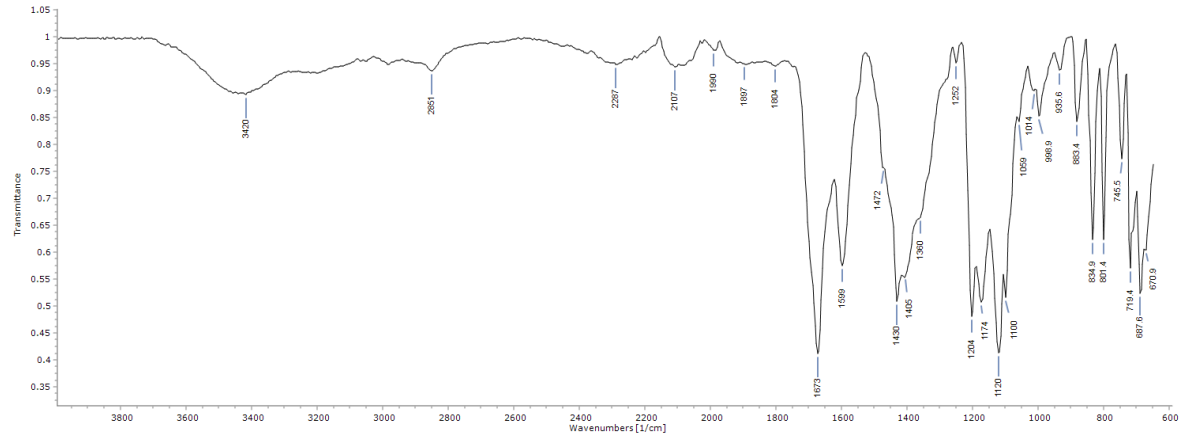

Figure S2-7. Solid-state infrared spectrum of **[La-DO3A-DTC-AuPPh$_3$]**.

Preparation of [Gd-DO3A-DTC-AuPPh$_3$]

[AuCl(PPh$_3$)] (99 mg, 0.20 mmol) was dissolved in a 1:3 mixture of acetone and water (10 mL) and K[**Gd-DO3A-DTC**], prepared as described previously,[1] (0.15 g, 0.20 mmol) was added, causing the precipitation of a colorless salt. The solution was stirred in the dark, at room temperature for 1 h and the precipitate was removed by filtration through Celite. The solvent was removed under reduced pressure to afford the product as an off-white powder. Yield: 205 mg (87%). IR (solid state): 3385 [ν(O-H)], 2918 [aromatic ν(C-H)], 1679 [ν(C=N)], 1603 [ν(C=O)], 1396 [ν(C-N)], 1203, 1176, 1126 [ν(C-O)], 994 [ν(C-S)] cm^{-1}. NMR data not obtained due to paramagnetic nature of Gd(III) center. MS (MALDI +ve) *m/z* (abundance %): 1179 (3) [M]$^+$, 935 (37) [M – PPh$_3$ + H$_2$O]$^+$.

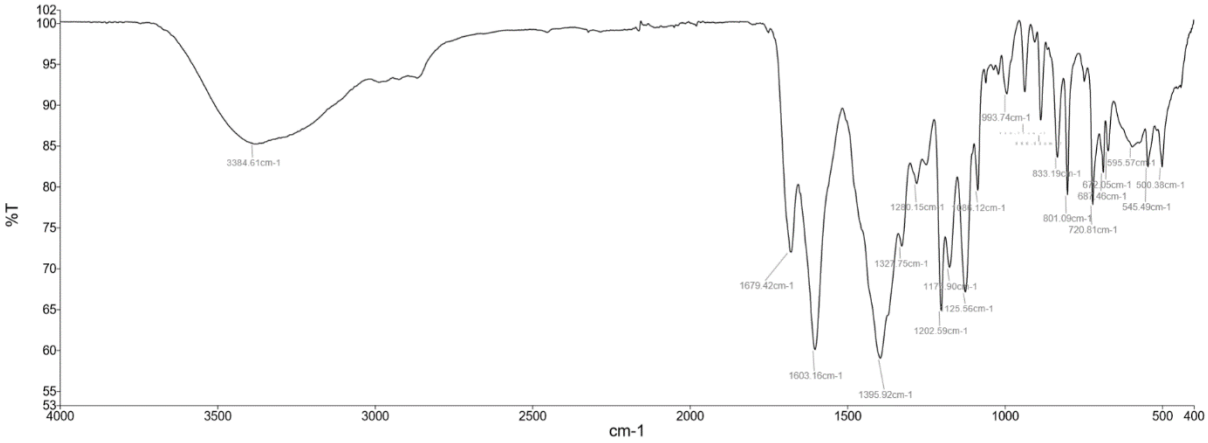

Figure S2-8. Solid-state infrared spectrum of **[Gd-DO3A-DTC-AuPPh$_3$]**.

Preparation of [Ni(La-DO3A-DTC)$_2$]

Ni(NO$_3$)$_2$·6H$_2$O (29 mg, 0.10 mmol) was dissolved in water (10 mL) to form a pale blue solution and K[**La-DO3A-DTC**] (150 mg, 0.20 mmol) was added, resulting in a color change to yellow. The solution was stirred at room temperature for 1 h before being filtered through Celite. The solvent was removed under reduced pressure to yield a pale green hygroscopic powder. Yield: 127 mg (87%). IR (solid state): 3408 [ν(O-H)], 1671 [ν(C=N)], 1599 [ν(C=O)], 1403 [ν(C-N)], 1200, 1174, 1119 [ν(C-O)], 1003 [ν(C-S)] cm^{-1}. ^{1}H NMR (400 MHz, D$_2$O) δ 1.92 - 3.94 (m(br), 64H) ppm. ^{13}C{^{1}H} NMR (126 MHz, D$_2$O) δ 214.1 (s, CS$_2$), 179.7, 171.7 (s x 2, C=O), 61.2, 58.5 (s(br) x 2, CH$_2$C=O), 54.0, (s(br), NC$_4$H$_8$N), 49.8, 45.9, 43.5 (s(br) x 3, NCH$_2$CH$_2$N) ppm. MS (MALDI +ve) *m/z* (abundance %): 1499 (22) [M + K]$^+$, 721 (74) [M – H$_2$O]$^{2+}$.

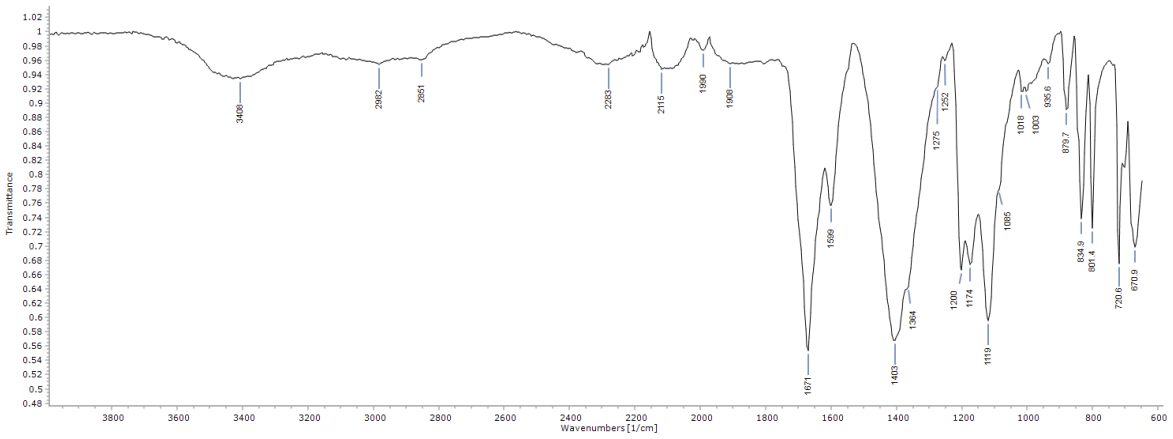

Figure S2-9. Solid-state infrared spectrum of **[Ni(La-DO3A-DTC)$_2$]**.

Preparation of [Ni(Gd-DO3A-DTC)$_2$]

$Ni(NO_3)_2 \cdot 6H_2O$ (29 mg, 0.10 mmol) was dissolved in water (10 mL) to form a pale blue solution and K[**Gd-DO3A-DTC**][1] (150 mg, 0.20 mmol) was added, resulting in a color change to cloudy yellow. The solution was stirred at room temperature for 1 h before being filtered through Celite. The solvent was removed under reduced pressure to yield the product as a pale green powder. Yield: 122 mg (81%). IR (solid state): 3356 [ν(O-H)], 1678 [ν(C=N)], 1606 [ν(C=O)], 1395 [ν(C-N)], 1203, 1175, 1123 [ν(C-O)], 993 [ν(C-S)] cm^{-1}. NMR data not obtained due to paramagnetic nature of Gd(III) center. MS (MALDI +ve) *m/z* (abundance %): 1521 (8) $[M + Na]^+$, 772 (36) $[M + 2Na]^{2+}$.

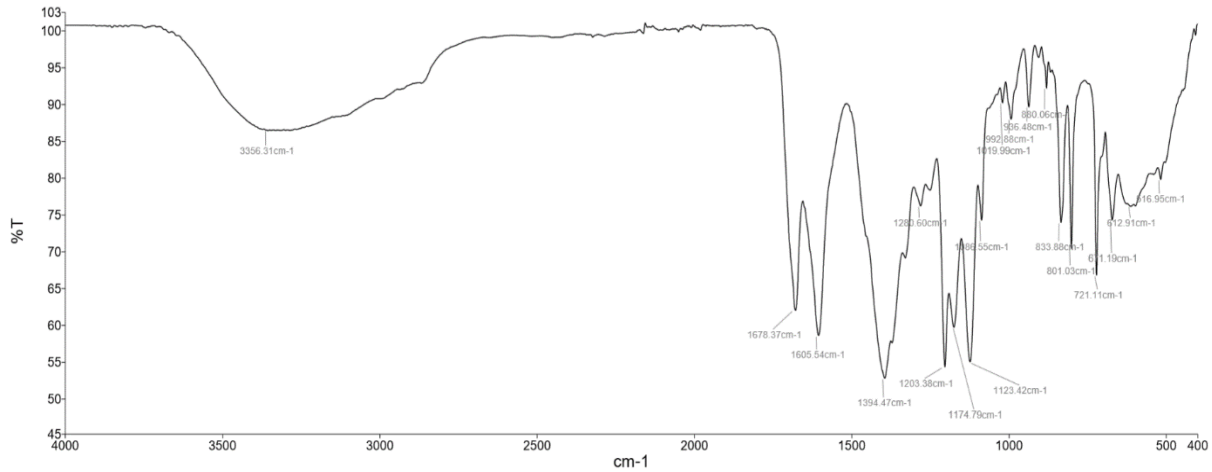

Figure S2-10. Solid-state infrared spectrum of **[Ni(Gd-DO3A-DTC)$_2$]**.

Preparation of [Co(La-DO3A-DTC)$_3$]

$CoCl_2 \cdot 6H_2O$ (17 mg, 0.07 mmol) was dissolved in water (10 mL) to form a pale pink solution and K[**La-DO3A-DTC**] (159 mg, 0.22 mmol) was added, resulting in color change to dark green. The solution was stirred at room temperature for 1 h before being filtered through Celite. The solvent was removed under reduced pressure to yield a dark green hygroscopic powder. Yield: 121 mg (78%). IR (solid state): 3440 [ν(O-H)], 1674 [ν(C=N)], 1599 [ν(C=O)], 1433 [ν(C-N)], 1200, 1174, 1121 [ν(C-O)], 1003 [ν(C-S)] cm^{-1}. ^1H NMR (400 MHz, D_2O) δ 2.20 - 4.20 (m(br), 96H) ppm. $^{13}C\{^1H\}$ NMR (126 MHz, D_2O) δ 210.4 (s, CS_2), 179.6, 172.1, 171.8 (s x 3, C=O), 61.4, 58.2 (s(br) x 2, $\underline{C}H_2C{=}O$), 54.5, (s(br), NC_4H_8N), 50.4, 46.0, 43.7 (s(br) x 3, NCH_2CH_2N) ppm. MS (MALDI +ve) *m/z* (abundance %): 2144 (4) $[M - H_2O]^+$, 1104 (34) $[M + 2Na]^{2+}$, 721 (48) $[M]^{3+}$.

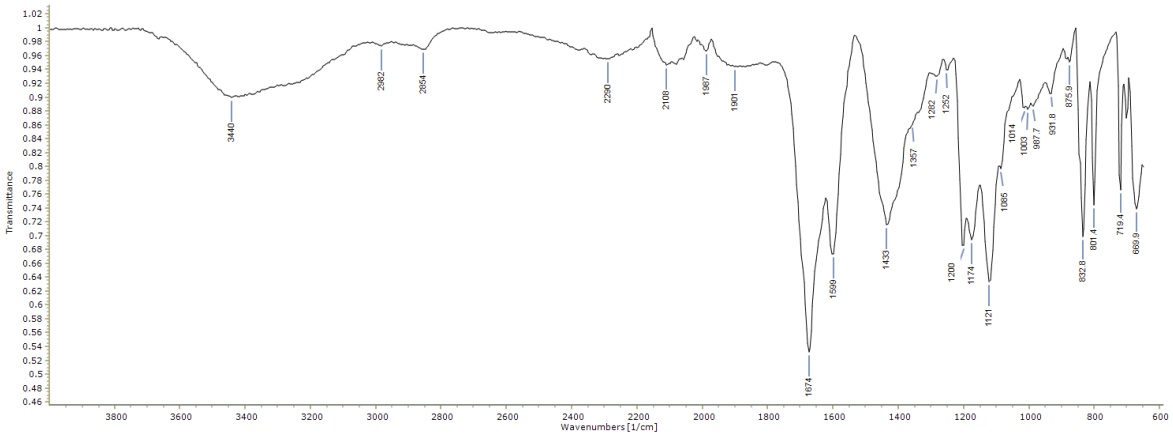

Figure S2-11. Solid-state infrared spectrum of **[Co(La-DO3A-DTC)$_3$]**.

Preparation of [Co(Gd-DO3A-DTC)$_3$]

$CoCl_2 \cdot 6H_2O$ (17 mg, 0.07 mmol) was dissolved in water (10 mL) to form a pale pink solution and K[**Gd-DO3A-DTC**][1] (163 mg, 0.22 mmol) was added, resulting in a color change to cloudy blue-green. The solution was stirred at room temperature for 1 h before being filtered through Celite. The solvent was removed under reduced pressure to yield a dark green hygroscopic powder. Yield: 120 mg (76%). IR (solid state): 3333 [ν(O-H)], 1678 [ν(C=N)], 1607 [ν(C=O)], 1397 [ν(C-N)], 1203, 1174, 1123 [ν(C-O)], 993 [ν(C-S)] cm^{-1}. NMR data not obtained due to paramagnetic nature of Gd(III) center. MS (MALDI +ve) *m/z* (abundance %): 763 (31) $[M + 3Na]^{3+}$.

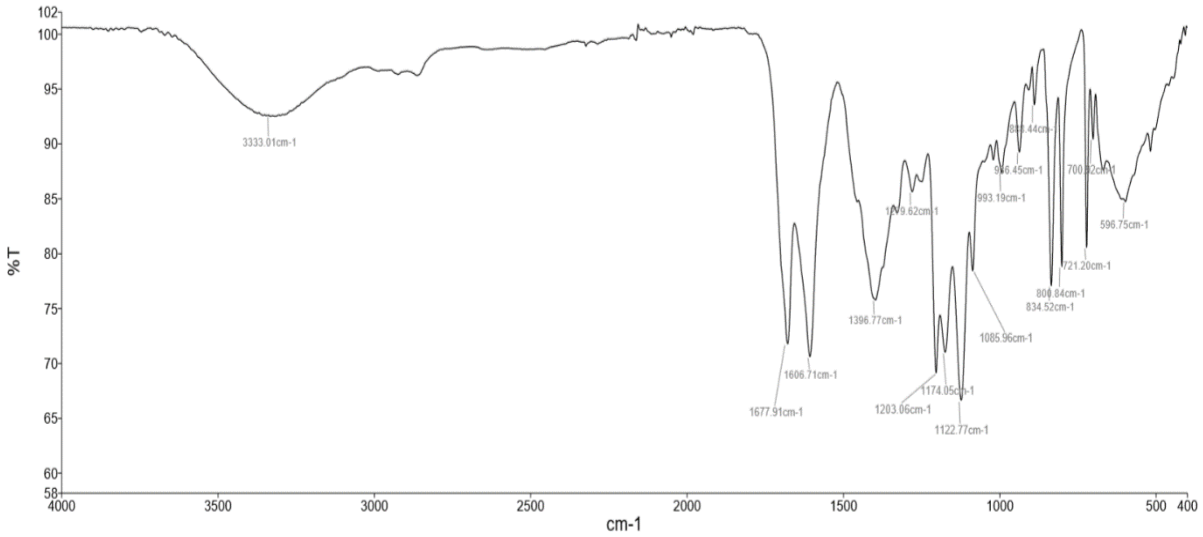

Figure S2-12. Solid-state infrared spectrum of **[Co(Gd-DO3A-DTC)$_3$]**.

Preparation of [Ru(La-DO3A-DTC)$_3$]

$RuCl_3 \cdot 3H_2O$ (17 mg, 0.07 mmol) was dissolved in water (10 mL) to form a black solution and K[**La-DO3A-DTC**] (150 mg, 0.20 mmol) was added, resulting in a color change to dark green. The solution was stirred at room temperature for 1 h before being filtered through Celite. The solvent was removed under reduced pressure to yield a dark green hygroscopic powder. Yield: 119 mg (77%). IR (solid state): 3406 [ν(O-H)], 1647 [ν(C=N)], 1625, 1593 [ν(C=O)], 1394, 1368 [ν(C-N)], 1282, 1204, 1122 [ν(C-O)], 1004 [ν(C-S)] cm^{-1}. NMR data not obtained due to paramagnetic nature of Ru(III) center. Magnetic moment was calculated using the Evans NMR method (μ_{eff} = 1.92 BM) and using a magnetic susceptibility balance (μ_{eff} = 1.92 – 2.10 BM). MS (MALDI +ve) *m/z* (abundance %): 2222 (31), $[M + H_2O]^+$, 735 (43) $[M]^{3+}$.

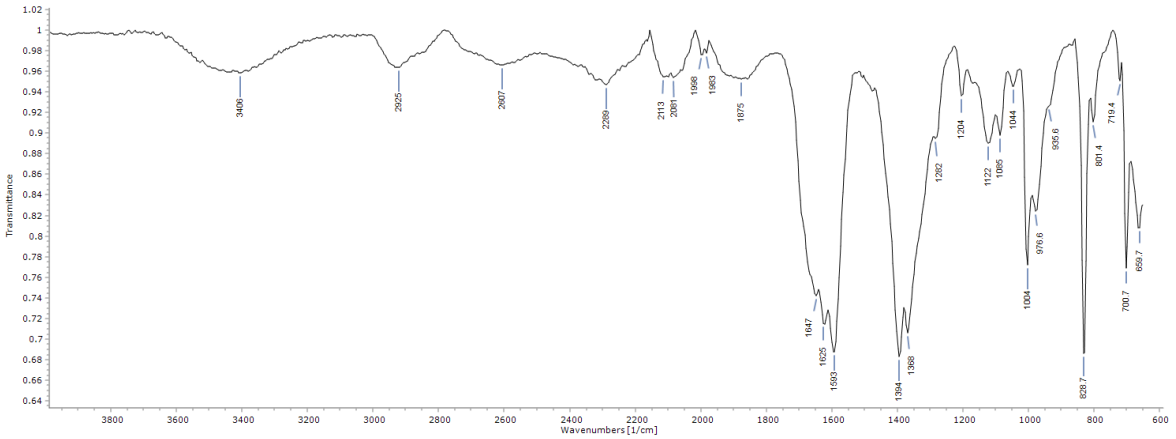

Figure S2-13. Solid-state infrared spectrum of **[Ru(La-DO3A-DTC)$_3$]**.

Preparation of [Ru(Gd-DO3A-DTC)$_3$]

$RuCl_3 \cdot 3H_2O$ (17 mg, 0.07 mmol) was dissolved in water to form a black solution and K[**Gd-DO3A-DTC**][1] (0.15 g, 0.20 mmol) was added, resulting in a color change to dark green. The solution was stirred at room temperature for 1 h before being filtered through Celite. The solvent was removed under reduced pressure to yield a dark green hygroscopic powder. Yield: 119 mg (81%). IR (solid state): 3441 [ν(O-H)], 1678 [ν(C=N)], 1606 [ν(C=O)], 1397 [ν(C-N)], 1204 [ν(C-O)], 993 [ν(C-S)] cm^{-1}. MS (MALDI +ve) *m/z* (abundance %): 2303 (10) $[M + MeCN]^+$, 1133 (73) $[M – H_2O + Na]^{2+}$.

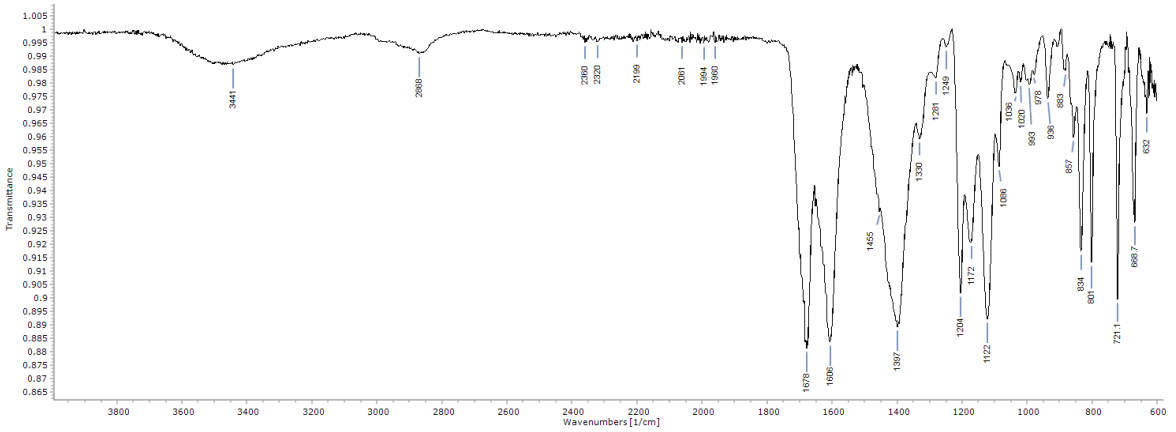

Figure S2-14. Solid-state infrared spectrum of **[Ru(Gd-DO3A-DTC)$_3$]**.

Preparation of K[Gd-DOTAGA-DTC-AuPPh$_3$]

[AuCl(PPh$_3$)] (99 mg, 0.20 mmol) was dissolved in a 1:3 mixture of acetone and water (10 mL) and K$_2$[**Gd-DOTAGA-DTC**]^2 (174 mg, 0.20 mmol) was added, causing the precipitation of a colorless salt. The solution was stirred in the dark, at room temperature for 1 h and the precipitate was removed by filtration through Celite. The solvent was removed under reduced pressure to afford the product as an off-white powder. Yield: 197 mg (76%). IR (solid state): 3379 [ν(O-H)], 2918 [aromatic ν(C-H)], 1680 [ν(C=N)], 1603 [ν(C=O)], 1392 [ν(C-N)], 1203, 1173, 1125 [ν(C-O)], 993 [ν(C-S)] cm^{-1}. NMR data not obtained due to paramagnetic nature of Gd(III) center. MS (MALDI −ve) *m/z* (abundance %): 1250 (50) [M]$^-$.

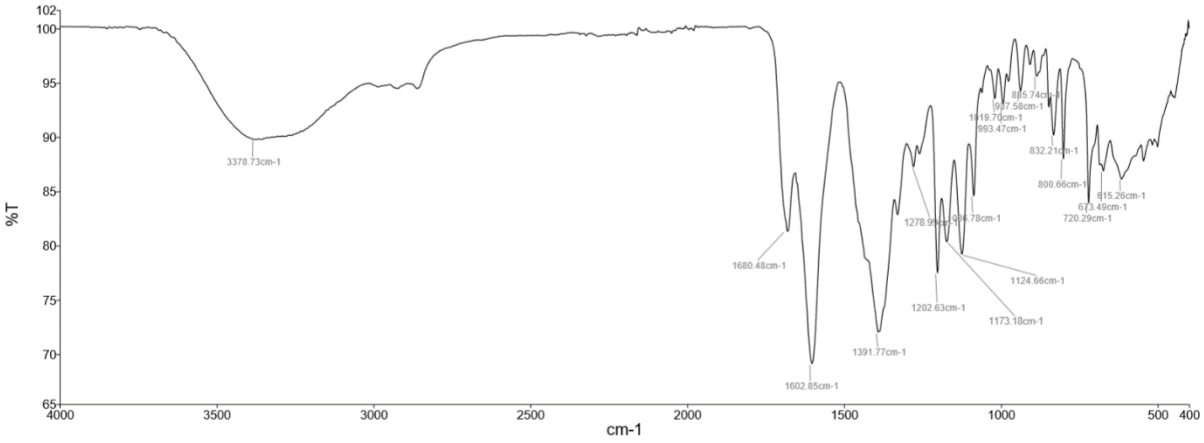

Figure S2-15. Solid-state infrared spectrum of **K[Gd-DOTAGA-DTC-AuPPh$_3$]**.

Preparation of K$_2$[Ni(Gd-DOTAGA-DTC)$_2$]

Ni(NO$_3$)$_2$·6H$_2$O (29 mg, 0.10 mmol) was dissolved in water (10 mL) to form a pale blue solution and K$_2$[**Gd-DOTAGA-DTC**]^2 (174 mg, 0.20 mmol) was added, resulting in a color change to cloudy yellow. The solution was stirred at room temperature for 1 h before being filtered through Celite. The solvent was removed under reduced pressure to yield the pale green hygroscopic product. Yield: 123 mg (72%). IR (solid state): 3240 [ν(O-H)], 1681 [ν(C=N)], 1606 [ν(C=O)], 1393 [ν(C-N)], 1203, 1174, 1125 [ν(C-O)], 994 [ν(C-S)] cm^{-1}. NMR data not obtained due to paramagnetic nature of Gd(III) center. MS (MALDI −ve) *m/z* (abundance %): 868 (100) [M + 2K + H$_2$O]$^{2-}$.

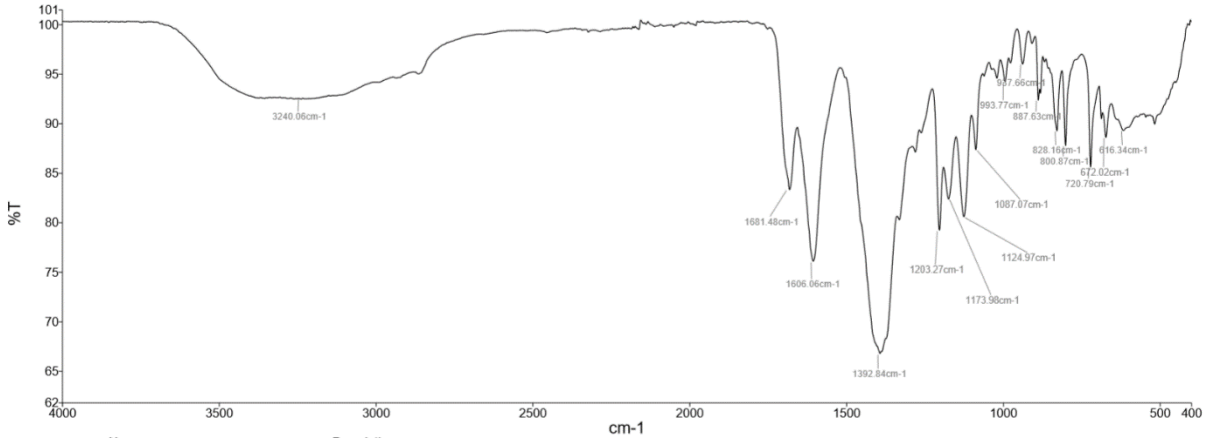

Figure S2-16. Solid-state infrared spectrum of K_2**[Ni(Gd-DOTAGA-DTC)$_2$]**.

Preparation of K_3[Co(Gd-DOTAGA-DTC)$_3$]

$CoCl_2 \cdot 6H_2O$ (17 mg, 0.07 mmol) was dissolved in water (10 mL) to form a pale pink solution and K_2[**Gd-DOTAGA-DTC**][2] (187 g, 0.22 mmol) were added, resulting in a color change to cloudy blue-green. The solution was stirred at room temperature for 1 h and filtered through Celite. The solvent was removed under reduced pressure to yield a dark green hygroscopic powder. Yield: 128 mg (70%). IR (solid state): 3375 [ν(O-H)], 1681 [ν(C=N)], 1606 [ν(C=O)], 1387 [ν(C-N)], 1203, 1174, 1124 [ν(C-O)], 994 [ν(C-S)] cm^{-1}. NMR data not obtained due to paramagnetic nature of Gd(III) center. MS (MALDI -ve) *m/z* (abundance %): 811 (40) $[M]^{3-}$.

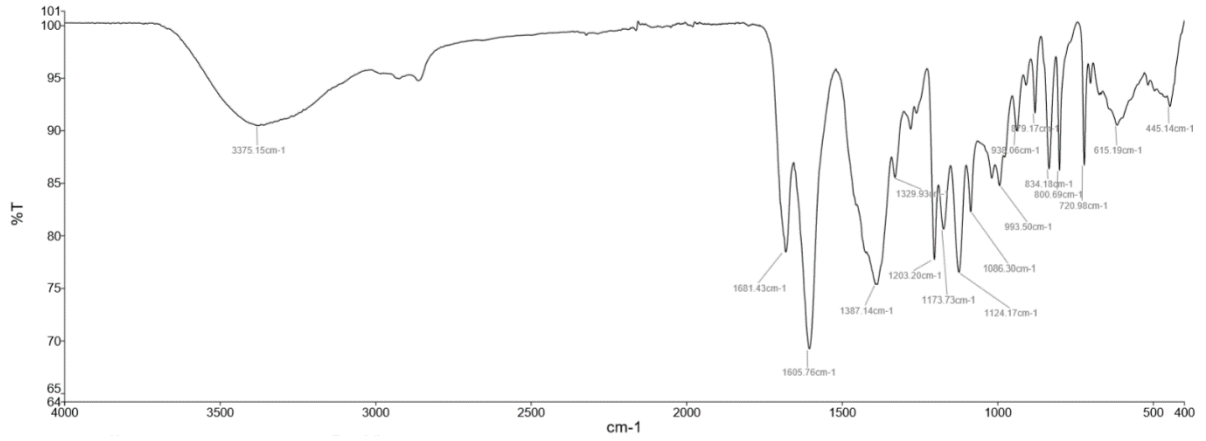

Figure S2-17. Solid-state infrared spectrum of K_3**[Co(Gd-DOTAGA-DTC)$_3$]**.

Preparation of K_3[Ru(Gd-DOTAGA-DTC)$_3$]

$RuCl_3 \cdot 3H_2O$ (17 mg, 0.07 mmol) was dissolved in water (10 mL) to form a black solution and K_2[**Gd-DOTAGA-DTC**][2] (0.17 g, 0.20 mmol) was added, resulting in a color change to dark green. The solution was stirred at room temperature for 1 h before being filtered through Celite. The solvent was removed under reduced pressure to yield a dark green hygroscopic powder. Yield: 119 mg (71%). IR (solid state): 3453 [ν(O-H)], 1678 [ν(C=N)], 1603 [ν(C=O)], 1391 [ν(C-N)], 1202, 1172, 1128 [ν(C-O)], 994 [ν(C-S)] cm^{-1}. NMR data not obtained due to paramagnetic nature of Gd(III) center. MS (MALDI -ve) *m/z* (abundance %): 1211 (22) $[M - 3H_2O]^{2-}$, 864 (41) $[M + 3K]^{3-}$.

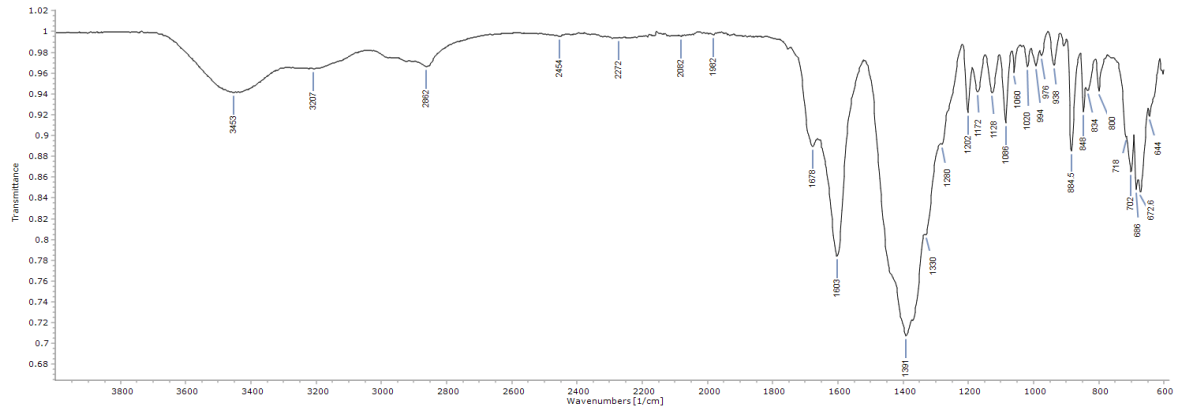

Figure S2-18. Solid-state infrared spectrum of **K_3[Ru(Gd-DOTAGA-DTC)$_3$]**.

Preparation of [Gd-DO3A-DTC-AuPPh$_2$C$_6$H$_4$COOH]

[AuCl(tht)][3] (59 mg, 0.18 mmol) was dissolved in dichloromethane (10 mL) and $PPh_2C_6H_4COOH$ (61 mg, 0.20 mmol) was added. After stirring for 15 min, the solvent volume was reduced to ca. 2 mL under vacuum and *n*-pentane added to afford [AuCl($PPh_2C_6H_4COOH$)] as a colorless solid, as reported previously.[4] Yield: 87 mg (88%). This solid was then dissolved in methanol (10 mL) before adding K[**Gd-DO3A-DTC**] (0.12 g, 0.16 mmol) and stirring at room temperature for 1 h. After evaporation of the solvent, the product was dissolved in dichloromethane and filtered through Celite. The solvent was then removed under reduced pressure to yield a pale yellow solid. Yield: 174 mg (88%). IR (solid state): 3355 [ν(O-H)], 2948 [aromatic ν(C-H)], 1681 [ν(C=N)], 1595 [ν(C=O)], 1394 [ν(C-

N)], 1182, 1137 [ν(C-O)], 999 [ν(C-S)] cm^{-1}. NMR data not obtained due to paramagnetic nature of Gd(III) center. MS (MALDI +ve) *m/z* (abundance %): 612 (5) $[M]^{2+}$.

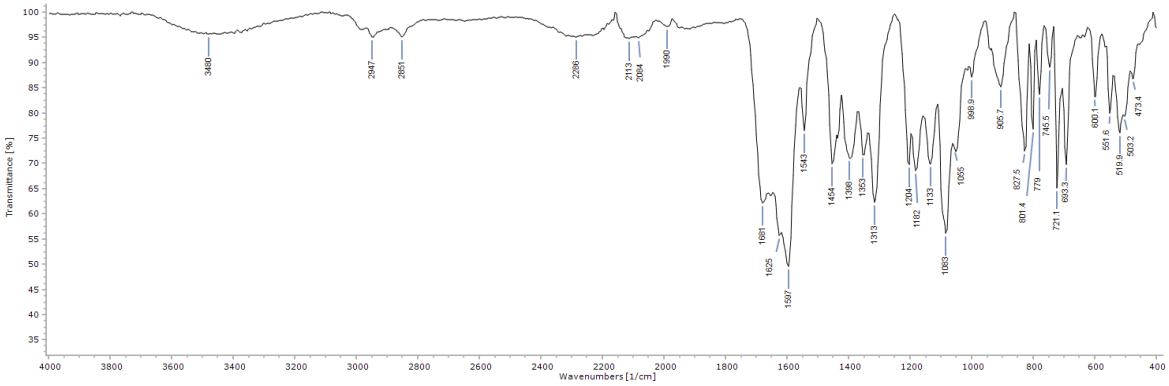

Figure S2-19. Solid-state infrared spectrum of **[Gd-DO3A-DTC-AuPPh$_2$PhCOOH]**.

S3. NMRD profiles

The NMRD profiles were measured at ^{1}H Larmor frequencies from 0.01 to 10 MHz using a 0.25 T Fast Field Cycling NMR relaxometer (SMARtracer, Stelar), equipped with a VTC90 temperature control unit. The R_1 values were acquired at 25 °C and 37 °C and converted into r_1 values using the below equation, where R_1 is the observed relaxation rate, R_{1d} the diamagnetic constant of the solvent and [CA] the concentration of Gd^{3+} (determined using the Evans Method).[5]

$$R_1 = r_1[CA] + R_{1d}$$

The data point at 63.87 MHz was acquired using a 1.5 T clinical MRI scanner, which operates only at room temperature (25 °C). For more details of MRI with these compounds, see section S7.

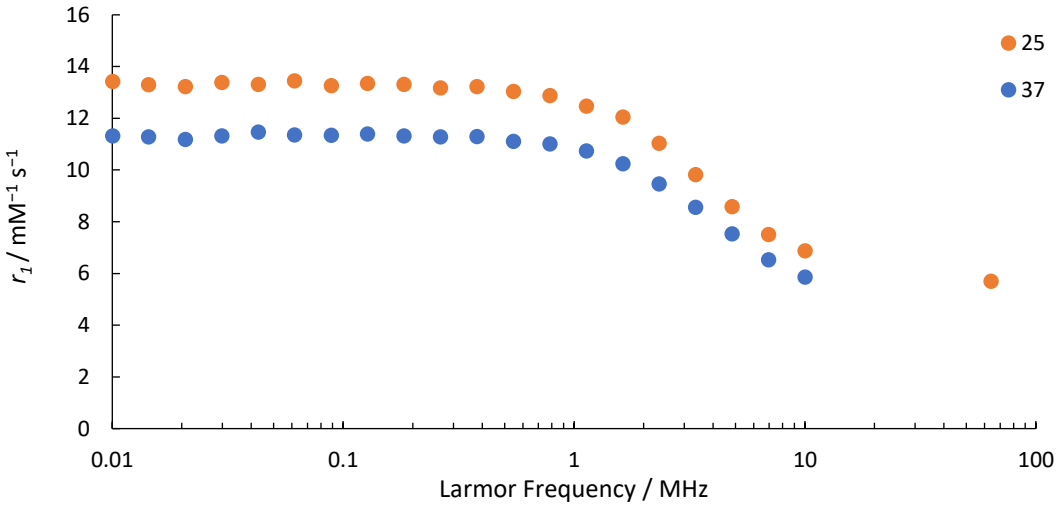

Figure S3-1. The relaxivity values per Gd^{3+} ion for K**[Gd-DOTAGA-DTC-AuPPh$_3$]** at 25 and 37 °C.

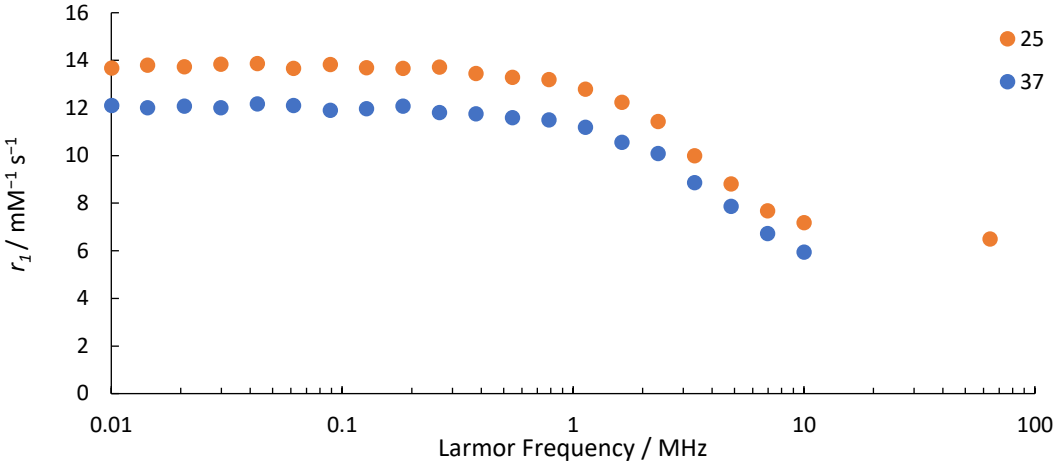

Figure S3-2. The relaxivity values per Gd^{3+} ion for K_2**[Ni(Gd-DOTAGA-DTC)$_2$]** at 25 and 37 °C.

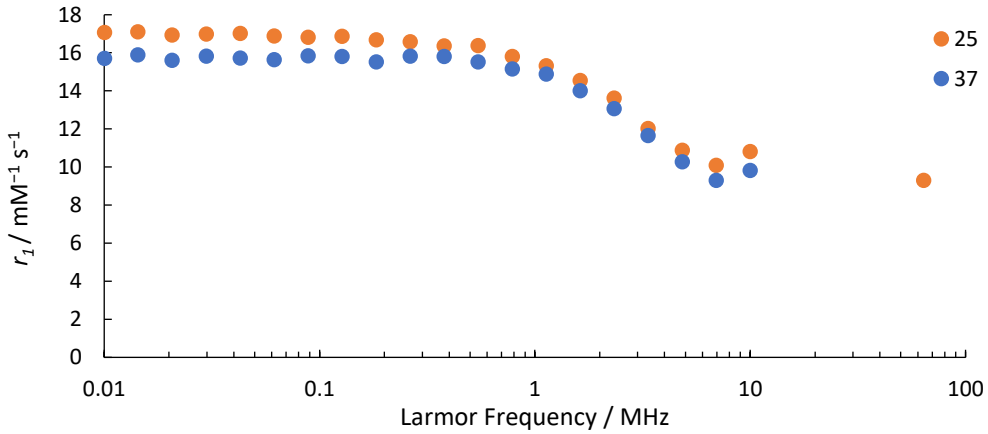

Figure S3-3. The relaxivity values per Gd^{3+} ion for K_3**[Co(Gd-DOTAGA-DTC)$_3$]** at 25 and 37 °C.

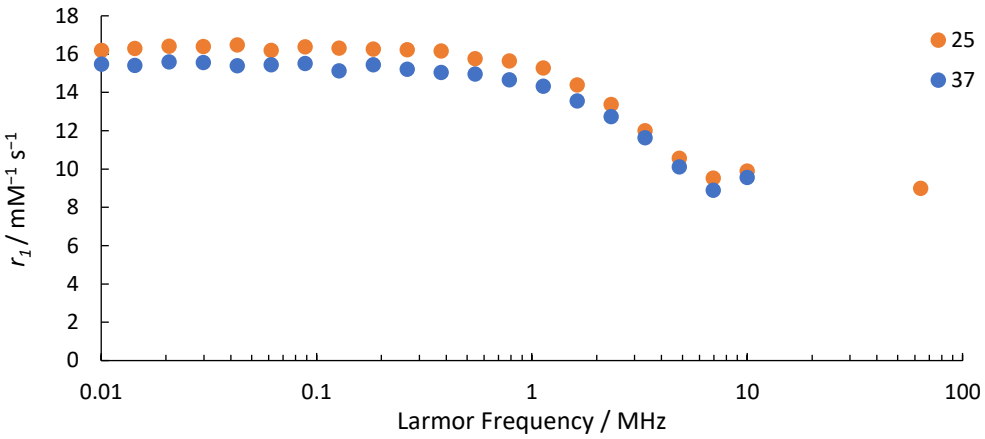

Figure S3-4. The relaxivity values per Gd^{3+} ion for K_3**[Ru(Gd-DOTAGA-DTC)$_3$]** at 25 and 37 °C.

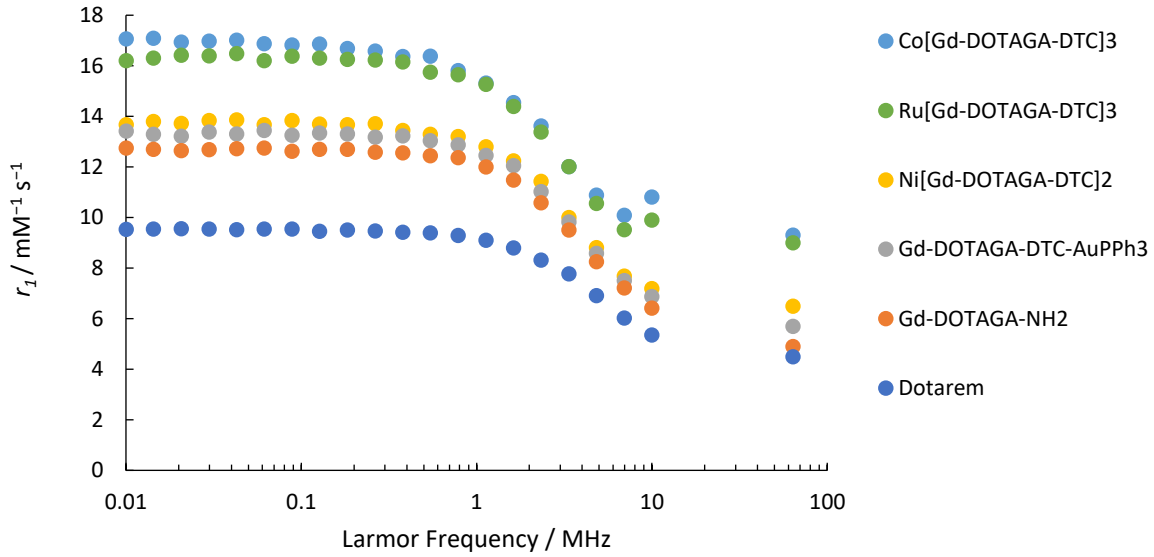

Figure S3-5. Summary of the relaxivity values per Gd^{3+} ion for **Dotarem®**, **[Gd-DOTAGA-NH$_2$]**O_2CCF_3, K**[Gd-DOTAGA-DTC-AuPPh$_3$],** K_2**[Ni(Gd-DOTAGA-DTC)$_2$]**, K_3**[Co(Gd-DOTAGA-DTC)$_3$]**, K_3**[Ru(Gd-DOTAGA-DTC)$_3$]** at 25 °C.

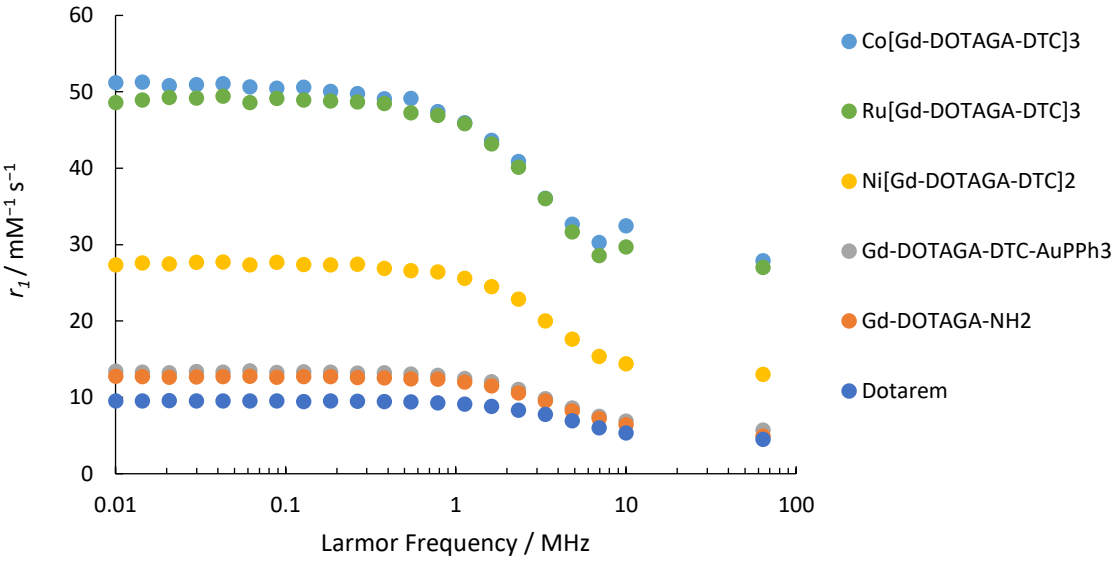

Figure S3-6. Summary of the relaxivity values per complex for **Dotarem®**, **[Gd-DOTAGA-NH$_2$]**O$_2$CCF$_3$, K**[Gd-DOTAGA-DTC-AuPPh$_3$],** K$_2$**[Ni(Gd-DOTAGA-DTC)$_2$]**, K$_3$**[Co(Gd-DOTAGA-DTC)$_3$]**, K$_3$**[Ru(Gd-DOTAGA-DTC)$_3$]** at 25 °C.

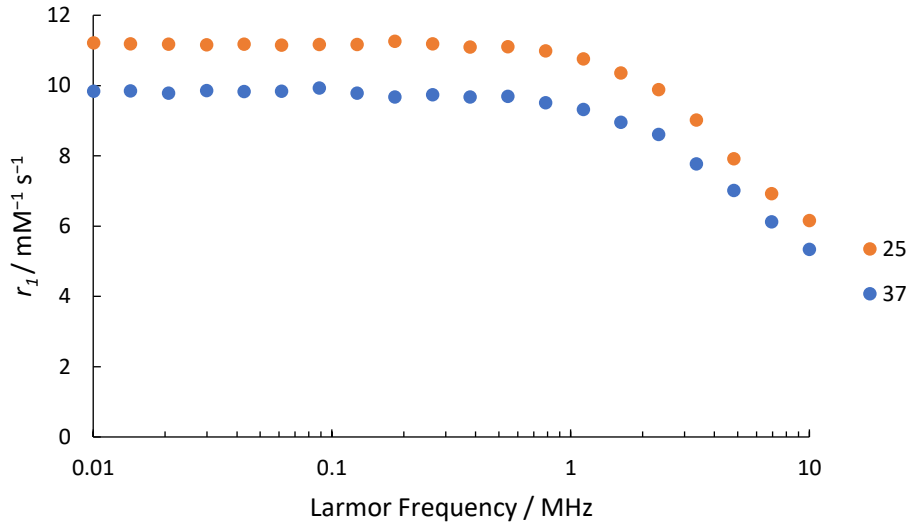

Figure S3-7. The relaxivity values per Gd^{3+} ion for **Gd-DO3A-DTC-AuPPh$_2$PhCOOH** at 25 and 37 °C.

S4. Stability studies

Stability studies were performed using a benchtop relaxometer (SMARtracer, Stelar). Multimetallic complex was dissolved in PBS (phosphate buffered saline, 200 µM) (with and without 10 eq. zinc acetate) and incubated at 37 °C and the relaxation rate (R_1) was determined at time points over 72 hours. The R_1 value relative to R_1 at t=0 was plotted against time.

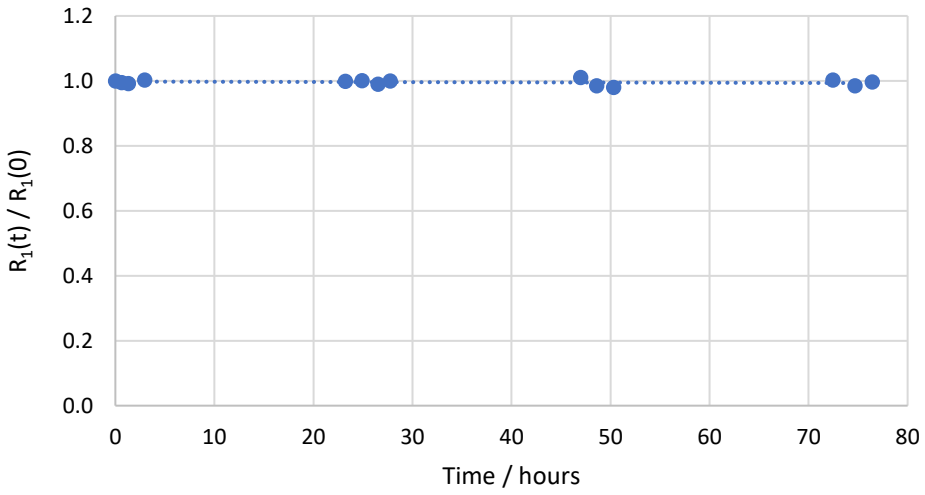

Figure S4-1. Relative R_1 of **Gd-DO3A-DTC-AuPPh$_3$** over a period of 72 hours.

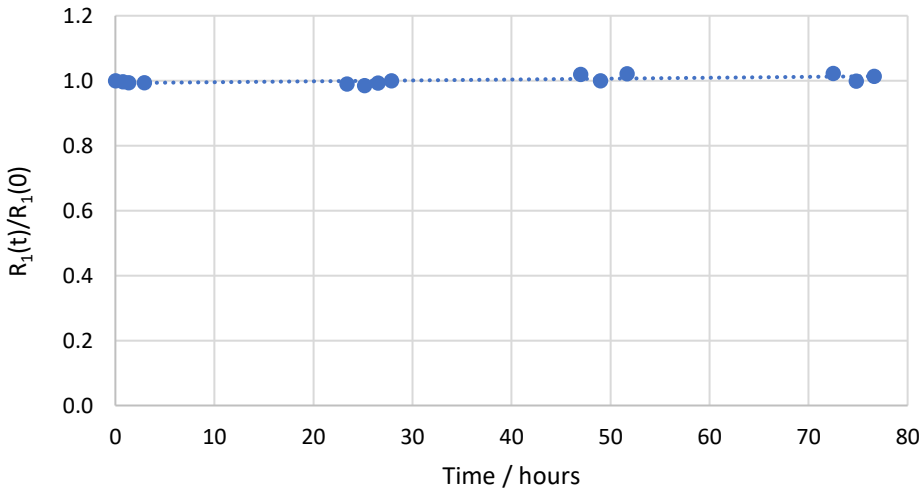

Figure S4-2. Relative R_1 of **Ni(Gd-DO3A-DTC)$_2$** over a period of 72 hours.

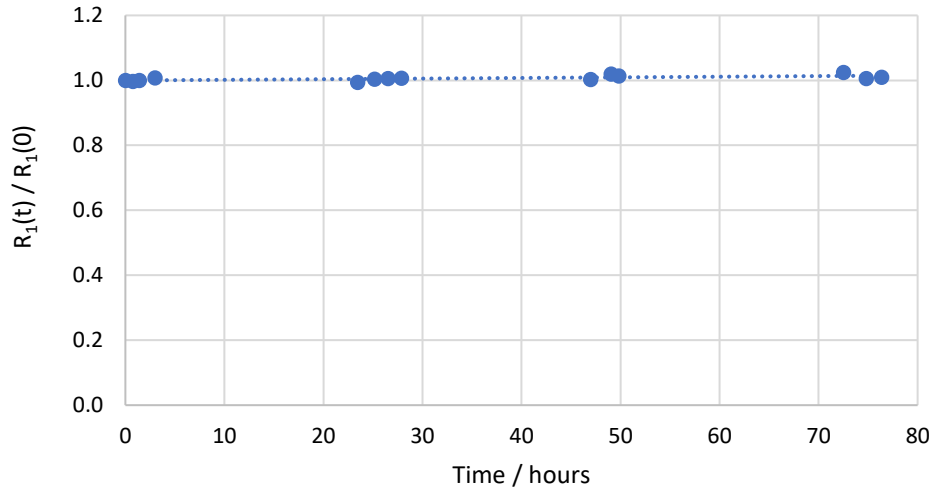

Figure S4-3. Relative R_1 of **Co(Gd-DO3A-DTC)$_3$** over a period of 72 hours.

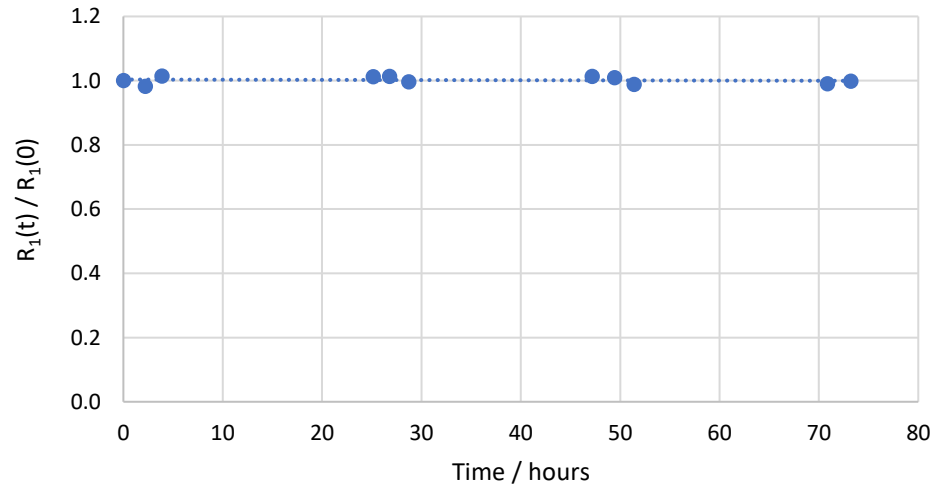

Figure S4-4. Relative R_1 of **Ru(Gd-DO3A-DTC)$_3$** over a period of 72 hours.

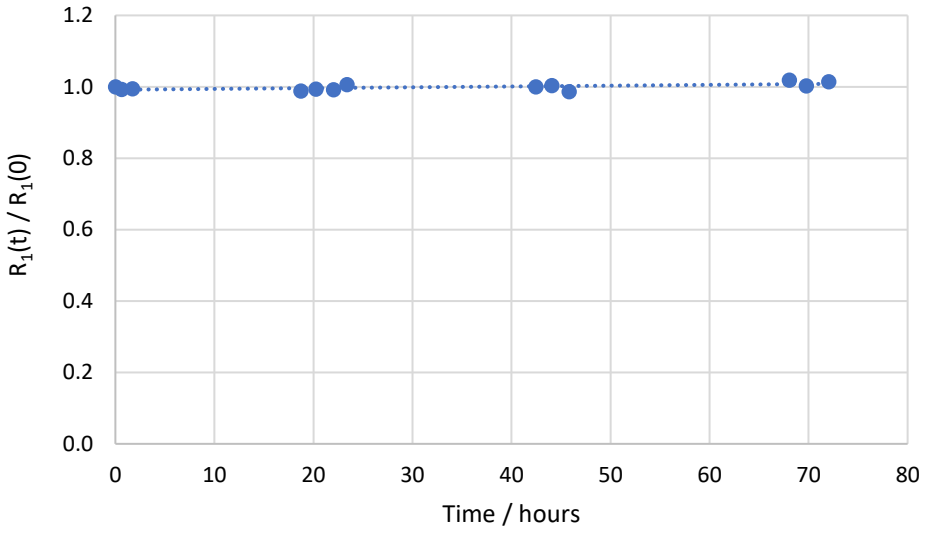

Figure S4-5. Relative R_1 of K**[Gd-DOTAGA-DTC-AuPPh$_3$]** over a period of 72 hours.

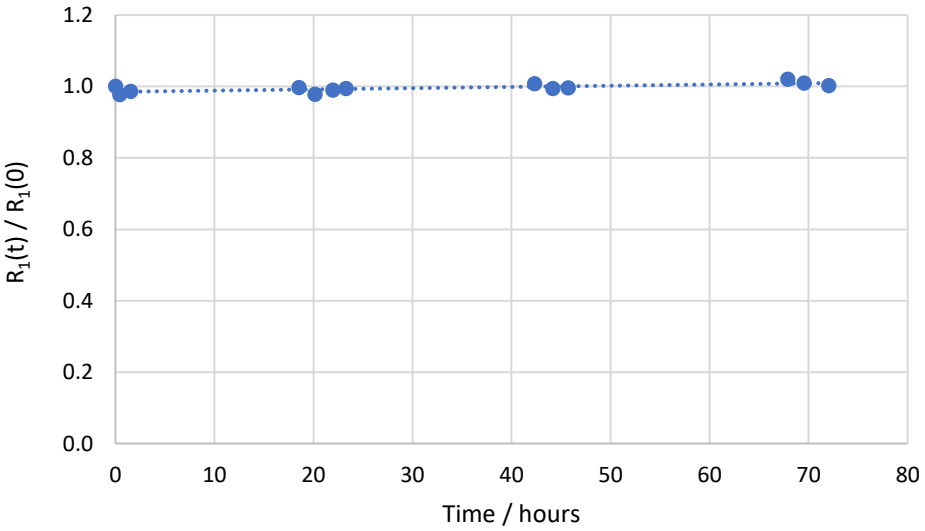

Figure S4-6. Relative R_1 of K_2**[Ni(Gd-DOTAGA-DTC)$_2$]** over a period of 72 hours.

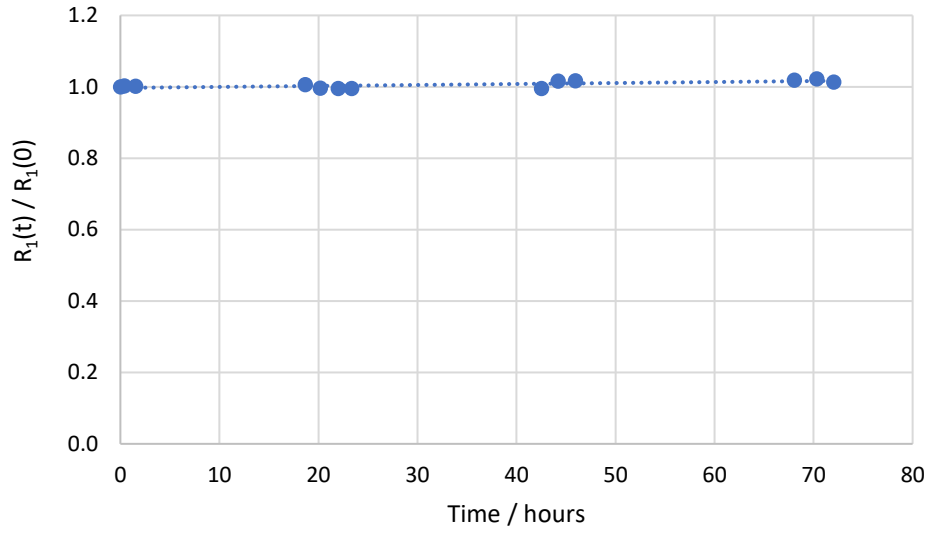

Figure S4-7. Relative R_1 of K_3**[Co(Gd-DOTAGA-DTC)$_3$]** over a period of 72 hours.

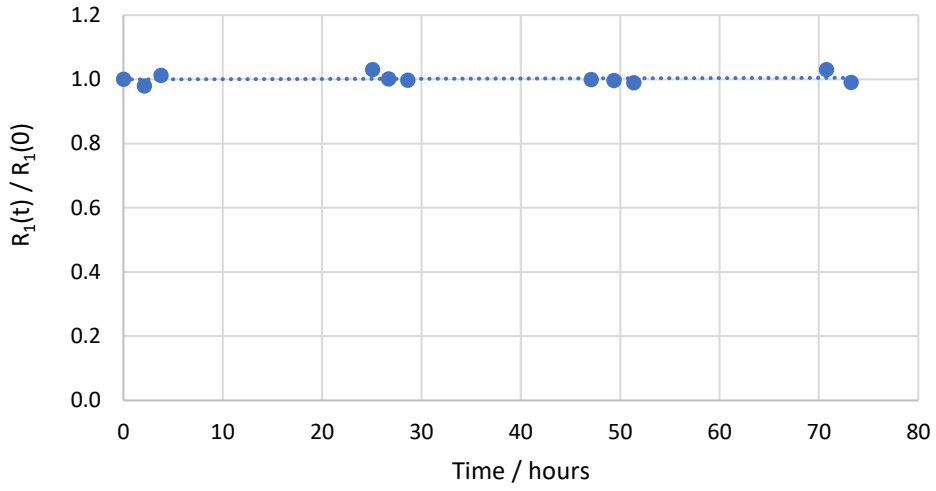

Figure S4-8. Relative R_1 of K_3**[Ru(Gd-DOTAGA-DTC)$_3$]** over a period of 72 hours.

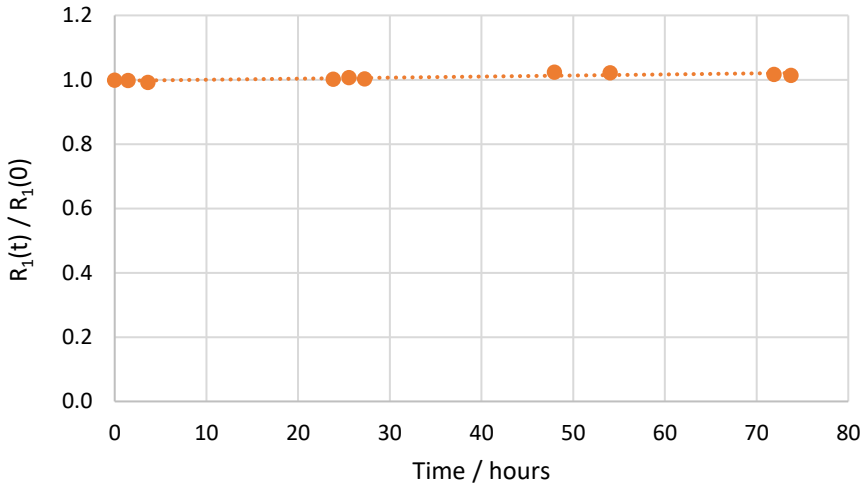

Figure S4-9. Relative R_1 of **Gd-DO3A-DTC-AuPPh$_3$** over a period of 72 hours whilst in the presence of 10 eq. zinc acetate.

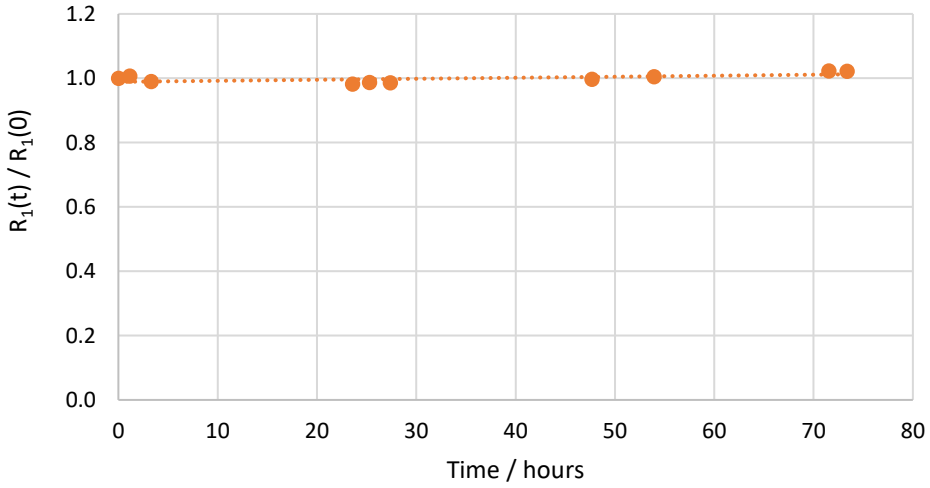

Figure S4-10. Relative R_1 of **Ni(Gd-DO3A-DTC)$_2$** over a period of 72 hours whilst in the presence of 10 eq. zinc acetate.

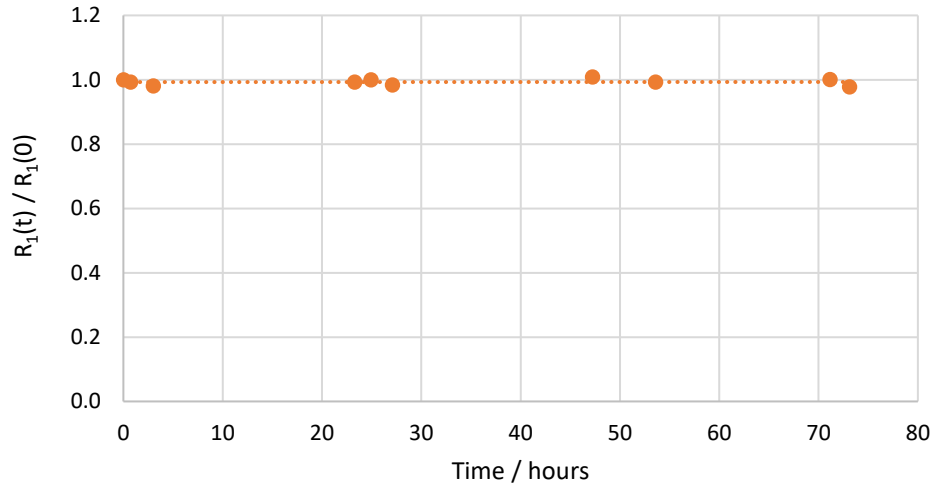

Figure S4-11. Relative R_1 of **Co(Gd-DO3A-DTC)$_3$** over a period of 72 hours whilst in the presence of 10 eq. zinc acetate.

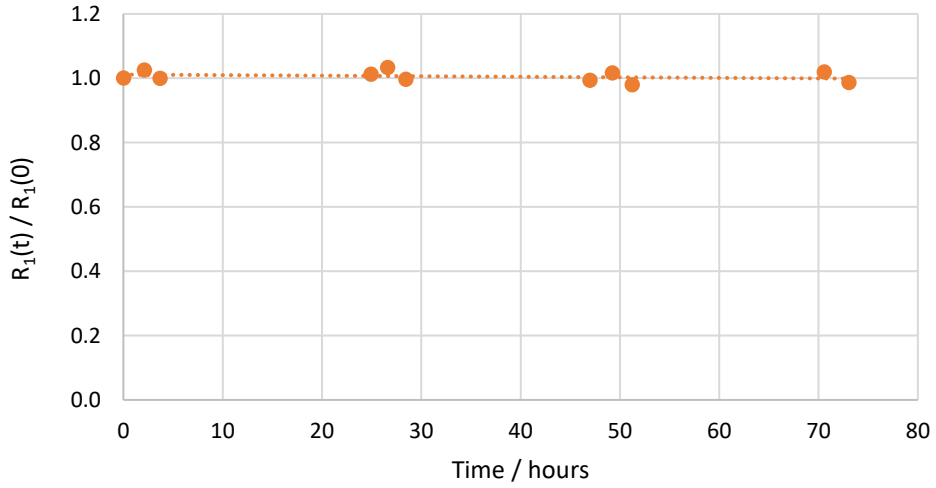

Figure S4-12. Relative R_1 of **Ru(Gd-DO3A-DTC)$_3$** over a period of 72 hours whilst in the presence of 10 eq. zinc acetate.

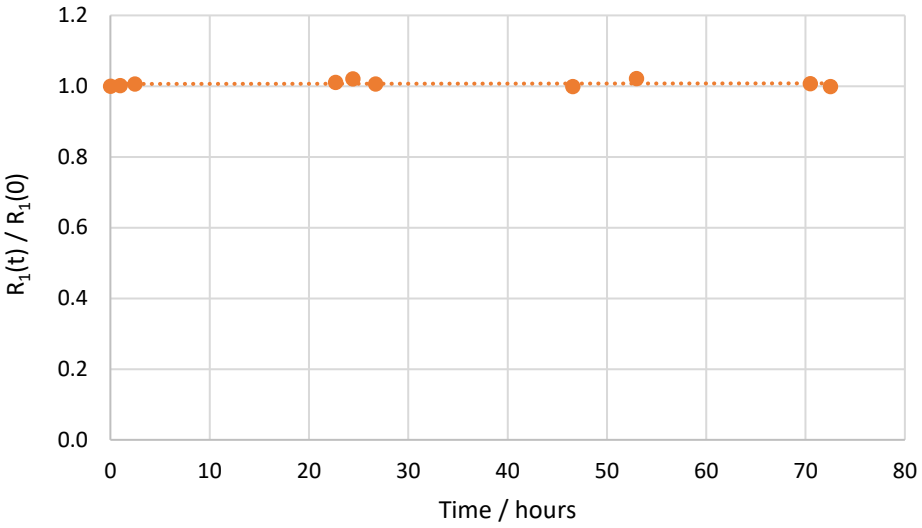

Figure S4-13. Relative R_1 of K**[Gd-DOTAGA-DTC-AuPPh$_3$]** over a period of 72 hours whilst in the presence of 10 eq. zinc acetate.

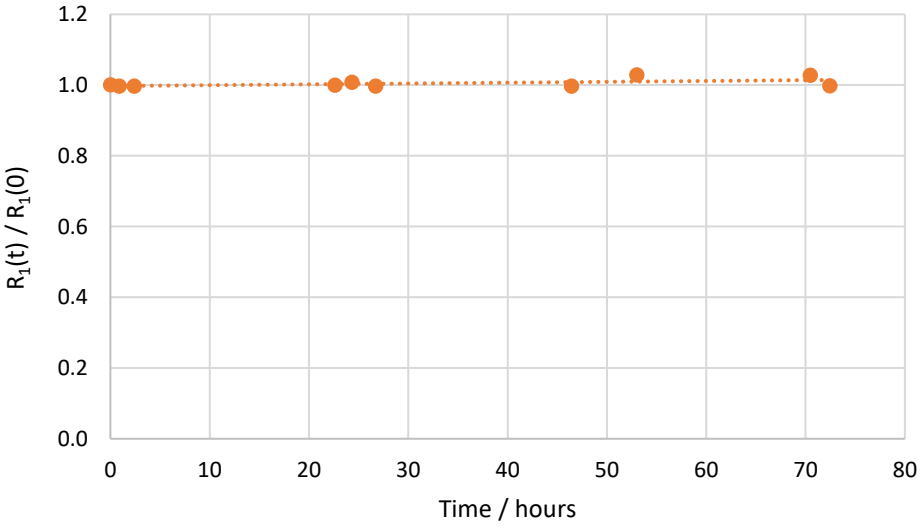

Figure S4-14. Relative R_1 of K$_2$**[Ni(Gd-DOTAGA-DTC)$_2$]** over a period of 72 hours whilst in the presence of 10 eq. zinc acetate.

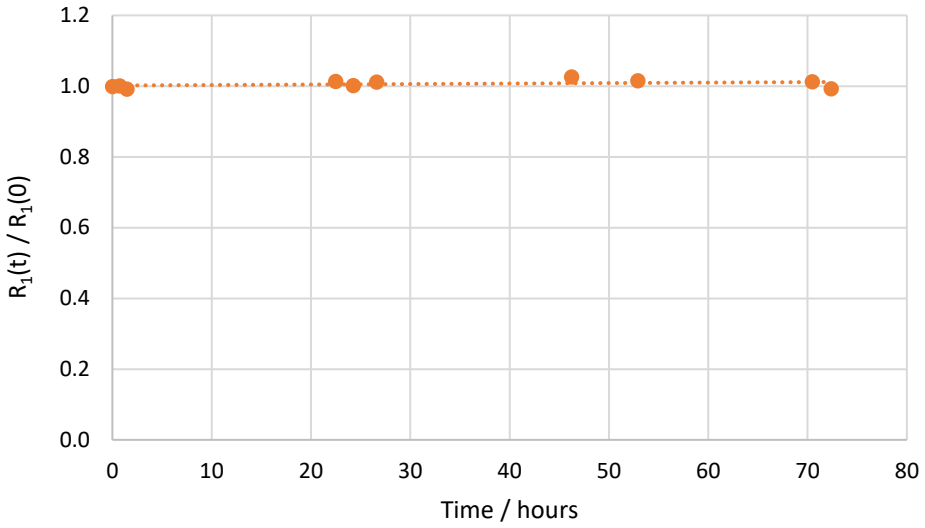

Figure S4-15. Relative R_1 of K_3**[Co(Gd-DOTAGA-DTC)$_3$]** over a period of 72 hours whilst in the presence of 10 eq. zinc acetate.

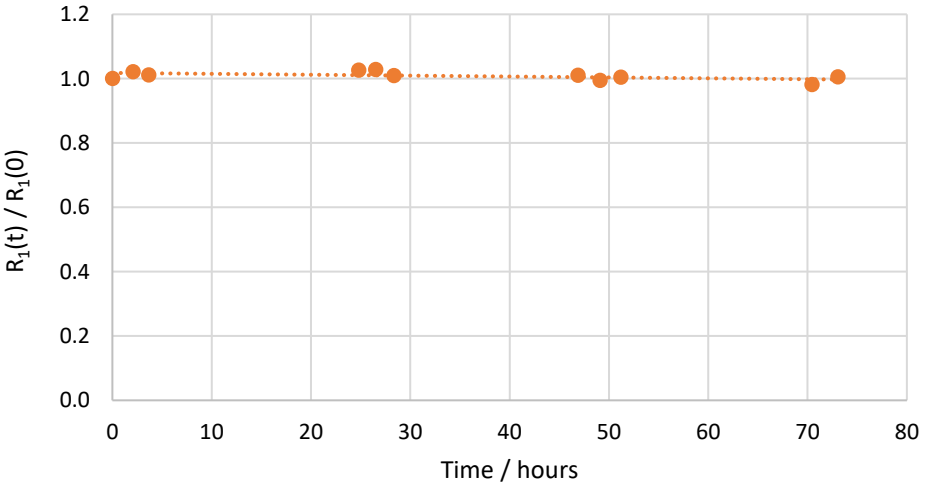

Figure S4-16. Relative R_1 of K_3**[Ru(Gd-DOTAGA-DTC)$_3$]** over a period of 72 hours whilst in the presence of 10 eq. zinc acetate.

S5. Cell viability studies

MTT assays were used to investigate the toxicity of our multimetallic complexes to HEK and HeLa cell lines. Wells of a 96-well plate were seeded with 15,000 cells and incubated for 24 hours at 37 °C, 5% CO_2. The media was removed before replacing with fresh media (200 µL), containing increasing concentrations of multimetallic complex (0 to 250 µM), and incubating for a further 24 hours 37 °C, 5% CO_2. Each concentration was repeated six times. The media was removed and replaced with a solution of MTT in PBS (1 mg/mL, 100 µL) and incubated for 2 hours at 37 °C, 5% CO_2. The MTT solution was removed and replaced with DMSO (100 µL) and incubated at room temperature in darkness for 2 hours. Absorbance readings were acquired using a plate reader with a 492 nm filter.

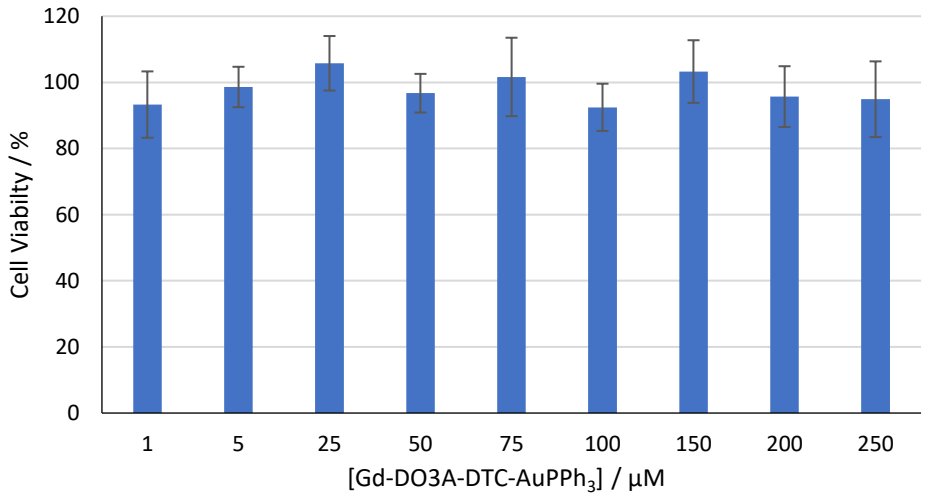

Figure S5-1. Percentage viability of HEK cells following 24-hour incubation with **Gd-DO3A-DTC-AuPPh3**.

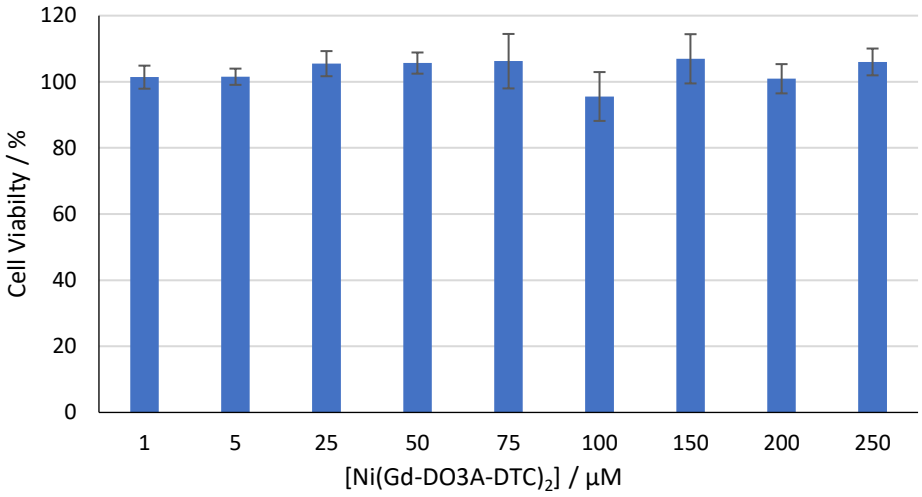

Figure S5-2. Percentage viability of HEK cells following 24-hour incubation with **Ni(Gd-DO3A-DTC)$_2$**.

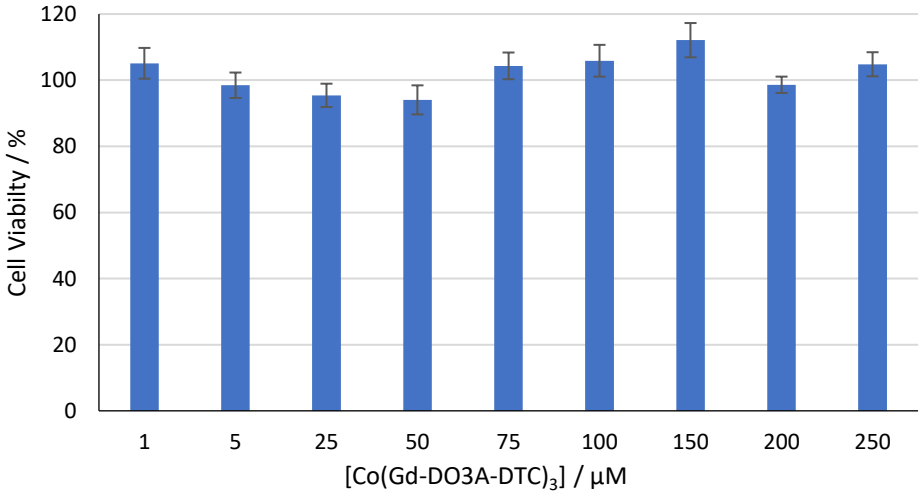

Figure S5-3. Percentage viability of HEK cells following 24-hour incubation with **Co(Gd-DO3A-DTC)$_3$**.

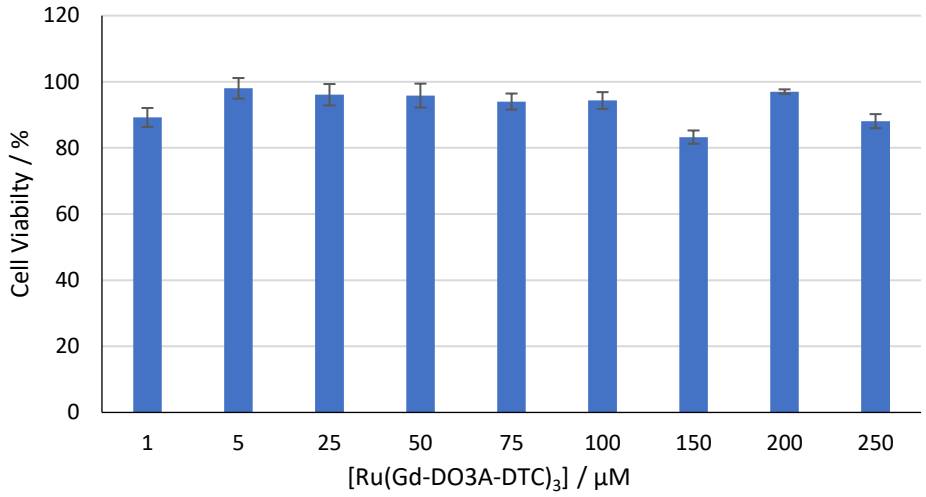

Figure S5-4. Percentage viability of HEK cells following 24-hour incubation with **Ru(Gd-DO3A-DTC)$_3$**.

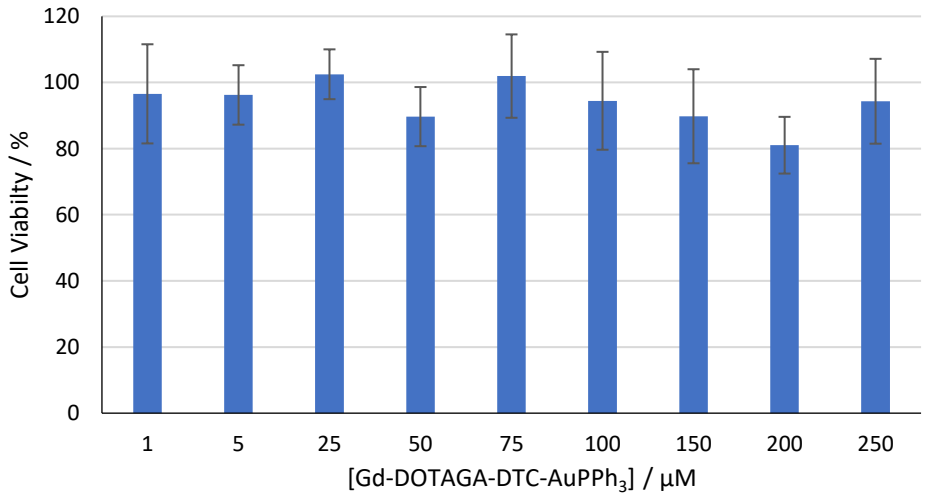

Figure S5-5. Percentage viability of HEK cells following 24-hour incubation with K**[Gd-DOTAGA-DTC-AuPPh$_3$]**.

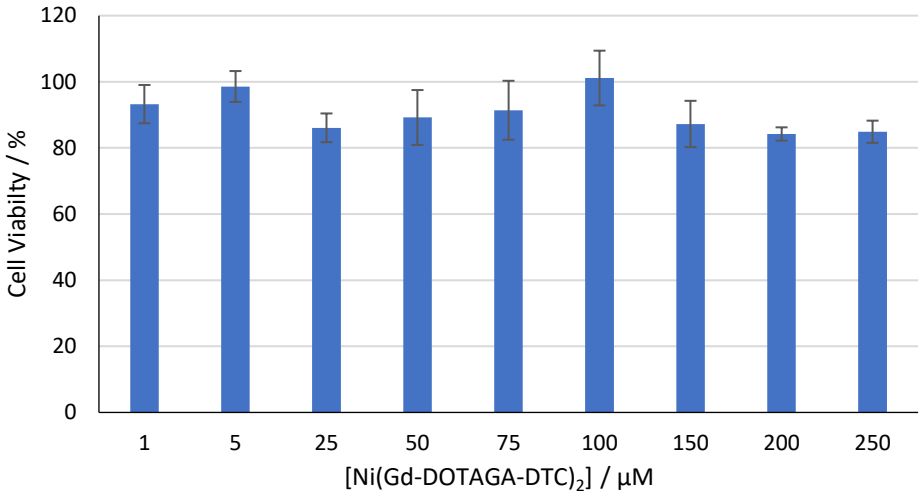

Figure S5-6. Percentage viability of HEK cells following 24-hour incubation with K_2**[Ni(Gd-DOTAGA-DTC)$_2$]**.

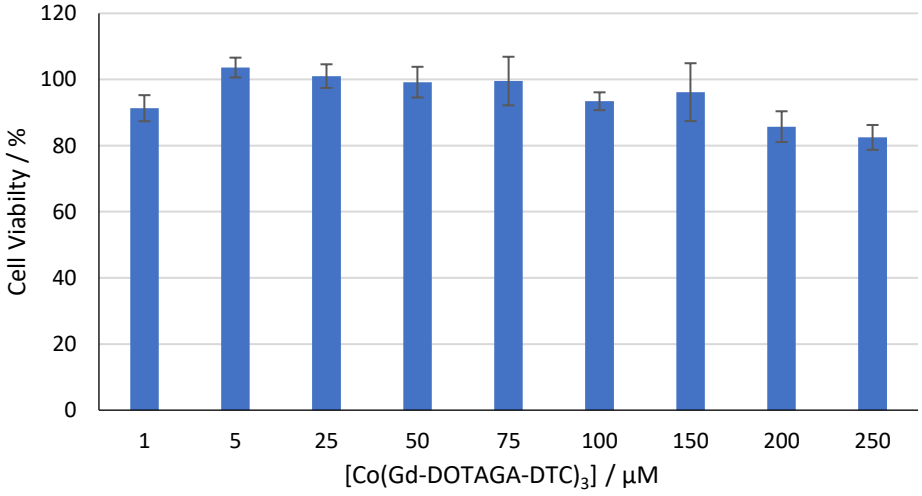

Figure S5-7. Percentage viability of HEK cells following 24-hour incubation with K_3**[Co(Gd-DOTAGA-DTC)$_3$]**.

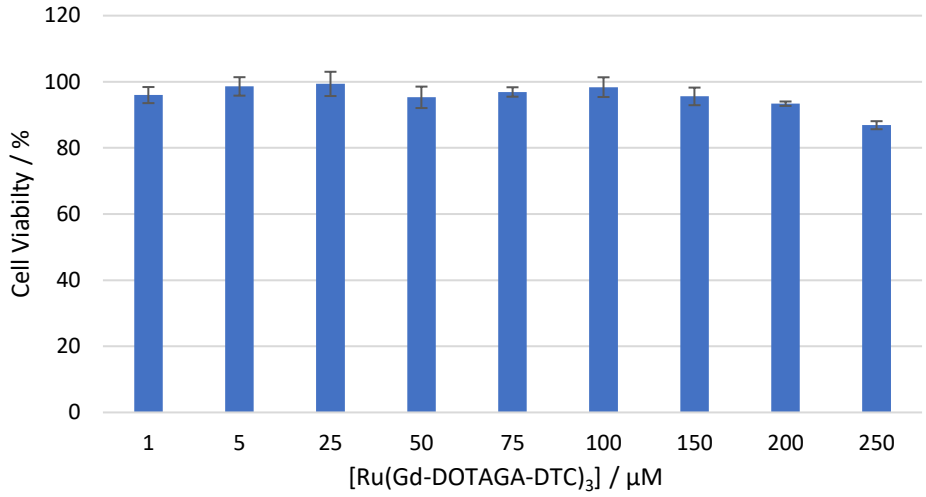

Figure S5-8. Percentage viability of HEK cells following 24-hour incubation with K_3**[Ru(Gd-DOTAGA-DTC)$_3$]**.

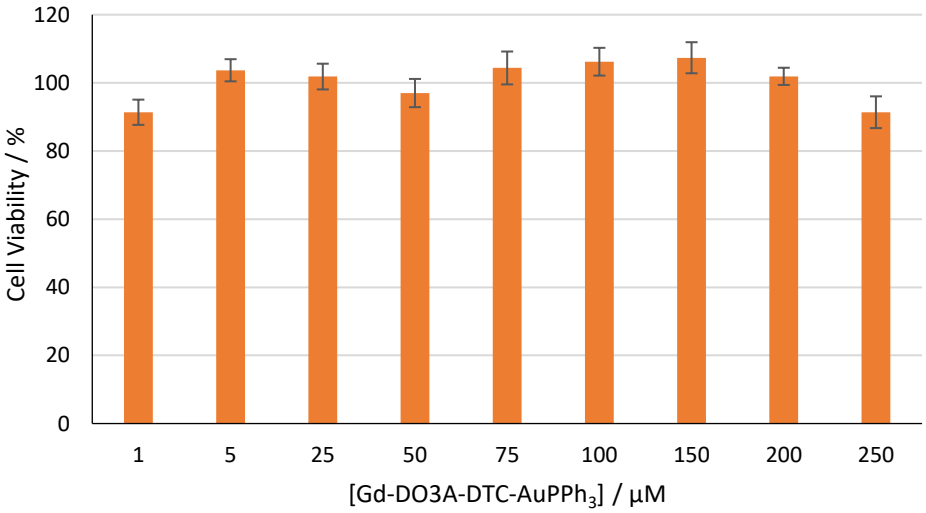

Figure S5-9. Percentage viability of HeLa cells following 24-hour incubation with **Gd-DO3A-DTC-AuPPh$_3$**.

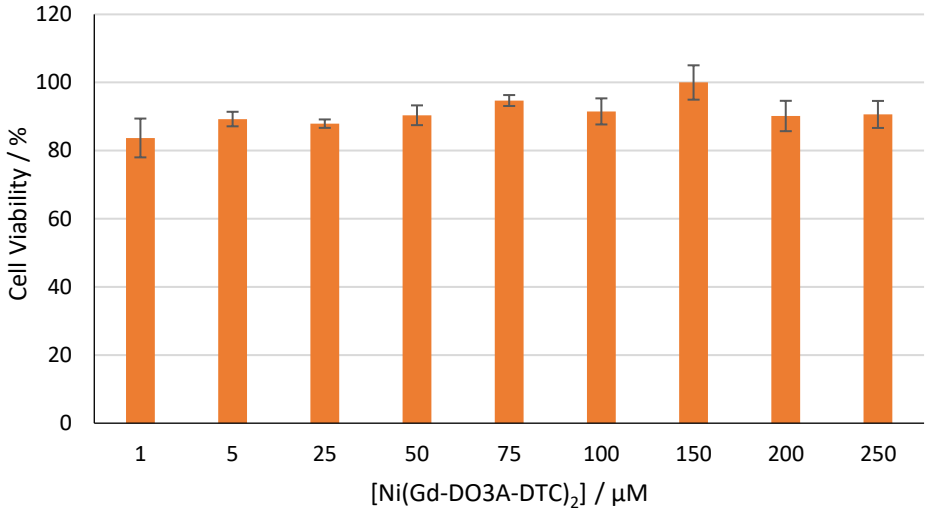

Figure S5-10. Percentage viability of HeLa cells following 24-hour incubation with **Ni(Gd-DO3A-DTC)$_2$**.

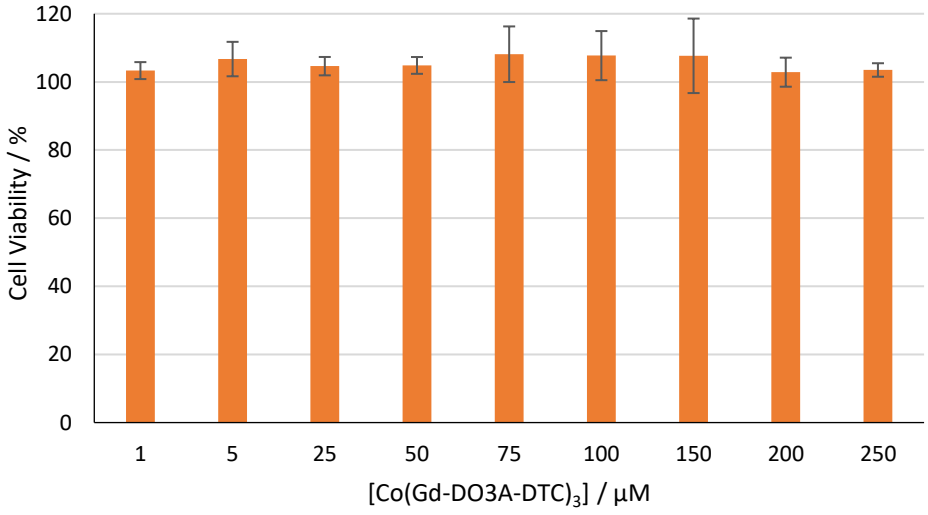

Figure S5-11. Percentage viability of HeLa cells following 24-hour incubation with **Co(Gd-DO3A-DTC)$_3$**.

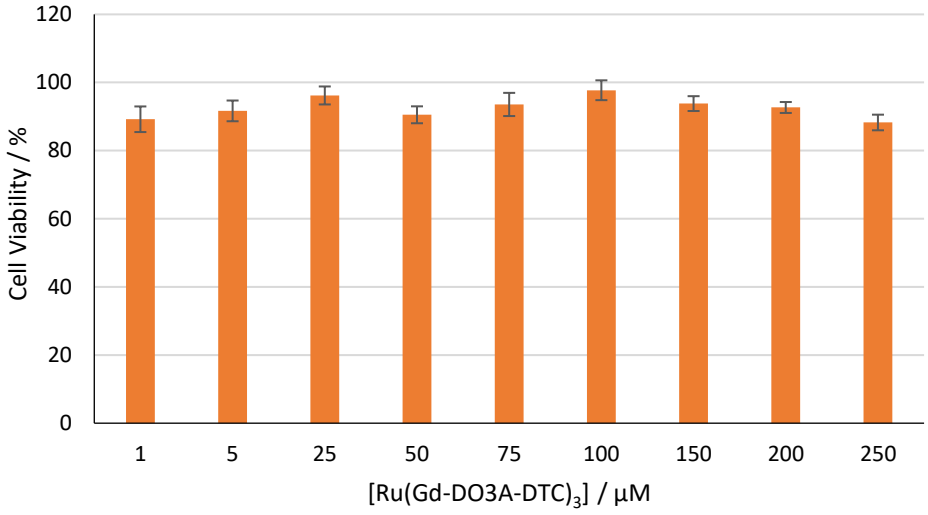

Figure S5-12. Percentage viability of HeLa cells following 24-hour incubation with **Ru(Gd-DO3A-DTC)$_3$**.

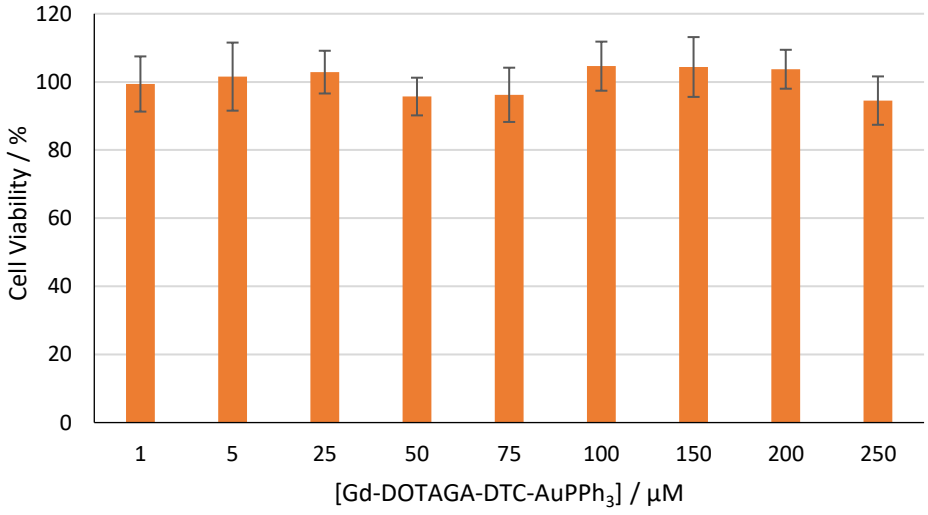

Figure S5-13. Percentage viability of HeLa cells following 24-hour incubation with K**[Gd-DOTAGA-DTC-AuPPh$_3$]**.

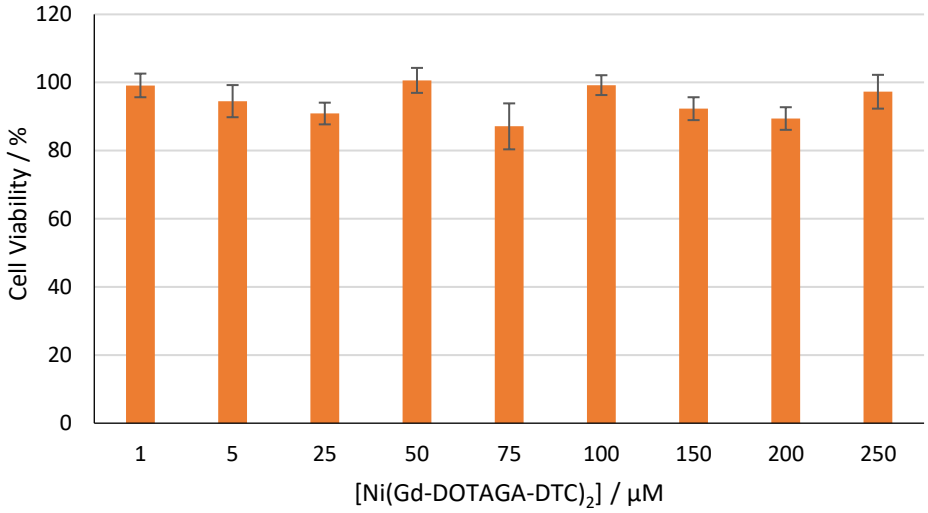

Figure S5-14. Percentage viability of HeLa cells following 24-hour incubation with K_2**[Ni(Gd-DOTAGA-DTC)$_2$]**.

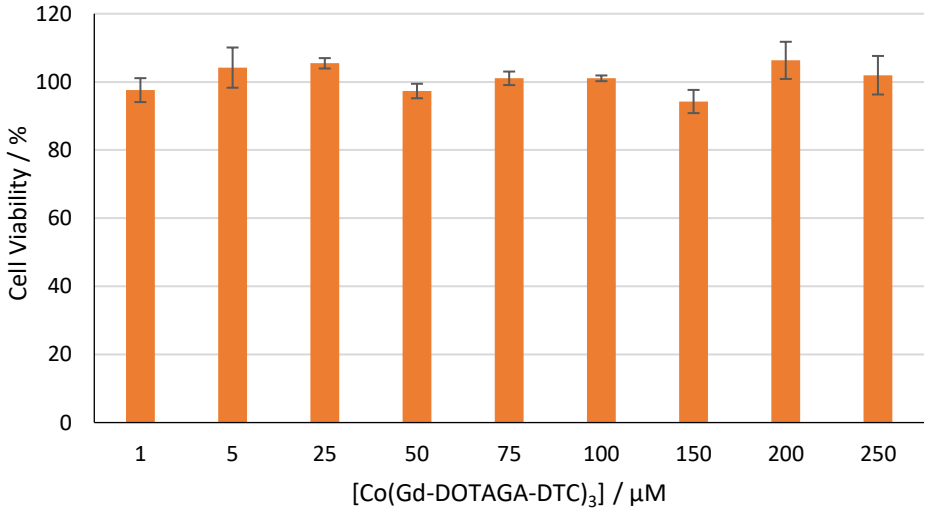

Figure S5-15. Percentage viability of HeLa cells following 24-hour incubation with K_3**[Co(Gd-DOTAGA-DTC)$_3$]**.

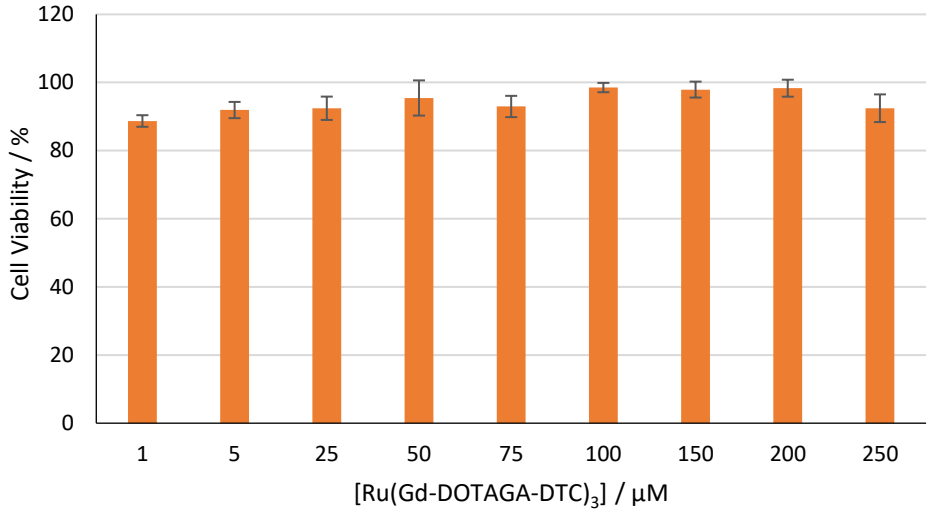

Figure S5-16. Percentage viability of HeLa cells following 24-hour incubation with K_3**[Ru(Gd-DOTAGA-DTC)$_3$]**.

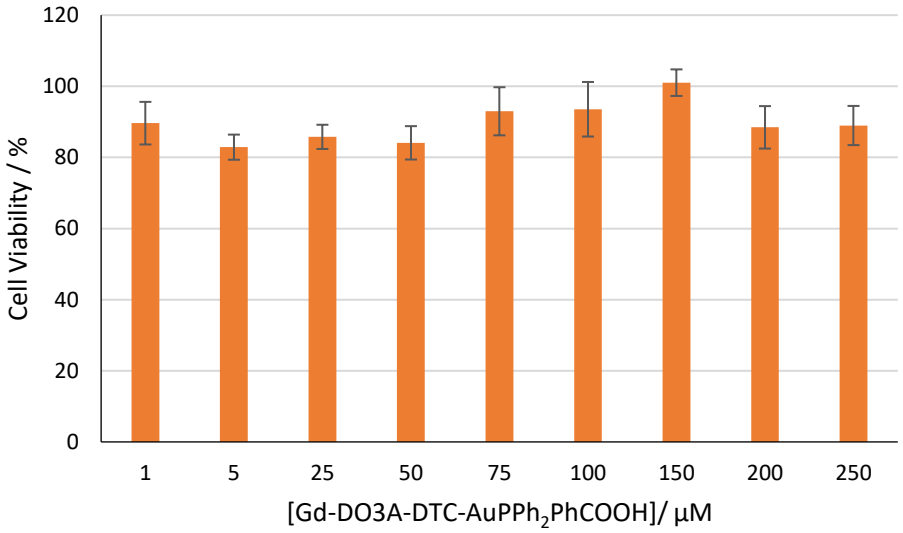

Figure S5-17. Percentage viability of HeLa cells following 24-hour incubation with **Gd-DO3A-DTC-AuPPh$_2$PhCOOH**.

S6. Cell uptake studies

Wells of a 96-well plate were seeded with 15,000 cells and incubated for 24 hours at 37 °C, 5% CO_2. The media was replaced with a solution of metallostar complex dissolved in media ([Gd^{3+}] =10 µM, 100 µL) and incubated for either 1, 4 or 24 hours at 37 °C, 5% CO_2. Each time point for each complex was repeated four times. The media was collected, the cells were washed three times and the washings were also collected. Samples were analyzed for metal content by ICP-MS. The mass detected was subtracted from the mass added to the cells to determine mass taken up by cells and a percentage uptake value was calculated.

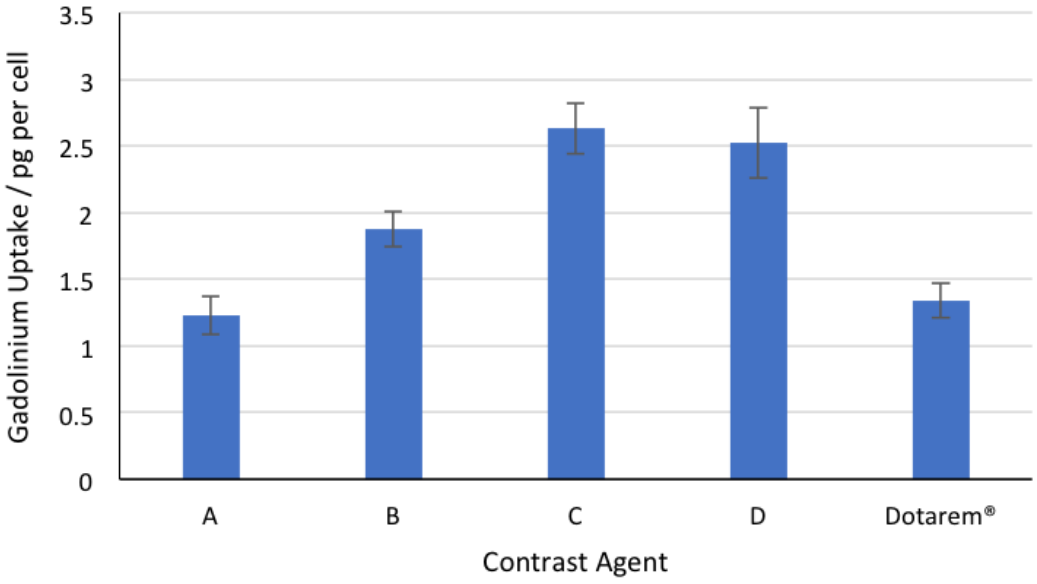

Figure S6-1. Uptake of Gd by HeLa cells after 24 hours incubation with **Gd-DOTAGA-DTC-$AuPPh_3$ (A), $Ni(Gd\text{-}DOTAGA\text{-}DTC)_2$ (B), $Co(Gd\text{-}DOTAGA\text{-}DTC)_3$ (C)**, **$Ru(Gd\text{-}DOTAGA\text{-}DTC)_3$ (D)** and Dotarem®.

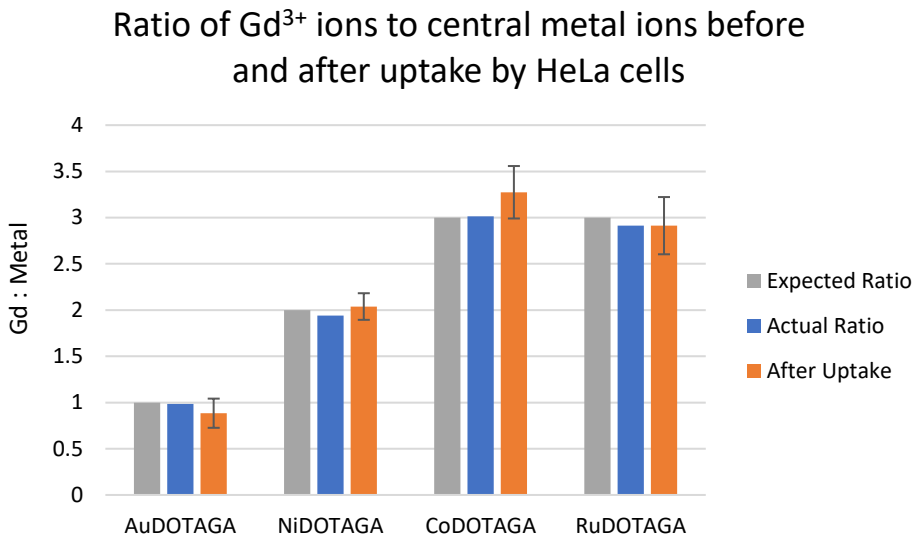

Figure S6-2. Comparison of the ratio of gadolinium ions to central metal ions (Au, Ni, Co or Ru) before and after uptake by HeLa cells for K**[Gd-DOTAGA-DTC-AuPPh$_3$],** K_2**[Ni(Gd-DOTAGA-DTC)$_2$]**, K_3**[Co(Gd-DOTAGA-DTC)$_3$]** and K_3**[Ru(Gd-DOTAGA-DTC)$_3$]**.

S7. Magnetic resonance imaging

Magnetic resonance imaging was performed at 25 °C on a clinical 1.5 T MRI Scanner (Philips Ingenia, Philips Medical Systems) using a Modified Look-Locker Imaging (MOLLI) T_1 sequence. The scan parameters were as follows: 15 x 300 x 300 mm field of view, 300 x 300 mm acquisition matrix, 3 mm slice thickness, 2.145 ms echo time, 4.290 ms repetition time and 50° flip angle. Each metallostar complex was prepared at 3 different gadolinium concentrations (ICP-MS) between 0.02 and 0.6 mM. A phantom of ultrapure water was also prepared to obtain the diamagnetic constant of the solvent. The 1 mL phantoms were submerged in water during acquisition to reduce Gibbs artefacts. The T_1 maps were analyzed using Philips DICOM Viewer 3.0. T_1 values were extracted for each metallostar complex across 5 slices and a mean average value was taken. R_1 was then plotted against gadolinium concentration and the gradient of the straight line was taken to be the relaxivity.

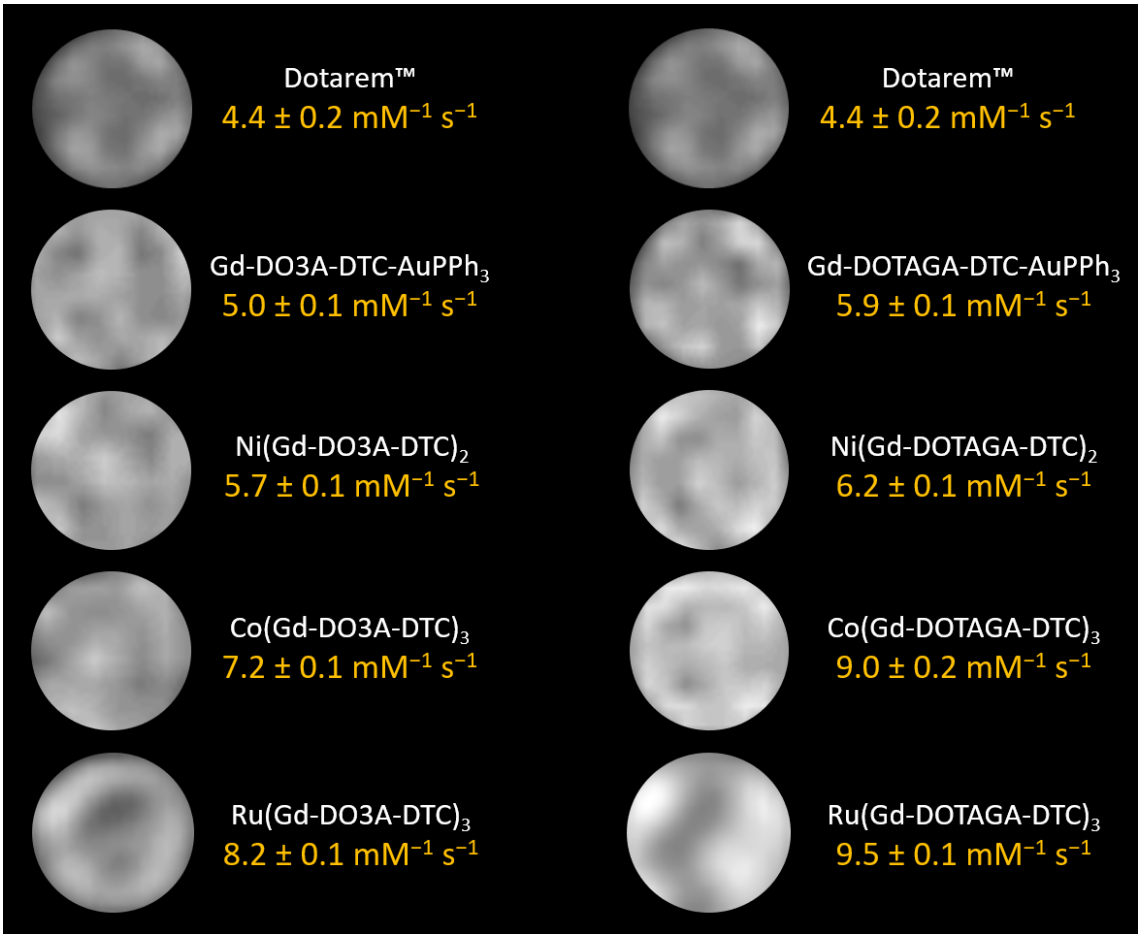

Figure S7-1. MR images and relaxivity values of the **metallostar complexes** and **Dotarem®** (1.5 T, 25 °C, [Gd^{3+}] = 0.1 mM).

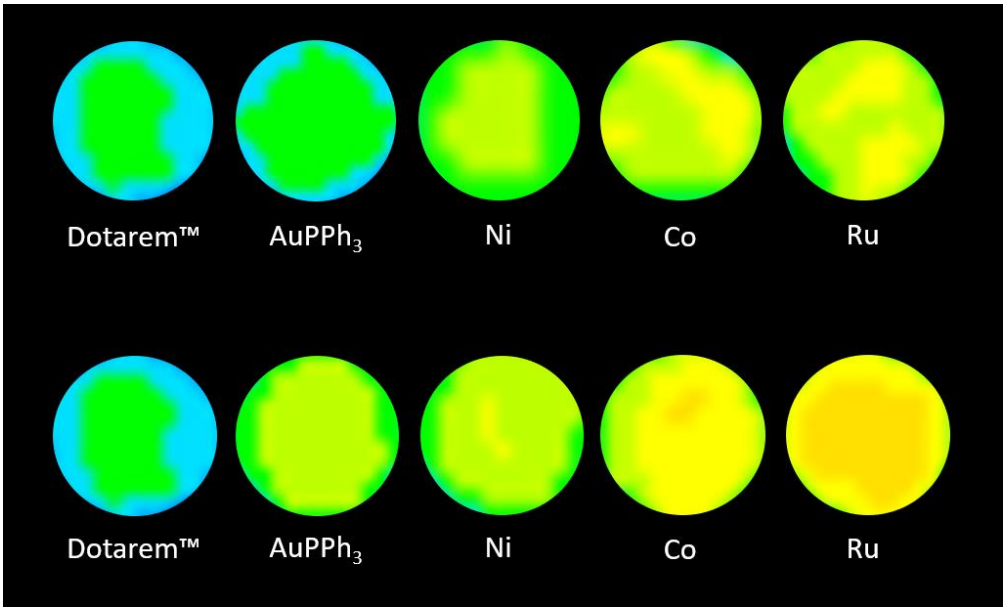

Figure S7-2. MR images (shown in '16 colors', ImageJ) of the **metallostar complexes** and **Dotarem®** (1.5 T, 25 °C, $[Gd^{3+}]$ = 0.2 mM).

S8. References:

1. Chabloz, N. G.; Wenzel, M. N.; Perry, H. L.; Yoon, I.-C.; Molisso, S.; Stasiuk, G. J.; Elson, D. S.; Cass, A. E. G.; Wilton-Ely, J. D. E. T. Polyfunctionalized nanoparticles bearing robust gadolinium surface units for high relaxivity performance in MRI. *Chem. Eur. J.* **2019**, *25*, 10895-10906.

2. Chabloz, N. G.; Perry, H. L.; Yoon, I.-C.; Coulson, A. J.; White, A. J. P.; Stasiuk, G. J.; Botnar, R. M.; Wilton-Ely, J. D. E. T. Combined magnetic resonance imaging and photodynamic therapy using polyfunctionalized nanoparticles bearing robust gadolinium surface units, *Chem. Eur. J.* **2020**, *26*, 4552–4566.

3. Uson, R.; Laguna, A.; Vicente, J. Novel anionic gold(I) and gold(III) organocomplexes, *J. Organomet. Chem.* **1977**, *131*, 471-475.

4. Kriechbaum, M.; List, M.; Himmelsbach, M.; Redhammer, G. J.; Monkowius, U. Peptide coupling between amino acids and the carboxylic acid of functionalized chloride-gold(I)-posphane. *Inorg. Chem.* **2014**, *53*, 10602-10610.

5. Evans, D. F. The determination of the paramagnetic susceptibility of substances in solution by nuclear magnetic resonance. *J. Chem. Soc.* **1959**, *0*, 2003-2005.